1-1-2017

Analysis Of The Secondary Neurodegenerative Consequences Of Primary Oligodendrocyte Stress Through The Use Of The Novel Obiden Mouse Model

Daniel Zdzislaw Radecki
Wayne State University,

ANALYSIS OF THE SECONDARY NEURODEGENERATIVE CONSEQUENCES OF PRIMARY OLIGODENDROCYTE STRESS THROUGH THE USE OF THE NOVEL *OBIDEN* MOUSE MODEL

by

DANIEL ZDZISLAW RADECKI

DISSERTATION

Submitted to the Graduate School

of Wayne State University,

Detroit, Michigan

in partial fulfillment of the requirements

for the degree of

DOCTOR OF PHILOSOPHY

2017

MAJOR: MOLECULAR BIOLOGY AND GENETICS

Approved By:

Advisor Date

DEDICATION

This work is dedicated to my parents and my sister. For encouragement, help, patience and intelligence that have helped me for 28 years. Thank you for everything you have done and everything you continue to do, none of this would be possible without you. I will continue to push myself, my work and my life with everything you've taught me at my back.

ACKNOWLEDGEMENTS

I would like to acknowledge many people for their help and guidance along the way. First, Kathleen Maheras and Chelsea Richardson for their help and thoughts and cooperation through our graduate work, you two are awesome. I will never forget my time with you and a wish nothing but the best for you in the years to come.

To all the summer and rotation students who contribute to the work including Ashley Brown, Kate VanPelt and Nicholas Meshkin, thank you for your help and effort.

To all the mice that gave themselves for the sake of science and furthering our understanding of the nervous system and Multiple Sclerosis.

To CMMG department, especially Suzanne Shaw and Dave Wissbrun, your help and problem solving have been invaluable and made this work all the better.

To my committee and faculty members who have given advice, guidance, help or a kick to get going over the years, including Dr. Gregory Kapatos, Dr. Joyce Benjamins and Dr. Leon Carlock, thank you for your patience and help.

Finally, I would like to thank my mentor Dr. Alexander Gow and Cherie Southwood. For taking me into the lab, showing me everything from experimental designs, and mouse work and analysis and how to fix equipment and keep it running. Also, for your encouragement, support, conversations and pushing me to do and be everything I set out to be, thank you and I will never forget you or my time in your lab.

TABLE OF CONTENTS

LIST OF TABLES

LIST OF FIGURES

LIST OF ABBREVIATIONS

1H	hydrogen
3V	third ventricle
ABR	auditory brainstem response
AnkG	ankyrin-G
APP	amyloid precursor protein
ATF3	activating transcription factor 3
ATF4	activating transcription factor 4
AUC	area under the curve
β4-Spec	beta four spectrin
BBB	blood brain barrier
CA1	cornu ammonis 1
CC	corpus collosum
CD68	cluster of differentiation 68
CHOP	CAAT-enhancer binding protein homologous protein
CING	cingulate cortex
cm	centimeter
CNPase	2', 3'-cyclic nucleotide 3'-phosphodiesterase
CNS	central nervous system
CSF	cerebrospinal fluid
Ctip2	COUP-TF-Interacting Protein 2
dB	decibels
DHC	dorsal hippocampus
DTI	diffusion tensor imaging
EAE	experimental autoimmune encephalomyelitis

EC	external capsule
EDSS	extended disability scoring system
EEG	electroencephalography
ENT	entorhinal cortex
EPI	exploratory preference index
FA	fractional anisotropy
FOV	field of view
GABA	gamma amino butaric acid
i.msd	inducible myelin synthesis deficient
IC	internal capsule
ICC	immunocytochemistry
INF-b	interferon beta
INF-g	interferon gamma
IRE1	inositol-requiring enzyme 1
kHz	kilohertz
Kv	potassium channel
LFB	luxol fast blue
LV	lateral ventricle
MBP	myelin basic protein
Mcre	MBP promoter-enhancer Cre recombinase
min	minute
mm	millimeter
mm	micrometer
MR	magnetic resonance
MRI	magnetic resonance imaging

MRS	magnetic resonance spectroscopy
MS	Multiple Sclerosis
ms/msec	millisecond
msd	myelin synthesis deficient
mV	microvolt
Nav	sodium channel
NeuN	neuronal nuclei
NF-L	neurofilament light chain
NN	neuronal nuclei
nNF	non-phosphorylated neurofilament
PBS	phosphate buffered saline
PERK	protein kinase RNA-like endoplasmic reticulum kinase
PIRI	piriform cortex
PLP1	proteolipid protein 1
PMD	Pelizaeus-Merzbacher Disease
PNS	peripheral nervous system
PPMS	primary-progressive multiple sclerosis
Rost-ENT	rostral entorhinal cortex
Rost-PIRI	rostral piriform cortex
RPM	revolutions per minute
RRMS	relapse-remitting multiple sclerosis
S	Siemens
sec	second
SPG2	spastic paraplegia type 2
SPL	sound pressure level

SPMS	secondary-progressive multiple sclerosis
SYN	synapsin 1
SYP1	synaptophysin 1
TBS	tris buffered saline
TE	time of echo
THAl	thalamus
TR	time of relaxation
UPR	unfolded protein response
VHC	ventral hippocampus
VTA	ventral tagmental area

INTRODUCTION

The central nervous system (CNS) in mammals is a highly ordered structure of multiple cell types, functions and interactions. It works to maintain homeostatic balances throughout the body for temperature, digestion, blood pressure and oxygenation and all the fine sensory inputs and motor controls throughout the body. In addition, it shapes the behavioral and cognitive landscape of the animal and governs its interactions with other organisms and the environment. To achieve its function, the CNS is composed of four primary cell types; neurons and the glial cells, oligodendrocytes, astrocytes and microglia.

Through much of modern neuroscience and biology, neurons have been the focus of study and analysis as they generate the large electrical signals detectable as electroencephalographs (EEG) (Yeager, 1950). They are also the cells with the most apparent, extensive branching patterns and the only cells in the CNS that discretely connect physical nuclei (Liska et al., 2015; Witter, 2006). This view was strengthened upon post-mortem analysis of CNS tissue form neurodegenerative diseases where intracellular inclusions, neuronal loss, axonal spheroids and axonal transections were all readily visible phenotypes, suggesting neurons are vulnerable to these diseases (Adams and Kubik, 1952). However, this was a simple view that was quickly altered as more information regarding the other cell types of the CNS was discovered.

Oligodendrocytes and Myelin

The last major glial type to be described microscopically was the oligodendroglia lineage of cells in 1921 (Garrosa, 2012; Rio-Hortega, 1921). Their similarity to Schwann cells, the peripheral nervous system (PNS) lipoprotein producing cells that sheath axons was a major focus, however the organization, morphology and clustering was distinctly different. The glial cells described have fewer processes than other glial types and with their cell bodies were linearly arrayed in white matter and often located near blood vessels and neuronal cell bodies. Subsequently, oligodendrocytes were confirmed to be synthesizing myelin for axons, not just

arranged in juxtaposition to myelin sheaths (reviewed in Boullerne, 2016). Although the physical relationship between myelin and axons was established, the exact purpose of myelin was still in debate. Myelin increases the conduction velocity and the fidelity of signal transduction that allows action potentials to cover greater distances with less energy expenditure (Peters, 1960; Rasminsky, 1972). However, the benefit in conduction to neurons does come with a cost to oligodendrocytes because the large amount of myelin a single cell synthesizes for up to one hundred axons leaves it susceptible to metabolic disruptions.

In addition to ensheathing multiple axons, the number of myelin wraps depends on the diameter of the axons. As the diameter of the axon grows, so too will the number of myelin wraps creating a constant relationship between the outer diameter of a myelin sheath and the inner axonal diameter called the *g*-ratio (Waxman, 1975). This is further evidence that an individual oligodendrocyte can be placed under a large metabolic load to initially synthesize the myelin for the axons it contacts and to maintain myelin throughout life (Gow et al., 1994b)

Oligodendrocyte Metabolic Stress

The concept for a metabolic stress phenotype in oligodendrocytes originated with the characterization and observation of mice, rats and patients with hypomyelination and an oligodendrocyte phenotype (Bischoff, 1975; Knapp et al., 1986; van Noort et al., 1995). The initial characterizations identified decreased myelination and oligodendrocyte populations without identifying the cause of the cellular loss. Some work suggested that the loss may be due to immune involvement depleting oligodendrocytes, similar to the immune infiltrating lesions in MS that attack and degenerate myelin (Gardinier and Macklin, 1988; Turnley et al., 1991). However, further investigation revealed a different, common mechanism for many of the diseases resulting from overexpression of myelin proteins or expression of mutant proteins.

The initial insights into the pathology of oligodendrocyte metabolic stress pathology began with the identification of anomalous gene transcript and transcript levels for the major myelin gene,

proteolipid protein 1 (*Plp1*) in mice developing a spontaneous demyelinating phenotype (Dautigny et al., 1986; Gardinier and Macklin, 1988; Ikenaka et al., 1988). These observations identified deficits and changes to the *Plp1* transcript and protein level, but did not address fully how these changes were affecting oligodendrocytes. Indeed, a complete knockout of *Plp1* resulted in no overt phenotype until mice were over one year of age, when the mutant mice would often die by postnatal day 30 (Raskind et al., 1991; Rosenbluth et al., 1996).

A more complete understanding of the phenotype came from work in the early to mid 1990s that identified protein trafficking and the unfolded protein response (UPR) as contributors to the oligodendrocyte phenotype (Gow et al., 1994a, b; Gow et al., 1998). Mutations in *Plp1*, or its smaller splice isoform *DM20*, will cause the protein to misfold as it is translated in the ER and will either be degraded or accumulate in the ER (Gow et al., 1992; Southwood et al., 2002). The location of the mutation in the *Plp1* gene contributes to the severity of the misfolding and cellular stress that in turn leads to more or less pronounced phenotypes in animals and in patients (Garbern, 2007; Gow and Lazzarini, 1996; Gow et al., 1998). This understanding of the primary etiology of dysmyelinating disease enabled alternate interpretation of oligodendrocyte involvements and particularly the importance of maintaining oligodendrocyte homeostasis (Southwood et al., 2016).

Unfolded Protein Response in Disease

Maintaining a balance between peptide synthesis, folding and degradation of damaged or misfolded proteins is important to all cell types. Depending on the metabolic demands of the cell, disruptions to these processes will negatively impact cellular health. Specifically, in this pathway, there is a need to monitor the higher order structure of peptides to prevent misfolding of peptides and enhance degradation of aberrant products (reviewed in Kaufman, 2002). This UPR maintains cellular health but sustained, long term activation of this pathway can have negative effects on cellular survival.

The UPR pathway evolved to protect cells from the toxic effects of excess misfolded proteins when those peptides utilize chaperones, ATP and metabolites at a rate significantly above the basal level (Gow and Wrabetz, 2009). It was originally identified in yeast where the dimerization of the IRE1 protein in the endoplasmic reticulum membrane led to splicing and activation of the *Hac1* mRNA and transcription of chaperone and proteins for degradation (Kohno et al., 1993). However, during evolution in multicellular organisms the UPR grew in complexity to include three major factors.

In mammals, one of the main arms of the UPR involves dimerization and autophosphorylation of the PERK protein (protein kinase RNA-like endoplasmic reticulum kinase) after binding to the ER lumen protein BiP (binding immunoglobin protein). When hydrophobic domains or cytosolic regions of proteins are exposed in the ER, BiP activates PERK, which then phosphorylates eIF2α (eukaryotic initiation factor 2) and removing eIF2α from the translation initiation complex and halting translation of some mRNAs. Next, ATF4 (activating transcription factor 4) is translated and allows for the transcription of a number of proteins involved with reinitiating translation and degrading the unfolded proteins by endoplasmic reticulum associated degradation (ERAD) (Southwood et al., 2016). One of the important targets of ATF4 is the CHOP protein (CCAAT-enhancer-binding protein homologous protein).

The CHOP protein was thought to be a pro-apoptotic protein as expression of nuclear CHOP often preceded apoptosis in cells undergoing the UPR (Maytin et al., 2001). Further investigation, though, revealed that CHOP in oligodendrocytes, Schwann cells and osteoclasts is not a pro-apoptotic protein, even when it is overexpressed as the dogma predicted (Gow and Wrabetz, 2009; Southwood et al., 2002). Increased expression of apoptotic markers, such as caspase-3, is more likely to result from a failure to establish homeostasis after activation of the UPR and an eventual depletion of cellular energy stores.

Due to their high level of metabolic activity during myelinogenesis, oligodendrocytes are reliant on the proper functioning of the UPR to maintain their synthetic activity. Overwhelming the

UPR through excess synthesis or the inability to remove toxic, misfolded proteins is the hallmark of two leukodystrophies; the mild Spastic Paraplegia Type 2 (SPG2) and Pelizaeus-Merzbacher Disease (PMD) (Gow et al., 1998).

Focusing on one type of protein disruption, several point mutations in the *PLP1* gene result in severe developmental and physical phenotypes and truncated lifespans in PMD patients and rodent models of the disease. One of these is the myelin synthesis deficient (*msd*) A242V mutation, with extensive hypomyelination and a life expectancy of 30 days for mice and from weeks to a decade for affected males (Gencic and Hudson, 1990). Numerous point mutations in *PLP1* have been described for PMD patients with varying degrees of severity depending on the mutation locations. The severity is defined by the ability of *PLP1* to correctly traffic appropriately to the cell surface of oligodendrocytes, or in *in vitro* systems to the cell surface of HeLa cells or COS7 fibroblasts (Gow et al., 1994a).

A similar degenerative phenotype in patients and animal models can be achieved through overexpression of the PLP1 protein when the *PLP1* gene is duplicated (Inoue et al., 1999; Readhead et al., 1994). Severe hypomyelination, developmental delay and premature death can all result from the *PLP1* duplications, a convergent phenotype with *PLP1* mutations. Molecularly the phenotypes are also conserved because mutant PLP1 protein will accumulate in the ER, and supra-normal transcription and translation of *PLP1* will also result in an ER buildup of PLP1 protein (Gow et al., 1998). The severity of the mutations and duplications is also a result of their constitutive expression during development because most myelination occurs post-natal in the first three weeks in mice or first 5-6 years in humans (Dautigny et al., 1986; Raskind et al., 1991).

Interestingly, not all mutations of *PLP1* produce severe disease, and some have manifested clinically as MS but subsequent genomic sequencing confirmed a PMD diagnosis (Warshawsky et al., 2005). The presentation of PMD as MS in addition to studies showing similar axonal and neuronal pathologies between the diseases. These observations lend weight to the idea that MS is not a primary immune disease and that oligodendrocyte dysfunction could be an

alternative etiology (Edgar et al., 2010; Gow et al., 1998; Trapp et al., 1998). This, along with evidence from Hans Lassman in Austria and John Prineas in Australia regarding UPR markers in oligodendrocytes of MS patients were encouraging ideas for the *OBiden* project (Ozawa et al., 1994; Prineas et al., 1984).

Multiple Sclerosis History and Model Development

Multiple Sclerosis is a demyelinating, neurodegenerative disease that typically manifests in patients during their early to mid 20s. Symptoms can be mild, including: transient numbness, slight loss of visual acuity to severe with limb paralysis, temporary blindness and gastrointestinal distress (Confavreux and Vukusic, 2006; Haussleiter et al., 2009; Polak et al., 2011; Rovaris et al., 2006). Originally, axonal and neuronal damage was widely noted in post-mortem examinations of the brains of MS patients in addition to immune cell infiltration that became the focus of MS investigation for much of the 20th century (reviewed in Adams and Kubik, 1952).

Accurate diagnosis, monitoring and treatment of MS remained elusive until the first animal model replicating some of the symptoms was established, experimental autoimmune encephalomyelitis (EAE) (Rivers et al., 1933; Vogel, 1951). The EAE model, in its original and improved iterations involved immunizing animals with a myelin peptide in an immunopotentiator adjuvant emulsion to trigger a peripheral immune response. This model led to increased research into the active, immune reactive lesions in MS and led to the development of one of the first, and arguably most effective treatments, interferon-beta (INF-β) (Jacobs et al., 1982). Additional interferons were contemplated and used in small clinical trials but were found to be ineffective or, as in the case of INF-γ, exacerbated the disease for many patients (Panitch, 1987).

Interferon-beta remained the standard of treatment for MS for decades and was evaluated in additional mouse models such as ethidium bromide injections into CNS white matter, lysolecithin CNS injections and cuprizone (copper chelator) feeding (Dousset et al., 1995; Franklin et al., 1993; Gao et al., 2000; Goldberg et al., 2015). These chemical models, depending on the

dose, effect oligodendrocytes and can cause demyelinating lesions at injections sites, or more widespread in the CNS. They were primarily used to evaluate the immune and glial responses to demyelination and mechanisms and effectiveness of treatments developed since INF-β. The treatments that were developed worked by eliminating B or T cells before they could mature, blocking immune cell exit from lymph nodes, or inhibiting antigen presentation from B to T cells. These therapies were developed and tested in murine models but in patients the therapies did not prevent disease progression and in some cases exacerbated disease course (Calabresi et al., 2014; Coles et al., 2004; Coles et al., 2008; Duddy and Palace, 2015; Giovannoni et al., 2014; Kappos et al., 2014).

For example, observations of MS lesions, and staining studies, identified cytotoxic CD4+ T-cells as a component of active MS lesions. Clinical trials on anti-CD4 cell therapies showed significant reductions in the amount of T-cells present in circulation and CSF, without a significant alteration of disease course (Oosten et al., 1997). Later results showed that this may have been due to the fact that even though CD4 or CD8+ T-cells react to myelin peptides, they do not directly cause neuronal damage (Reuter et al., 2015). Therefore, even a total elimination of these cell populations would not prevent continuing neural degeneration if the disease has a significant non-immune component.

As T-cell therapies proved disappointing in most MS cases, some attention shifted to the involvement of B-cell populations in the disease etiology. As the B-cells are responsible for antigen presentation to activate T-cells, as well as antibody production, it appeared that B-cells becoming reactive to CNS proteins could account for MS symptoms. This led to the targeting of proliferating B-cells with anti-CD20 antibody therapies to reduce the population and halt MS. The B-cell therapies were more effective than T-cell therapies at reducing the some of the clinical signs of MS, such as MR lesions and circulating immune cells, however they failed to prevent transitions from the milder RRMS to secondary progressive MS (SPMS) (Montalban et al., 2016). Although substantial effort has focused on identifying immune targets for treatment in MS, single

or combination therapies have failed to cure the disease or prevent progression in many patients. In addition, alterations or suppression of the immune system can have significant side effects including increased likelihood and severity of infection.

The increased understanding that the immune system is only part of the etiology of MS has led to a rediscovery of the axonal and neuronal phenotypes first identified in the 19th and early 20th centuries. Indeed, new MS treatments originally designed for immune suppression have been found to be beneficial because of effects on neurons within the CNS (Lublin et al., 2016). The notion that a primary CNS etiology for MS causes the pathology and patient decline independent of the well documented peripheral cytotoxic immune infiltration is one of the tenets leading to the development of our new mouse model.

This model, the *OBiden* mouse, was designed to recapitulate MS-like pathology by inducing primary dysfunction in oligodendrocytes and monitoring the secondary glial, neuronal and behavioral deficits. Rather than exogenous agents, the *OBiden* mouse relies on induction of the UPR in mature oligodendrocytes by inducing expression of the mutant *Plp1*^{msd} protein and metabolic stress and cell death in a subset of mature oligodendrocytes (Gow, 2011). A strength of this approach is that the mechanism of oligodendrocyte death is extensively characterized allowing focus to shift to the secondary effects of altering mature oligodendrocytes in adult mice (Gow et al., 1994b; Gow and Lazzarini, 1996; Gow et al., 1998; Gow and Wrabetz, 2009; Sharma and Gow, 2007; Southwood et al., 2002). Because MS commonly presents in adult life after myelination of most white matter tracts is complete this approximates the apparent timeline seen in MS patients.

Gray Matter Pathology

The white matter and oligodendrocyte etiologies may be a novel avenue of MS investigation, however, the mechanism must still result in gray matter damage that is key to MS pathophysiology. This is especially important for the progressive forms of disease whether it is

SPMS or primary progressive MS (PPMS). These are the more debilitating forms of MS, and as of yet there are no effective treatments in reducing the neurodegenerative progression in either subclass of MS.

Although the degeneration of gray matter is a well-established feature of MS, the mechanism and the development of efficacious treatments have proven elusive. Indeed, the nature and timeline of neurodegeneration in MS is difficult to determine with the limits of imaging techniques that are not always sufficiently sensitive to detect lesions and atrophy, and tests for cognitive performance have only recently become more widespread (Walker et al., 2016). This makes investigating the cognitive changes and underlying neuronal deterioration in the *OBiden* mouse especially important. For example, they could open up new avenues of research as well as identify some of the underlying degenerative changes that have been overlooked for years in MS.

Past and current work on axonal or neuronal degeneration is MS have been limited and focused on descriptive studies of pathology (reviewed in Kornek and Lassmann, 1999). However, how these pathologies develop, whether through axonal transport deficits, protein degradation or as a result of immune infiltrates, and their effect on neuronal function remains to be determined (Hampton et al., 2013; Huizinga et al., 2008; Lidster et al., 2013). Interestingly, more and more work has also identified connection deficits in the CNS through the use of electroencephalography (EEG) (Gschwind et al., 2016). These suggest interhemispheric communication disruptions likely as a result of changes to the action potentials of principal cells and changes to the action potential generating axon initial segment (AIS). Although EEG changes will not be investigated here, they provide additional insight into the distribution and type of pathology in MS, as well as novel ways by which the *OBiden* model can be investigated.

Axon Initial Segment in MS Pathology

A specific aspect of neuronal architecture that has not been extensively investigated in MS is the axon initial segment (AIS). The AIS is a region of the proximal axon with a highly structured organization where sodium and potassium channels are densely clustered along its length. This allows the AIS to generate action potentials because of the high conductance within its boundaries, for communication between neurons (Inda et al., 2006; Palay et al., 1968; Susuki and Rasband, 2008). In addition, the AIS is known to be extensively innervated with GABAergic synapses. The nature of these synapses, the density and distribution of channels and the length and location of the AIS relative to the soma all depend on the state of the pre-synaptic neuron (Evans et al., 2015; Inda et al., 2006; Kole and Stuart, 2012; Schafer et al., 2009; Szabadics et al., 2006). The interplay of the abundance and location of ion channels, especially the sodium channel variant $Na_v1.6$ and the potassium channel variants, $K_v7.2$ and $K_v7.3$, are critical to the rate and timing of action potential generation (Battefeld et al., 2014; Kole et al., 2008).

Because the AIS is highly regulated and structured, molecular changes to neurons within a cortical region and cell subtype should be readily detectable with antibody staining techniques, and broader changes to large areas should be evident with western blotting. For ICC, the pyramidal cells of layer 5 and 6 have distinct AIS usually beginning at the medial surface of the neuron and continuing for 15 – 30μm. In addition, they express unique markers such as the transcription factor COUP-TF interacting factor 2 (Ctip2), a negative regulator expressed primarily in post-mitotic pyramidal cells of the cortex and hippocampus (Chen et al., 2008). Together, these markers are useful tools for targeting specific cortical regions especially in human tissue where the cortical layers are less dense and well defined compared to mice. Changes to the AIS and gray matter regions in the *OBiden* mouse could yield valuable new insights in the etiology and progressive pathology in MS.

Applicability of the OBiden Mouse

With a potential for changing perspective on the etiology of MS, new insights into potential pathologies and their relevance to the disease are needed. The *OBiden* mouse could identify new pathogenic mechanisms in MS, and potentially other neurodegenerative diseases that involve the myelin producing oligodendrocytes. Through the use of induction of established oligodendrocyte stress pathways, in this case metabolic stress and the UPR, the *OBiden* model can more accurately recapitulate pathways that may be active within the CNS. This contrasts with models using exogenous toxins or proteins to generate toxic stresses in oligodendrocyte, or artificial induction of peripheral immunoreactivity that replicates just one aspect of MS. The *OBiden* mouse has the potential to model both the chronic and acute phases of MS, depending on the extent of oligodendrocyte metabolic stress. The acute phase can give insights into lesion development and spread, while the chronic stress, which is used in this project, serves to model the chronic, neurodegenerative phase of MS. Together, the development, characterization and analysis of the *OBiden* model, including potential new neurodegenerative consequences, allows for new perspectives and insight in MS and hopefully neuroscience generally.

Chapter 1 Results

In Chapter one, the genetic structure of the transgenes and their long term stability and activation were analyzed in the *OBiden* mice. Specifically, the genetics of how inducible metabolic stress is achieved through activation of the UPR by an endogenous oligodendrocyte protein. Because the inducible transgene eliminated the endogenous *Plp1* gene, a rescue transgene and its long term expression are also described. To analyze the mice, levels of myelin proteins were quantified instead of mRNA levels, because levels of *Plp1* mRNA from transgenic mice are consistently greater than the level of protein (Inoue et al., 1996).

In addition to the molecular analysis of the mice, a longitudinal *in vivo* electrophysiological evaluation of the *OBiden* animals was conducted. Using auditory brainstem responses (ABR) to

pure tone sounds of various frequencies and intensities two aspects of the *OBiden* mice were measured. First, the functional rescue of the inducible *Plp1* transgene knock out phenotype was analyzed for degeneration in the brainstem of aging mice. Because much of the pathway is myelinated, it allows for the determination of myelin disruptions locally, and can be used as a surrogate indicator of more global myelin disturbances.

Finally, it is critical to confirm that the oligodendrocytes in the CNS are undergoing metabolic stress and have activated the UPR pathway chronically. Downstream targets activated during cellular UPR have been previously characterized, and these markers were used to confirm that oligodendrocytes in the *OBiden* mice were undergoing UPR related stress compared to none in the controls. Critically, the presence of UPR markers in 12 month mice was important to demonstrate because it shows sustained activation of the UPR pathway in either established oligodendrocytes or in newly differentiated oligodendrocytes.

Chapter 2 Results

The *OBiden* model possesses the unique ability to create a relatively moderate level of cellular stress in oligodendrocytes, thereby not creating global demyelinating events and allowing the CNS to function but with a disrupted function. Behavioral and cognitive changes have been identified, not only in MS, but across neurodegenerative diseases (Koenig et al., 2014; Llufriu et al., 2014). Although for years the cognitive and behavioral impact of MS was either unknown or underreported, it is now recognized as an important factor in the disease and a sign of continued progression of MS even in the absence of physical decline.

To test for these changes in the *OBiden* mice, the animals were put through a battery of behavioral tests. These tests were to identify changes in working memory, spatial memory, fear conditioning, and the development of depression-like endophenotype in the mice. Changes to analogous cognitive pathways has been identified in MS patients (Koenig et al., 2014; Llufriu et al., 2014). Other animal models of MS, such as EAE, have difficultly performing behavioral tests

due to the physical paralysis that occurs as acute disease progresses in the mice. Because *OBiden* mice do not have overt sensorimotor deficits compared to Controls, this makes them well suited to the study of long term cognitive changes.

The analysis of the *OBiden* mice was conducted at three time points to test for which behaviors *OBiden* mice were abnormal in and when these deficits arose. Baseline testing began at 2 months of age immediately prior to the induction of metabolic stress followed by tests at 6 months of age (4 months of metabolic stress induction) and at 12 months of age (10 months of metabolic stress induction). The *OBiden* mice showed deficits in multiple paradigms, including working memory testing and the development of a depression-like endophenotype. Importantly, some behaviors remained unchanged, indicating that degeneration in the *OBiden* mice, at least through 12 months of age, is specific and not global. This specificity allows for the study of specific CNS regions.

Chapter 3 Results

The clinical evaluation of MS was significantly enhanced by the development of magnetic resonance (MR) imaging techniques adapted from physical chemistry and applied to patients to obtain *in vivo* images of the CNS (Scherzinger and Hendee, 1985; Young et al., 1981). MR techniques evolved by increasing magnet power, field strengths and coil sensitivities to give more detailed images of the CNS and allowed for more sophisticated scanning parameters to highlight functional and structural aspects of the CNS.

In this chapter, MR techniques are utilized to evaluate the *OBiden* mice *in vivo* to determine if degeneration can be detected *in vivo*, and if so where and when it arises. Two main series of scans were utilized; T1 and T2 weighted ^{1}H structural scans to differentiate white and gray matter and the CSF filled ventricles in the brain. One signature of degeneration noted in MS, and other neurodegenerative diseases, is expansion of the ventricles within the CNS (Nijeholt et al., 1988). In addition, volumetric changes to gray matter nuclei have been noted in MS, as well

as the more common feature of periventricular white matter lesions (Pardini et al., 2014; Seewann et al., 2009). Therefore, if the MR structural techniques were sensitive enough and degeneration significant enough in the *OBiden* mice, an analysis for multiple parameters could be undertaken.

MR techniques can also be used to assess more functional aspects of the CNS as well and one well adapted technique to many diseases is diffusion tensor imaging (DTI). This techniqued is based on the constriction or free flow of water molecules within the CNS, as is designed to highlight axonal bundles with parallel trajectories where more water molecules are confined to the axonal space and restricted in their movement (Llufriu et al., 2014). Because the *OBiden* model is a primary stress in the white matter of the animals, DTI was used to determine if there were changes to white matter fiber tracts or the less tightly bundled axons of gray matter.

Chapter 4 Results

In this chapter, the *OBiden* mice were directly compared to MS post-mortem tissue through the use of histological and immunocytochemical (ICC) techniques. This analysis was performed to identify details about the location and extent of pathology in the CNS and their similarities to MS patients. Histological techniques have an extensive history in many diseases because they were extensively used to stain and analyze tissue before the advent of antibody and molecular biology techniques. Therefore, they are often extremely well characterized in their methods and the types of pathology that can be detected.

The focus of the histological analysis was on the detection of white and gray matter lesions through the use of two stains, luxol fast blue (LFB) for myelin and Bielschowsky modified silver stain for axons (Snodgress et al., 1961; Yamamoto and Hirano, 1986). These stains have been shown to differentiate between intact and demyelinating areas, detect axonal spheroids as well as neurofibrillary tangles and are robust in terms of their effectiveness regardless of the preparation or state of the tissue. By comparing the stains between MS tissue and the *OBiden*

mice, the similarities, differences and effectiveness of these techniques on the mice can be analyzed.

In addition to the histological techniques, antibody staining to detect more specific secondary molecular changes in microglia, astrocytes and axons was utilized. The reaction of microglia and astrocytes to CNS stress, disease, dysfunction or degeneration has been widely repeated and is an important, albeit incompletely understood aspect of neurodegenerative diseases (Corbin et al., 1996; Fischer et al., 2013; Tang and Le, 2016). Nevertheless, as part of the analysis of the *OBiden* mice, the secondary reaction of these cells was important to analyze and confirm that we see secondary gliosis and where because the location of gliosis could elucidate CNS areas more susceptible to disease or more resilient to damage as the glial cells work to maintain homeostasis. Together with the histological analysis, this chapter looks into the broad CNS changes occurring in the *OBiden* animals.

Chapter 5 Results

The final chapter deals with the analysis of the secondary molecular neuronal changes in the *OBiden* mice as a result of primary oligodendrocyte stress, and again, their similarities or differences to MS tissue. To analyze the secondary neurodegeneration, a number of staining and molecular techniques were employed. These included western blots of tissue punches obtained from gray matter regions throughout the CNS, as well as staining and semi-quantitative analysis of fluorescence antibody staining. The goal was to detect regions of general neuronal dysfunction, then focus the analysis to a particular feature of interest that was altered in the *OBiden* mice compared to controls.

To begin the analysis, forms of the structural neurofilament (NF) proteins, heavy, medium and light chain, were blotted for in addition to a general marker for neurons, NeuN, and synapses, amyloid precursor protein (APP) (Elder et al., 1998b; Gusel'nikova and Korzhevskiy, 2015). Markers such as NeuN and APP should be reduced in areas of gross tissue loss and

neurodegeneration, while the NF proteins could build-up as has been noted in early degenerative disease processes, or dropout if there was a significant loss of neurons or processes in the gray matter (Jacomy et al., 1999; Lee et al., 1994). Changes seen in the *OBiden* mice allowed for more specific analysis in cortical and hippocampal areas that also correlated with deficits seen in earlier behavioral tests.

These changes focused on a section of the axon proximal to the cell body called the axon initial segment (AIS) where high densities of sodium and potassium channels are located to create an area of high conductance and low resistance across the membrane and maintain neuronal polarity. (Inda et al., 2006; Palay et al., 1968; Rasband, 2010; Song et al., 2009). The AIS is critical for the appropriate functioning of the CNS as action potential generation and transmission is the mechanism of long range communication in the CNS. Therefore, alterations to the timing, or threshold for action potential firing can have dramatic effects on CNS performance (Liska et al., 2015).

The analysis of the *OBiden* mice revealed alterations to AIS length and ion channel composition. Both have implications for connectivity and electrophysiological properties of the CNS that are the arena of future projects. However, the results are consistent with increasing evidence that the AIS is critical in neurodegenerative diseases but its link to MS is relatively unexplored making it an interesting area of study in the *OBiden* mouse.

CHAPTER 1 – GENERATION AND CHARACTERIZATION OF THE *OBIDEN* MOUSE

Introduction

The goal of much of this work is to understand the longitudinal consequences of chronic metabolic stress in oligodendrocytes and if, how and when it causes observable phenotypes in our mice. Specifically, we were trying to recapitulate the phenotype from the demyelinating, degenerative disease multiple sclerosis (MS), in response to recent failures in clinical trials of immune modulatory therapies as well as the fact that the current view of MS as a primary immune disease appears to be relatively untenable for the future (Kappos et al., 2014). The *OBiden* mouse is based off cumulative evidence on the similarities between the leukodystrophy, PMD and MS as well as the current lack of treatments to halt disease progression (Bauer et al., 2002; Gow et al., 1998). To determine if secondary neurodegeneration could be generated from a known primary insult to oligodendrocytes, and what phenotype that degeneration would take, the *OBiden* mouse was developed.

One of the most important aspects of the *OBiden* mouse is that it does not use an exogenous chemical, cocktail, protein or other method to infect the mouse or breakdown the blood brain barrier (BBB) or result from direct injection or ingestion of a toxin foreign to the animal (Gao et al., 2000; Shaw et al., 1962). These models create aspects of demyelinating and neuro-immune diseases, but do so at the cost of causing gross physical damage to the animals making behavioral or other testing unreliable, and more importantly they likely only represent a subset of the pathology seen in the actual disease. This has been borne out in a way because the vast majority of treatments for MS have been based on the suppressing the immune infiltration seen in some white matter lesions of patients, and the infiltration of immune cells into the CNS seen most dramatically in the EAE model. The treatments based off suppressing or modulating the immune system did result in treatments for patients that could suppress the frequency of relapses linked to active demyelinating lesions, but did not eliminate these lesions, nor did the treatments

mitigate the arguably more debilitating aspect of MS, namely the buildup of gray matter lesions and neurodegeneration (Calabresi et al., 2014; Feinstein et al., 2015; Giovannoni et al., 2014; Kappos et al., 2014).

This, in part, led to the idea behind the *OBiden* mouse, to develop a model primarily affecting oligodendrocytes in the CNS, rather than the peripheral immune system, and using an endogenous stressor rather than an injectable or chemical method to affect cells. In theory, we could acutely or chronically affect oligodendrocytes to create our primary disease trigger using the expression of mutant protein, an extremely well characterized cause of pathology in oligodendrocytes (Gow et al., 1998; Karim et al., 2007; Southwood et al., 2002). This method utilizes a disease cellular mechanism that is already known, eliminating the need to characterize the type of stress the oligodendrocytes would be undergoing and in addition takes advantage of the observation that the human disease resulting from mutant protein expression in oligodendrocytes can present with MS like symptoms and even respond to MS first line treatments (Southwood et al., 2013). The idea was to create a model that recapitulated MS phenotypes with little to no peripheral immune involvement to separate and identify different aspects of disease including what and how significant is the contribution from dysfunction in oligodendrocytes and could that be a primary etiology or major contributor to the disease process.

Material and Methods

Transgenes and Breeding

The *Plp1-i.msd* inducible transgene was created by taking the *Plp1*^{msd} gene and inserting an antisense *LoxP* flanked cassette containing the *PGKNeo* gene 3' to exon 7. The *Plp1-i.msd* transgene is homologously recombined onto the X-chromosome in place of endogenous *Plp1*, which means males will either be *Plp1-i.msd* $^{-/y}$ or *Plp1i.msd* $^{+/y}$ and females can be *Plp1-i.msd* $^{-/-}$ or *Plp1-i.msd* $^{+/-}$ or *Plp1-i.msd* $^{+/+}$. To differentiate we used 3 primers which give product sizes of 493bp for wildtype *Plp1* and 428bp for *Plp1-i.msd*: primer1 antisense –

TTTCCCACCAGAGACTACCGAG, primer 2 sense – GAGGTTGACACTTAGGGAAGTG, primer 3 antisense – GCAGCCTCTGTTCCACATACAC. To remove the suppressive antisense transcript and allow expression of *Plp1-i.msd* we used CreER^{T2} under control of the *Mbp* promoter, and to identify *Mcre*$^{+/-}$ mice we used 2 primers to give a product of 290bp: primer 1 sense – GAGTACGTGCTCGCTCGATGC, primer 2 antisense – CTCCCACCGTCAGTACGTGAGAT. The KI transgene results in the mice being functional *Plp1* knockout (*Plp1-ko*), and to rescue the *Plp1-KO* we inserted the *Plp1* overexpressor (*Plp1-OeX*) transgene #72 from Klaus Armine-Nave's group in the heterozygous state to generate normal Plp1 protein levels and *Plp1-OeX*$^{+/-}$ mice. For genotyping we used Nave's primer pair to get a 400bp product: primer 1 sense – CAGGTGTTGGAGTCTGATCTACACAAG, primer 2 sense – GCATAATACGACTCACTATAGGGATC. Male mice with all 3 transgenes, *Plp1-i.msd*$^{+/y}$*::Mcre*$^{+/-}$*::Plp1-OeX*$^{+/-}$*,* were the experimental *OBiden* mice and mice null for the Mcre transgene, *Plp1-i.msd* $^{+/y}$*::Mcre*$^{-/-}$*:: Plp1-OeX* $^{+/-}$*,* were used as Control mice. Female *Plp1-i.msd* $^{+/+}$*::Mcre*$^{+/-}$*::Plp1-OeX*$^{+/-}$ and *Plp1-i.msd* $^{+/+}$*::Mcre*$^{-/-}$*:: Plp1-OeX* $^{+/-}$ mice were used as breeders and bred with male *Plp1-i.msd* $^{+/y}$*::Mcre*$^{-/-}$*:: Plp1-OeX* $^{-/-}$ or *Plp1-i.msd* $^{+/y}$*::Mcre*$^{+/-}$*:: Plp1-OeX* $^{-/-}$ mice, respectively to generate experimental mice.

Metabolic Stress Induction

Control and *OBiden* litter mates (when possible) were weaned between postnatal day 19 and 21 from their parents and placed into new microisolator cages. 2-4 mice were housed per cage and allowed lab chow and water *ad libidum*. At postnatal day 60 (2 months of age) mice had their weights recorded and were given 175mg/kg of Tamoxifen dissolved in corn oil and made at 20mg/ml concentration. To dissolve the Tamoxifen, 100mg of powder was weighed and placed into a glass scintillation vial to which 5ml of corn oil was added. The mixture was vortexed then heated to 55^{c} and then vortexed every 30min until all the Tamoxifen crystals had dissolved. The mixture was cooled to room temperature then stored at 4^{c} for up to one month. The administration

of Tamoxifen was through oral gavage and a 22-gauge needle with rounded edge attached to a 1ml disposable syringe. Mice were divided randomly into two groups; one group was gavaged on Monday the other group on Friday of every week. Weights were recorded every week.

Tissue Collection and Western Blotting

Spinal cord tissue and cerebellum punches were harvested at the same time as punches for western blots and neurochemistry. Dissections were done on fresh tissue where mice were decapitated, the brain removed and sliced into 2mm coronal segments and then 1.5mm outer diameter punches taken from various brain regions including the cerebellum. The spinal cord was extracted through the "spinal cord flush" method by using an 18-gauge needle to push 1 X PBS through the spinal cord through the lumbar end after cutting at the level of the cauda equina. The spinal cord was then divided into cervical, thoracic and lumbar segments and frozen at -80^{C} along with pooled left and right cerebellum punches.

Before removing samples from the freezer, phosphorylation preservation buffer was made, consisting of: 50mM HEPES, 140mM potassium acetate, 4mM sodium acetate, 20mM sodium pyrophosphate, 20mM β–glycerol phosphate, 0.1mM PMSF, 0.1% protease inhibitor cocktail (Sigma-P8340), and 0.1% of phosphatase inhibitor cocktails 2 and 3 (Sigma-P5726 and P0044) made in distilled water (referred to as P-buff). 50μl of P-buff was added to each protein punch on ice, and the samples were sonicated with 3 pulse trains 5min apart, and each train consisted of 5, 1sec pulses followed by a 2sec break. Samples were kept on ice and only removed for the 15sec sonication step. Protein concentration was determined using the Thermo Scientific Micro Bicinchoninic Acid (BCA) assay kit as per the manufacturer's instructions.

Samples were diluted in P-buff to 2x the required concentration, then mixed 1:1 in general sample buffer (1g SDS, .5f sucrose, 0.98 Tris-HCL, 25ml distilled H_2O and pH to 6.8 with bromophenol blue) to equal concentrations for each sample. Samples were vortexed 3 times for 5sec each, then heated at 60^{c} for 5min and then spun down for 3sec. 8, 10 or 12%, 1.5mm thick,

SDS-PAGE gels were made in house and cast for 10 or 15 well combs and samples were loaded and run at 25mA per gel with water circulated cooling. PVDF membranes were cut to size and equilibrated in transfer buffer containing 20% methanol for at least 1 hour prior to transfer. Gels were stacked onto membranes and transferred, with cooling, at 500mA for 1 hour.

Immunocytochemistry

Mice were anesthetized with 375mg/kg of a 2.5X dose of 2-2-2 tribromoethanol (TBE) made in 2-methyl-2-butanol at 40X and diluted in 1X PBS with vortexing to the working concentration. The thoracic cavity was opened on the mice and a catheter was inserted into the left ventricle while a small cut was made in the right atrium. Next, 4% paraformaldehyde (PFA) dissolved in 0.1M Phosphate Buffer pH 7.2 was allowed to flow through the catheter by means of gravity for 15min until the mouse was rigged and fixed. Brains were dissected by removing the skull from the body, removing the lower mandible and making a vertical cut through the hard palate. Next, the ventral skull was broken away until the optic chiasm was revealed and the optic nerves were cut rostral to the optic chiasm followed by an incision along the midline of the skull moving rostral from the forman magnum to the olfactory bulbs. The skull was then removed, the brain extracted and tissue of interest placed in 12.5% sucrose in1X PBS for 6-8 hours followed by placing the tissue in 25% sucrose overnight. Finally, tissue was placed in tissue molds, covered with OCT embedding media and frozen by slowly submerging in dry-ice cooled 2-methyl butane.

Frozen tissue sections were cut between -18^{o}C and -20^{o}C and attached to Fisher Superfrost Slides and immediately stored in a slide box on dry ice. Slides were maintained at -20^{o}C until use, at which time they were thawed in three, 10min washes of 1x Phosphate Buffer Saline (PBS) pH 7.5. Following washes, one of four permeabolization/blocking steps were used to remove lipids and create holes in the membranes for a more thorough and consistent infiltration by primary antibodies.

Methanol – Thawed slides were placed in methanol (MeOH) at either -20°C or at room temperature for 20min. Subsequently, the slides were washed in 1X PBS three times for 10min each and then Liquid Blocker Pap Pen was applied in a circle around the tissue approximately 0.5cm from the tissue. Sections were then blocked in 1x Tris Buffered Saline with 0.5% Glycine and 1% Bovine Albumin (TBSGBA) with 2% Goat Serum (2%Gts) for 30min while rocking followed by removal of the blocking solution and addition of primary antibodies in fresh TBSGBA-2%Gts and setup to rock overnight at room temperature.

Triton X-100 – Thawed slides were placed in a solution made of 1xPBS and 0.3% Triton X-100 for 30min. Slides were then washed three times for 10min each in 1xPBS and then Pap Pen was applied around the tissue sections and TBSGBA-2%Gts was added to block the sections while rocking for 30min. The old TBSGBA-2%Gts was removed and primary antibodies in fresh TBSGBA-2%Gts were added to sections to rock overnight at room temperature.

Phosphate Buffer/Goat Serum/Triton X-100 – Pap pen is applied around tissue that has been thawed in 1xPBS. The permeabolization and blocking steps are combined into one step by adding a solution of: 0.1M Phosphate Buffer, 0.3% Triton X-100, and 10% Goat Serum (PBTGS) for one hour while the slides are horizontal and not rocking. For the addition of primary antibodies, the old PBTGS is removed and antibodies are diluted in fresh PBTGS and added to sections. The sections must be maintained horizontal and cannot rock as rocking will cause the high Triton X-100 content to dissolve the Pap pen and potentially allowing the solution to leak off the tissue sections (Ho et al., 2014).

Primary Antibodies – Primary antibodies are diluted in either TBSGBA-2%Gts or PBTGS, depending on the blocking solution, and up to three antibodies are diluted in one solution. 100-150μl of diluted antibodies is placed on each tissue section and for TBSGBA-2%Gts the sections are rocked overnight, but for PBTGS staining the slides are left in the damp chamber on the bench top overnight as rocking can cause the Triton to remove the pap pen and allow antibody run off

from the sections. Sections from control and experimental animals were also taken for no primary controls to test the non-specific secondary staining, and in these cases the tissue received only blocking solution with no antibodies for overnight incubation. After staining, slides are washed three times for 5-10min in 1x PBS.

Secondary Antibodies – Isotype specific antibodies were used against primary antibodies, and all secondary antibodies are diluted at 1:1000 in TBSGBA-2%Gts. The most common fluorophores conjugated to secondary antibodies are Alexa488 (green), Alexa568 (red) and Alexa647 (infrared), as well as the addition of DAPI at 1:1000 to all secondary antibody mixes. Secondary antibodies were added to sections for 3 hours, with rocking, then washed in 1x PBS, 3 times for 5-10mintes each. Following washes, the pap pen was removed with a Q-tip dipped in chloroform, and then a drop of Vectashield to prolong fluorescence was added to each slide before the addition of the coverslips. Coverslips were allowed to settle overnight on the slides while at 4^{C} before excess Vectashield was vacuumed off and coverslips sealed to the slides with nail polish. Slides were stored at 4^{C} to prolong fluorescence before image acquisition.

Results

Transgenes and Protein Expression in the OBiden Colony

The concept of the transgenes in the *OBiden* mouse was published in 2011 highlighting the main components used to create longitudinal, inducible stress in oligodendrocytes and have been reproduced in Figure 1.1 (Gow, 2011). The first is the *Plp1-i.msd* construct that was homologously recombined into the locus for endogenous *Plp1* on the X-chromosome, thereby replacing *Plp1* with a silenced copy of $Plp1^{msd}$ harboring the severe myelin synthesis deficit (*msd*) mutation. The silencing element is a PGKneo cassette in intron 7 of *Plp1-i.msd* and is flanked by LoxP sites in the same orientation to facilitate excision of the PGKneo cassette upon exposure to Cre recombinase. The next transgene is the $CreER^{T2}$ transgene under control of the myelin basic protein (MBP) promoter, making it specific to myelinating, and not premyelinating,

Figure 1.1 – Transgenes in the *OBiden* Mouse

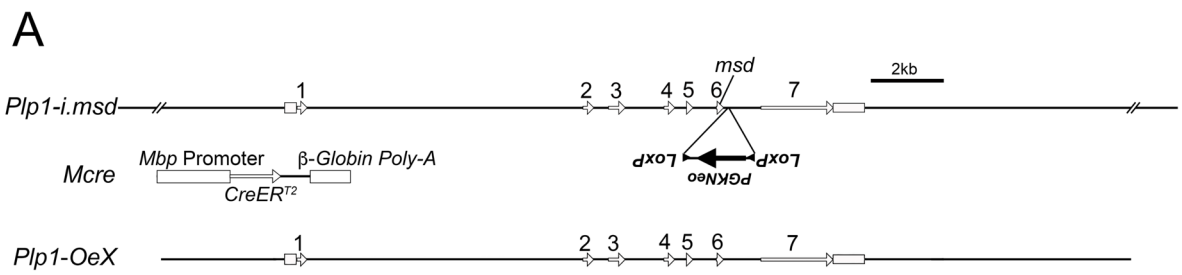

Figure 1.1– **A**) Schematic of the transgenes in the *OBiden* mice. Top is the knock-in inducible allele of *Plp1-i.msd* that upon expression causes metabolic stress in oligodendrocytes. The middle transgene is *Mbp* promoter/enhancer driven $CreER^{T2}$ that can excise antisense *PGKNeo* cassette in the top transgene. The bottom transgene is a 20kb genomic fragment of *Plp1* from Klaus Armin-Nave's transgenic #66 line to compensate for *Plp1-i.msd* suppressing normal *Plp1* expression.

Figure 1.2 – Protein Characterization of End Stage Myelin

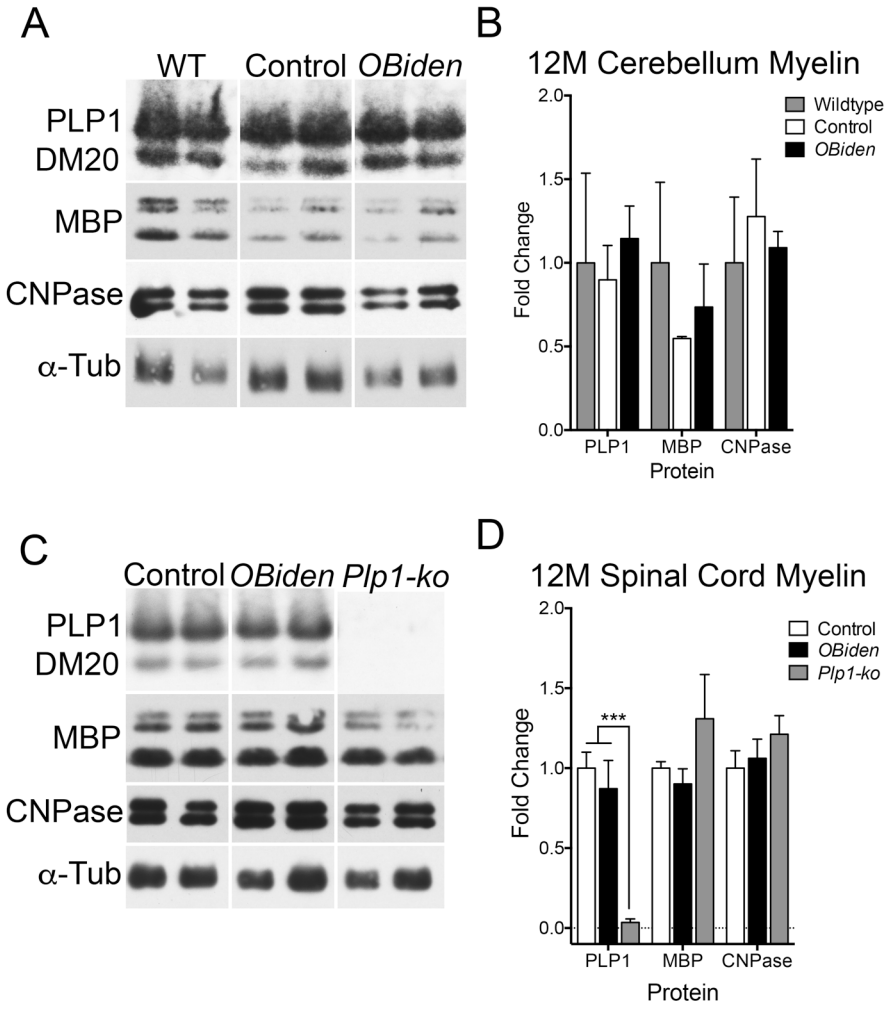

Figure 1.2 – **A**) Representative western blots from *OBiden* cerebellum at 12 months of age. Included are blots from wildtype (WT) non-gavaged animals and control, gavaged, mice. **B**) No significant differences were found in the levels of the major myelin proteins PLP1, MBP or CNPase at 12 months of age (2-way ANOVA). **C**) Representative western blots from *OBiden* spinal cord to analyze myelin protein expression in control, *OBiden* and *Plp1-ko* mice. **D**) Quantification of blots from **C**, that show a significant loss of PLP1 in *Plp1-ko* mice as expected. No changes to MBP or CNPase were seen at 12 months (n = 4 per group for each group).

oligodendrocytes. The Cre protein is expressed in oligodendrocytes but bound to HSP90 and only released upon the administration of the estrogen receptor agonist, Tamoxifen. These transgenes allow for induction of metabolic stress in oligodendrocytes, but the *Plp1-i.msd* construct creates a functional *Plp1-ko* mouse by suppressing *Plp1* translation through double stranded RNA mediated repression of the gene. To alleviate this feature, as *Plp1-ko* mice are known to undergo age related degeneration, we added a third transgene to compensate for the loss of *Plp1* gene expression. This transgene was a *Plp1* overexpressor (*Plp1-OeX*) line #72 originally developed by Klaus Armine-Nave and

Carol Readhead that in the homozygous state leads to overexpression of the Plp1 protein at 150-170% of wildtype levels (Readhead et al., 1994). We bred in the transgene to a heterozygous state to reduce its level of Plp1 production, but still maintain a level of Plp1 indistinguishable from wildtype mice (Figure 1.2). The addition of the *Plp1-OeX* transgene was critical to removing any potential phenotype from the *Plp1-i.msd* transgene as it causes the mice to become functional *Plp1-ko*s when bred to homozygosity. At 12 months of age (12M), control and *OBiden* mice had comparable levels of the three major myelin proteins, PLP1, MBP and CNPase, compared to wildtype (WT) mice in punches obtained from the cerebellum of aged mice (Figure 1.2 A,B). There was increased variability across samples from the cerebellum, potentially due to the heterogeneity of the tissue and the location of the punches. Additionally, we compared control and *OBiden* mice to functional *Plp1-ko* mice, that did not contain the rescue *Plp1-OeX* transgene, to confirm two processes. First, that the *Plp1-i.msd* transgene did indeed suppress endogenous Plp1 expression even at 12 months of age and second, that the *Plp1-OeX* transgene restored expression in experimental animals and that Plp1 expression was maintained through end stage at 12 months (Figure 1.2 C,D). In *Plp1-ko* mice it would have been optimal to test for expression of $Plp1^{msd}$ protein to confirm expression when the Cre protein is released upon administration of tamoxifen. However, the mutant Plp1 protein has a high level of toxicity and can cause cell death

Figure 1.3 – Longitudinal Auditory Brainstem Analysis in the *OBiden* Mouse

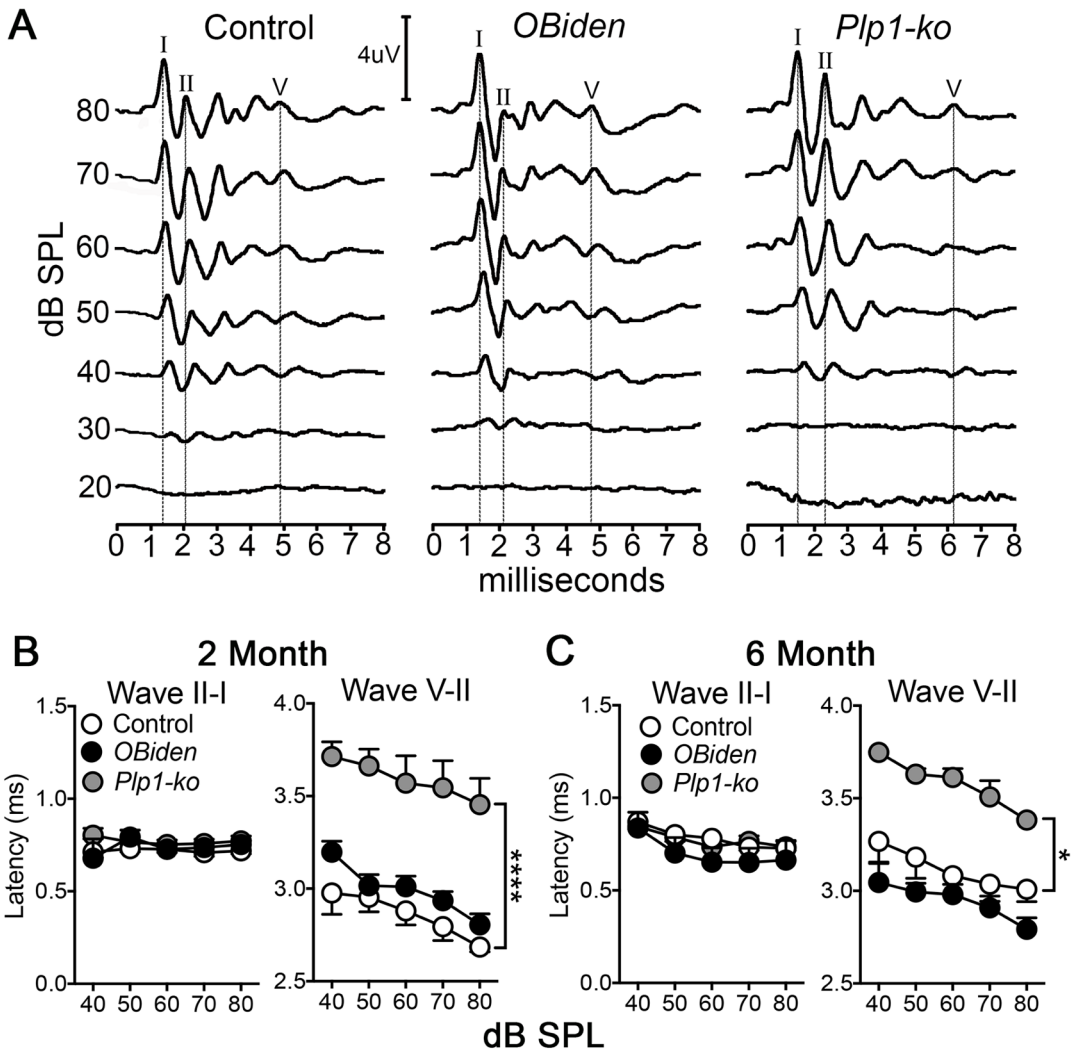

Figure 1.2 – **A**) Representative ABR traces from 2 month old animals. Peaks used for analysis are indicated as Wave I for cochlea, Wave II for cochlear nucleus and Wave V for medial lemniscus. **B**) Quantification of peripheral conduction velocity (Wave II-I) and central conduction (Wave V-II) in 2 month old animals in Control, *OBiden* and *Plp1-ko* animals (n = 3, 6, 6) that show a slowed central conduction only in *Plp1-ko* mice. **C**) Quantification of conduction velocities shows slowing only in the central component in *Plp1-ko* animals (n = 5, 4, 2)

Table 1.1 – Auditory Brainstem Response 2-way ANOVA Main Effects

2 Month 32kHz ABR

Wave II-I

ANOVA table	SS	DF	MS	F (DFn, DFd)	P value
Interaction	0.04035	8	0.005043	F (8, 70) = 0.6308	P = 0.7492
dB SPL	0.01161	4	0.002903	F (4, 70) = 0.3631	P = 0.8341
Gneotype	0.03748	2	0.01874	F (2, 70) = 2.344	P = 0.1034
Residual	0.5597	70	0.007995		

Wave V-II

ANOVA table	SS	DF	MS	F (DFn, DFd)	P value
Interaction	0.04546	8	0.005683	F (8, 40) = 0.7957	P = 0.6096
dB SPL	0.6807	4	0.1702	F (4, 40) = 23.83	P < 0.0001
Genotype	5.876	2	2.938	F (2, 10) = 22.08	P = 0.0002
Residual	0.2857	40	0.007141		

6 Month 32kHz ABR

Wave II-I

ANOVA table	SS	DF	MS	F (DFn, DFd)	P value
Interaction	0.0176	8	0.0022	F (8, 42) = 0.1213	P = 0.9981
dB SPL	0.1287	4	0.03218	F (4, 42) = 1.775	P = 0.1518
Genotype	0.0852	2	0.0426	F (2, 42) = 2.350	P = 0.1078
Residual	0.7614	42	0.01813		

Wave V-II

ANOVA table	SS	DF	MS	F (DFn, DFd)	P value
Interaction	0.04465	8	0.005582	F (8, 50) = 0.1597	P = 0.9951
dB SPL	0.4999	4	0.125	F (4, 50) = 3.575	P = 0.0122
Genotype	2.923	2	1.461	F (2, 50) = 41.80	P < 0.0001
Residual	1.748	50	0.03496		

Table 1.2 – Auditory Brainstem Response Post-hoc *t*-tests

	2M Wave II-I		2M Wave V-II		6M Wave II-I		6M Wave V-II	
Tukey's multiple comparisons test	**Summary**	**Adjusted P Value**	**Summary**	**Adjusted P Value**	**Summary**	**Adjusted P Value**	**Summary**	**Adjusted P Value**
40 dB SPL								
Control vs. *OBiden*	ns	0.7984	ns	0.204	ns	0.9379	ns	0.2217
Control vs. *Plp-ko*	ns	0.2245	****	< 0.0001	ns	0.975	*	0.0127
OBiden vs. *Plp-ko*	*	0.0469	***	0.0001	ns	0.9977	***	0.0002
50 dB SPL								
Control vs. *OBiden*	ns	0.4751	ns	0.8756	ns	0.5201	ns	0.231
Control vs. *Plp-ko*	ns	0.7863	****	< 0.0001	ns	0.9924	*	0.0165
OBiden vs. *Plp-ko*	ns	0.8556	****	< 0.0001	ns	0.7299	***	0.0004
60 dB SPL								
Control vs. *OBiden*	ns	> 0.9999	ns	0.5663	ns	0.2998	ns	0.6167
Control vs. *Plp-ko*	ns	0.878	****	< 0.0001	ns	0.9124	**	0.003
OBiden vs. *Plp-ko*	ns	0.8635	****	< 0.0001	ns	0.7484	***	0.0004
70 dB SPL								
Control vs. *OBiden*	ns	0.8736	ns	0.5178	ns	0.5967	ns	0.4699
Control vs. *Plp-ko*	ns	0.6351	****	< 0.0001	ns	0.9592	**	0.009
OBiden vs. *Plp-ko*	ns	0.9007	****	< 0.0001	ns	0.5735	***	0.0008
80 dB SPL								
Control vs. *OBiden*	ns	0.8019	ns	0.6154	ns	0.7414	ns	0.1229
Control vs. *Plp-ko*	ns	0.5868	****	< 0.0001	ns	0.9972	*	0.046
OBiden vs. *Plp-ko*	ns	0.9269	****	< 0.0001	ns	0.8044	***	0.0009

within hours of induction of expression as seen in cell culture and constitutive expression of *Plp1*^{msd} in mutant mice (Gow et al., 1998).

Auditory Brainstem Analysis of OBiden Mice

After confirming the *OBiden* mice maintained normal expression levels of major myelin proteins throughout the experiment, they were tested for electrophysiological function in the auditory brainstem to confirm the function of the nervous system was not disrupted. This involved testing the auditory brainstem response (ABR) that measures the compound action potential (CAP) firing through different brainstem nuclei as a result of stimulation through sounds of various frequencies and intensities (Shah and Salamy, 1980). The ABRs have a characteristic waveform after presentation and recording through sub-dermal electrodes, namely five peaks that occur at specific timeframes after presentation (Figure 1.3.A). Three representative waveforms from control, *OBiden,* and *Plp1-ko* are shown in Fig.1.3.A, with three peaks used for analysis highlighted in each genotype. Wave I is the initial firing of the spiral ganglia in response to stimulation from the cochlea, followed by Wave II at the cochlear nucleus that are the first set of neurons with the CNS as opposed to the PNS. The latency difference between Wave I and Wave II (i.e. Wave II-I) is the temporal component of the peripheral nervous system as signals travel on PNS myelinated nerves and there should be no difference in latency between any group of animal at any ages as we are not affecting the PNS myelin. At 2 month and 6 months of age, there is no difference between any genotype in the latency from Wave II-I, indicating that there is no developmental or developing deficit in peripheral signal transduction (Figure 1.3.B,C). Next, the CNS component of the ABR was analyzed, represented by the difference in latency between Wave II and Wave V, where Wave V is likely an ascending CAP from the brainstem to the inferior colliculus (Wenngren and Anniko, 1988). Represented by Wave V-II, in Fig. 1.3.B,C the control mice have decreasing latencies as the sound intensity increase from 40 to 80 dB SPL at both 2 and 6 months. The *Plp1-ko* mice show a significant increase in latency at all intensities at 2 and 6 months indicating a slowing of CAP processing through the auditory brainstem as a result of

knocking out *Plp1*. As this phenotype could be present in other CNS areas, it was important to rescue the phenotype through the use of the *Plp1-OeX* transgene to complete the *OBiden* mouse genetics. As it restored protein levels as seen in Fig. 1.2, the transgene also restored conduction velocity to the *OBiden* mice, where no difference is seen in Wave V-II latency at 2 months before tamoxifen gavage and activation of metabolic stress, and even at 6 months, with 4 months of weekly gavaging, the conduction velocity remained unchanged compared to controls (Figure 1.3.B,C). This indicated that not only does the *Plp1-OeX* transgene rescue PLP1 protein levels, but that it functionally rescues a gross conduction velocity deficit even after the beginning of gavage. Also, this shows that at least through the first 4 months of gavage (from 2 to 6 months of age) no significant degenerative consequences occur between 2 and 6 months of age, indicating relatively mild or no pathology at least in relation to the brainstem area.

Metabolic Stress in Aged OBiden Mice

The hypothesis and principle of the *OBiden* colony rests on the induction of primary metabolic stress chronically throughout the lifespan of the animals. As the central tenet of the model, it was necessary to identify the expression of metabolic stress markers in oligodendrocytes of aged, gavaged mice to confirm the expression of metabolic stress markers and the continued efficacy of the main *Plp1-i.msd* transgene.

Frozen coronal sections from 12 month mice at the level of the optic chiasm/optic tract were used to stain for mature oligodendrocytes with the marker CC-1 and one of the transcription factors activated during metabolic stress and the UPR, activating transcription factor 3 (ATF3). This staining procedure has been used by our lab to identify stressed oligodendrocytes in white matter tracts in the CNS (Gow et al., 1998; Southwood et al., 2016). In the optic tracts of mice, there was no difference in the total number of CC-1+ cells between control or *OBiden* mice indicating that if we are stressing oligodendrocytes and causing cell death, precursors are still adequately repopulating the mature cells, or the stressed oligodendrocytes have not undergone cell death yet (Figure 1.4A-C) (Mann-Whitney t-test, $p<.99$). However, there was significant

Figure 1.4 – Metabolic Stress in Oligodendrocytes of the *OBiden* Mouse

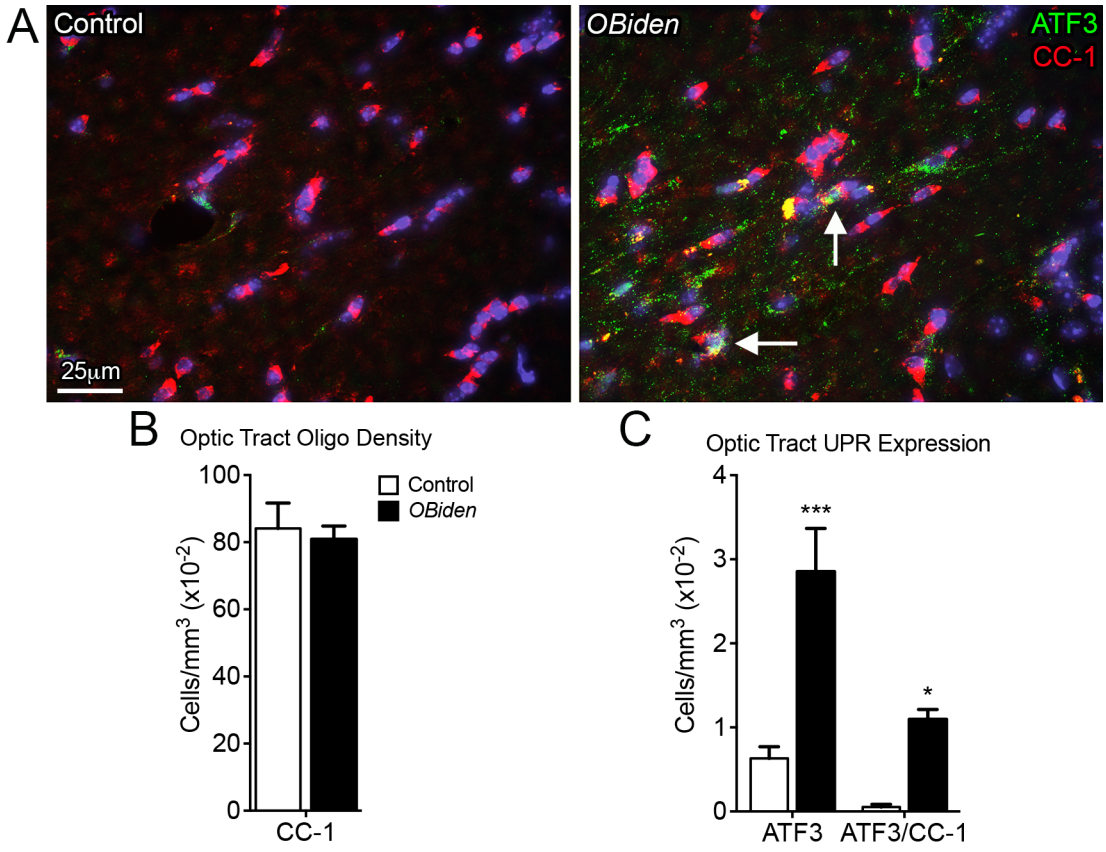

Figure 1.4 – **A**) Representative staining images from optic tract of 12 month old control and *OBiden* animals showing all mature oligodendrocytes (CC-1; red) and nuclear ATF3 staining in cells undergoing metabolic stress (green; arrows). **B**) There was no difference in oligodendrocyte density in the optic tract between control and *OBiden*. **C**) There was a significant increase in the number of ATF3+ cells and ATF3+/CC-1+ double positive cells in the *OBiden* animals compared to controls (n = 4 animals per group and 3 slides per animal)

Table 1.3 – White Matter Oligodendrocytes Metabolic Stress Statistics

Staining for Total Oligodendrocytes

Mann Whitney test

P value	> 0.9999
P value summary	ns
One- or two-tailed P value?	Two-tailed

Staining for ATF3 Expression in Oligodendrocytes

ANOVA table	SS	DF	MS	F (DFn, DFd)	P value
Interaction	1.389	1	1.389	F (1, 6) = 7.462	P = 0.0341
Marker	5.461	1	5.461	F (1, 6) = 29.34	P = 0.0016
Genotype	10.66	1	10.66	F (1, 6) = 26.25	P = 0.0022
Subjects (matching)	2.437	6	0.4062	F (6, 6) = 2.183	P = 0.1824
Residual	1.117	6	0.1861		

Sidak's multiple t-tests

Staining	Summary	Adjusted P Value
ATF3	***	0.0002
ATF3/CC-1	*	0.0374

increase in the total number of ATF3+ cells in the optic tract as well as a significant increase in the number of ATF3+/CC-1+ double positive oligodendrocytes (Figure 1.4C) (2-way ANOVA, $F(1,6)=29.4$, $p=.002$). This shows the *OBiden* mice continue to shows signs of metabolic stress in oligodendrocytes even after multiple months of gavage and multiple rounds of stress activation in white matter tracts throughout the CNS.

Discussion

The development of the *OBiden* mouse represents a change in direction from the historical and previously utilized models of the neurodegenerative disease, MS. While most of the research has been focused on the response, adaptation and suppression of the adaptive immune system to artificial stimulation or stress to the CNS, the *OBiden* model utilizes more biologically relevant pathology to attempt to recapitulate the disease. To achieve that goal, the necessary transgenes to induce metabolic stress in mature oligodendrocytes were inserted or recombined into the experimental mice. As will all transgenes, it was necessary to test the function and stability of the transgene to confirm that any future phenotypes we identified were not due to aberrant expression or lack of expression of critical proteins as well as the gross function of representative portions of the CNS.

The analysis of the *OBiden* mice confirmed that the recombination even to insert the *Plp1-i.msd* transgene did suppress *Plp1* expression and that the addition of the *Plp1-OeX* did restore normal levels of PLP1 protein, critically, without leading to an overexpression phenotype, the results of which are known to be degenerative. Additionally, chronic metabolic stress in mature oligodendrocytes is created through induction of the *Plp1-i.msd* transgene as given by the expression of ATF3 in oligodendrocytes out to the end point of 12 months of age. Unlike other models that create substantial, acute attacks or stresses on the CNS that might replicate some features of an acute MS attack, the *OBiden* model represents are the more chronic phases of the

disease. These phases are potentially times when subclinical damage is accumulating within the CNS that triggers, or is exacerbated by an acute immune or degenerative event.

The ATF3 analysis focused on 12 month old animals to confirm the long term maintenance of metabolic stress in oligodendrocytes. It is known that under nominal physiological conditions, CHOP and ATF3 will not be expressed in oligodendrocytes (Gow et al., 1998). Identification of UPR markers in aged animals likely indicates that metabolic stress in present at younger ages. Because of the chronic, long-term model utilized the focus was on an end stage analysis rather than earlier time points. A future analysis at 2 months of age baseline would be appropriate to confirm the lack of metabolic stress prior to activation of the transgenes.

Another facet of the *OBiden* model of interest was the integrity of the information processing pathway in the auditory brainstem. This pathway represents a mixture of small and large myelinated fibers, and conduction changes or block would manifest as alterations to the timing of different waves (Denninger et al., 2015; Maheras and Gow, 2013). In addition, the ABRs highlight a critical point in the importance of maintaining proper PLP1 levels until we initiate metabolic stress. The analysis was not carried past 6 months due to the fact that as mice age, their hearing thresholds increase making reliable ABR analysis difficult without prohibitively large numbers of mice to screen for those that maintain hearing levels.

The *Plp1-ko* mice do not express detectable levels of PLP1 protein, and although they display no overt signs of degeneration, at 2 months there is already an alteration to their ABRs seen in the delayed Wave V. This would make them dubious subjects for behavioral or neurochemical studies as this information processing would also occur in other myelinated tracts and result in potentially significant changes compared to mice expressing normal levels of PLP1 and confound any additional pathology. As the *OBiden* mice displayed normal levels of PLP1 and show no ABR processing deficits, they are suitable for further behavioral and degenerative studies where any detectable pathology should be solely due to the metabolic stress in myelinating oligodendrocytes.

CHAPTER 2 – *IN VIVO* BEHAVIORAL CHARACTERIZATION OF THE *OBIDEN* MOUSE

Introduction

The use of animal models for neurological diseases is critical to gain insight into degenerative conditions that are difficult that study and test in human populations. Through the years, it has become critical to be able to evaluate animal models *in vivo* for behavioral deficits in parallel to those seen in patients, to allow for analysis of how the deficits arise and how best they may be mitigated. This has led to the development, and refinement, of a number of behavioral testing paradigms for animal models of disease to allow researchers to better evaluate their models and their relevance to human pathophysiology.

This is especially true in MS research, where much of the research has focused on the massive immune infiltration that occurs within white matter lesions, to the exclusion of what is now understood to be extensive gray matter pathology (Bjartmar and Trapp, 2003; Hasselmann et al., 2016; Hemmer et al., 2015; Pryce et al., 2005). This means that there is relatively limited behavioral testing data from current MS models, in part due to different focus, but also because many of the models undergo significant, debilitating physical degeneration which makes behavioral testing nearly impossible. Evidence from early work on MS through the mid 20th century, and recent mounting evidence regarding the cognitive symptoms patients find most debilitating as the disease progresses, leaves a significant opening to develop a model that recapitulates the cognitive changes seen in MS and evaluate their underlying pathology (Adams and Kubik, 1952; Llufriu et al., 2014).

The extent of behavioral testing is limited mostly by what can be attributed to specific neuroanatomical pathways associated with conditions, or those tests that we known to react to treatments that are efficacious in patients (Acharjee et al., 2013; Can et al., 2012; Chen et al., 2015; Kitamura et al., 2015; Pardini et al., 2014). This includes testing for depression-like endophenotypes, spatial memory, novel object memory, recognition memory and anxiety related

phenotypes are some of the behaviors that can be tested, and those can be subdivided further depending on the level of specificity required (Eagle et al., 2015; Morellini et al., 2010; Porsolt et al., 1977).

Materials and Methods

Tail Suspension

For the apparatus, two retort were placed 45cm apart with bar held between them 40cm above the desktop. Behind the stand 20cm distant was a dark green curtain (mouse cage cover) was spread out to create and even background for the camera and to create a consistent, static view for the mice. A camera was placed 90cm away from the stands, with its line of sight perpendicular to the bar between the retort stands. Before beginning the test, a cylindrical piece of thin plastic was cut that measured 1cm long by 0.5cm and this was placed over the tail of the mice, resting at the base of the tail to prevent them from climbing up their tail during the test. Finally, a piece of tape 10-15cm long was measured and cut to attach the mouse to the horizontal bar. For the test, the mouse was removed from its home cage, the plastic cylinder was placed over its tail, then the last 0.5cm of the mouse tail was bound with tape and the free end of the tape was wrapped over the bar between retort stands so that the mouse was in the middle of the camera's FOV with legs facing the camera. A timer was started and the mouse was allowed to hang, with video recording, for 6min, at which point the video was stopped first, the mouse removed from between the stand and the tape cut gently from the tail. For the analysis, all 6min of the videos were analyzed at 2x speed and the time immobile was quantified as times when there was no movement form the mouse, only small paw motions, or swinging from the base of the tail without torso bending. Any attempts at climbing, running like behavior, and torso twisting were considered "escape-like" behaviors and were counted as movement. An independent, blinded rater was utilized to confirm the original immobility times and scoring criteria.

Learned helplessness forced swim test

Forced swim was performed over two days, the first was a training/acclimation day to overcome the novelty and shock of the test and the second day was used to assay for the helplessness behavior as quantified by immobility time, similar to the original testing paradigm (Porsolt et al., 1977). The test container was a 4-liter glass beaker, filled to 3 liters so the water depth would be 16cm and the surface of the water was 10cm from the top of the beaker so the mice cannot touch the bottom nor escape the container. Water temperature was 24-26^{C} for each mouse, and 4 mice could be run between changing or adjusting the water temperature. On day 1, mice were gently scruffed, still allowing most movement but the inability to turn and reach the handler, then gently placed tail first into the water to prevent the mice from sinking below the surface. Mice were video recorded for 10min in the water and then removed to a clean cage containing no bedding, and instead a blue absorbent pad was in the cage and the cage was on a heating pad turned to high to maintain a warm, dry environment for the mice to recover before returning to their home cage. On day 2, the mice were again placed in the water and recorded but only for 6min, after which they were removed to the dry heated cage. The first 6min of day 1 and the full 6min of day 2 were analyzed at 2x video speed for floating only or small, one rear leg only kicks as the sign of immobility.

Inverted Screen

This was a modified version of Kondziela's Inverted Screen test (Deacon, 2013). A 40cm x 40cm x 10cm deep frame was made out of 2in x1in wood planks, and a 19-gauge wire screen composed of 1.2cm x 1.2cm squares was attached to one side across the opening of the wooden square. This creates an area to place the mice so they are enclosed by the wooden frame while on the wire grid. On the outside of the grid we painted lines to designate areas 5 squares x 5 squares (6cm x 6cm) for use in movement counting. For the test, a large, deep (40cm) plastic bin was lined with soft blue pads as a cushion if the mice fall. A mouse was placed in the center of the screen, and then the screen was rotated over 2-5sec so as not to jolt the mouse and give it a

chance to cling to the wire screen as it was inverted. If a mouse fell off immediately after inversion it was given a second chance at the test, two immediately falls in a row were counted as a score of 0. Once inverted, the test lasted for a maximum of 2min, and if the mouse fell before the 2min end point the time was recorded. In addition, the painted grid was used to asses for movement while inverted where the number of times both front paws crossed a painted line was counted to give a movement score. Each mouse was run once a week before gavage and the time and movement scores were recorded. To calculate cumulative scores, the time score was converted to a 1-10 scale: 1=1-10sec, 2=11-20sec, 3=21-30sec, etc. up to 9=81-90sec and 10=91-120sec, and this gave us a maximum score of 10. With initial testing we found that the maximum number of lines a mouse would cross in 2min was ~30 lines, so we divided all movement scores by 3 which converted them to an approximate 1-10 scale to match the time scores. This means the mice could achieve a cumulative score from 0-20. Since each mouse was being tested weekly we had running scores for each mouse from which we could calculate mean and median scores per mouse and at each age from the 8-week start point until the 52-week end point. We found the median score better reflected the overall performance of the mice as mean was susceptible to weighting due to extreme scores outside the typical performance of the mice, so each mouse had its weekly score normalized to its overall median score. This normalization meant each mouse score should fluctuate around 1, and allowed us to identify weeks when the score deviated from one. We looked for deficits in the mice defined by a score of 1 on one week followed by a score >.33 (3x reduction in the score), and then a return to a score of approximately 1 following the dip. This gave us a characteristic signature, "V" shaped on graphs, which we looked for across all mice and quantified the number of deficits in each genotype compared to the number of total weeks analyzed across all mice.

Win-Shift T-Maze

The T-maze apparatus was custom made to the size of mice following published protocols for T-maze design (Deacon and Rawlins, 2006). The T-maze was made of clear plastic to allow

for the alteration of color or pattern on the walls of the floor to guide the mouse in correct arm identification. Each arm of the maze was 30cm long x 10cm wide x 20cm high so the mouse could not see the surrounding environment, and the maze was small enough where no large open spaces were present for the mice to avoid. At the end of the start arm, a 7cm long divider was placed between the 2 goal arms, this allows for more directed decisions by the mice and does not allow them to observe both arms simultaneously, as is the case without the divider. Finally, guillotine doors were placed at the entrance to each goal arm so the arm could be closed off from the rest of the maze. For training and testing, the walls and floor of each goal arm were made unique, in our experiments one goal arm had a horizontal stripe pattern and the other goal arm had large 3cm circles to create a polka dot pattern. Both patterns were equilibrated for overall gray intensity so neither pattern caused a darker environment than the other pattern, which could influence mouse arm choice. An additional cue was the floors of the goal arms which were covered in 29cm x 9.8cm bench coat paper with either the smooth or rough side of the paper facing up to differentiate the texture of the floors. To enhance the drive for the mice to leave the start arm, there was a spotlight 40cm above the mice focused on the area where mice where initially placed, and the goal arms of the T-maze were covered to create a darker environment. The T-maze procedure was run over 3 days, the first was used as a training day to acclimate the mice to the maze and to learn the paradigm. In the first trial of each day, the right goal arm was closed off and a piece of food from the home cage was placed at the end of the left arm as incentive, and the mice were placed in the start arm then allowed 2min to enter the left goal arm. After entering the arm, the guillotine door was closed and the mouse was allowed 30sec to explore before being removed and placed back in its home cage. The T-maze was not cleaned between trials of a single mouse, but the floor was changed and the maze cleaned with water than 70% ethanol between mice. On the following trial, both arms were open for the mouse, but the food incentive had moved to the right arm. Again, the mouse was given 2min to explore and if it chose and arm the guillotine door for that arm was closed and the mouse confined for 30sec in the arm

before moving back to its home cage. 9 more trials were repeated on the training day and for each trial the food incentive was in the opposite arm compared to the previous trial. The arm chosen and time to completion was recorded for each mouse. On days 2 and 3, the initial trial was the same where only the left arm was open for the mouse, and on all subsequent trials both arms were open and the food incentive moved to the previously unoccupied arm. Again, choices and time to completion were recorded for each trial and the percent correct alterations (i.e. the mouse correctly followed the food and changed arms) was calculated for day 2 and day 3, then the average across both days was used in analysis.

Novel Object

Novel object testing was performed in a 61cm x 61cm black Plexiglas box with floor. No cues were used inside the box, but external cues including the camera mount and holder and walls of the room were visible to the mouse. However, the box was placed in the middle of the room with equivalent lighting direction and intensity (~100 lux) to avoid biases and give a consistent arena. Novel object consisted of 3 trials over 1 day, the first trial was a training trial to acclimate the mice to the arena and remove novelty by allowing 10min of free exploration, which was video recorded for future analysis if needed. The maze was cleaned with water than 70% ethanol following every trial. There was then a 30min break between trials, and before the second trial two identical objects (round plastic ramekins, 8cm in diameter, 4cm high, with ridges along the outside and a 20-30g stainless steel bolt glued inside the ramekin to hold it down) were placed opposite to each other in the corners of the arena 8-10cm from the walls. The mouse was placed in the middle of the arena, not facing any object and allowed 10min to explore while being video recorded. After the trial, the mouse was moved back to its home cage and the arena and objects were cleaned with water than 70% ethanol. After another 30min break, the final trial began with one object from the previous training trial (familiar object) and a new object (glass star-shaped candle holder, 7.5cm in diameter, 2.5cm tall, called novel object) placed in the same locations as the previous trial so one corner has a novel object, one corner has a familiar object. The mouse

is placed in the middle of the arena facing the same way as the second trial and allowed to explore for 5min while being video recorded. For analysis, we used Ethovision XT Ver. 8.5 (courtesy of Dr. Shane Perrine, Dept. of Psychiatry and Behavioral Neurosciences), which allowed us to define the entire maze, the quadrants of the maze, and areas around the object for automated quantitation. The area around the objects was defined as a circle, encompassing the object that had a diameter 2.5x greater than the object (this was an area large enough for an entire mouse body so we can track either nose point or center point for analysis). The mice were tracked with a center and nose point tracking, and nose point was used for the majority of analysis to track time around objects and time in different quadrants, where center point was used for velocity and distance measures as center point has less tendency to undergo quick changes that could influence velocity and distance measures. To quantify the novel object preference, we used a metric called the exploratory preference index;

$$\text{(EPI)}= \left(\frac{Time\ at\ Novel\ Object}{Total\ time\ at\ Objects} * 100\right)$$

and substituted Object 1 or 2 for Novel Object in the numerator for Trial 2 analysis to determine if there was a preference between similar objects.

Spatial Memory

Spatial memory was run in the same in the same box as novel object, however, we had a clear Plexiglas insert with patterns attached to it so the smooth side of the Plexiglas faced the mouse and the patterns were between the two layers of Plexiglas. This allowed us to add patterns to the walls of the spatial memory chamber that are critical as reference points for the mouse when determining locations within a distinct environment. Spatial memory was run with the same timing as novel object, with a similar paradigm. It was a one-day test, trial 1 was a 10min training trial in the empty arena then a 30min break, trial 2 was 10min and had two identical objects placed in opposite corners of the maze followed by a 30min break, and trial 3 was 5min and one of the objects moved positions to a new corner of the maze. Between each trial the maze and objects

were cleaned with water followed by 70% ethanol. All trials were video recorded for analysis with Ethovision, with the same parameters as novel object with quadrants, and areas around the object defined for analysis.

Barnes Maze

An opaque, white, circular platform 36in in diameter, with 2in holes driller around the circumference and each hole is centered 3in from the edge of the platform. Under one hole an escape-goal box was placed that measured 4in x 4in x 2in deep with a fine wire mesh ramp for the mice to use to enter the box. Mice were first trained to identify the goal box as an escape by placing the mice inside the goal hole, then near the goal hole so they would enter the box voluntarily. Barnes maze testing lasted for a total of 11 days, with 3 x 5min trials per day per mouse, with the following days: days 1-5 were training days for the mouse to learn the location of the goal hole and to enter the goal hole in the minimum time with the minimum number of errors. Day 6 was a 90^{o} rotation probe day where the platform was rotated 90^{o} clockwise, and the mouse run as before where it should return to the location it was trained to on days 1-5. Day 7 was a retraining day with the maze in its original orientation, and day 8 was the curtain probe day where a curtain was hung around the entire circumference of the maze to block the visual cues that the mouse was using to find the goal box before to test if there was any intrinsic property to the maze that allowed the mice to locate the goal hole. On day 9, mice were retrained the same as on days 1-5 and day 7. Day 10 was a change where the goal hole was moved 180^{o} from its original location and the mouse was trained to find the new location, this day was meant to test how well the mice could learn a new location and day 11 was a probe day to see if the mice remembered the 180^{o} change defined by the latency it too the mice to reach the new goal hole location. Latency to reach the correct goal hole was recorded each trial, as were the number of errors the mouse made, defined by poking part or all of its head or body through and incorrect hole. All trials were also video recorded from directly above for subsequent analysis if necessary.

Rotorod

A Med Associates Rotorod was used for testing with an acceleration set to maximum giving a ramp speed from 4-40 RPM over a course of 5min (300sec). The first day of rotorod analysis consisted of a training day to teach the mice to walk and maintain balance on the rotorod and to avoid falling off the bar. As an aversion, a water/ice mixture was placed below each mouse where they would land if they fell off the bar. The rotorod was turned to the slowest speed and the mice placed on the bar until the walked for approximately 30sec at 4 RPM. Mice that gave up immediately or jumped off landed in the ice bath and were placed back on the bar up to 5 times or until they walked continuously on the bar. On the subsequent testing day(s), the rotorod is started on the non-accelerating lowest speed so all mice are facing forward and walking at speed. Then the rotorod is switched to acceleration and as it increases speed the time the mouse falls off the bar is recorded and the mouse is removed back to its home cage. If the mouse holds on to the bar and rotates one full cycle then continues walking, the time of the spin is noted but the mouse is allowed to continue, this is also true if the mouse completes two spins but continues to walk. However, if the mouse completes 3 or more spins at once the time is noted and is counted as a fall and the mouse is finished, even if it recovers after numerous spins as this is considered a sign of inability to accurately balance and walk in the test. Three trials over 300sec are run per day and the average across all three trials is reported as the time for that day.

Fear Conditioning

Fear conditioning was run in an 18cm x 18cm x 30cm arena with alterable walls, overhead recording camera and floor within an insulated, sound deadening chamber (Coulbourn Instruments Habitest System; Holliston, MA). Testing consisted of a training day with 5 shock trials separated by 100sec of rest and the following parameters were used for the trials and following shock; multi-Hz, 80 dB-SPL hiss tone for 20sec, then 2sec of a 0.4-0.6 mA foot shock. For the extinction days the following paradigm was used; 20sec hiss tone followed by 40sec of recovery, repeated 10 times per day for 12 days. The entire box was cleaned with 70% ethanol

between mice and 10% bleach between training and extinction days while being allowed to air dry overnight to remove contaminating odors. To analyze the extinction days, each 20sec hiss period was broken in 5 x 4sec bins and averaged together, while the 40sec recovery period was broken in 4 x 10sec bins and averaged. (Freezeframe 3, Coulbourn Instruments). Contextual freezing was the percentage of time spent immobile during the first 20sec exposure to the arena on the day following fear training. Tone freezing was the average freezing across a day for trials 2-9 (trials 1 and 10 were excluded to obtain a consistent average not including initial sound/box stress from trial 1 or long term acclimation form trial 10).

Results

Physical Deficit Testing

To investigate the *OBiden* mice, cohorts of male mice were tested longitudinally beginning at 2 months of age prior to the first round of metabolic stress induction, then at 6 and 12 months of age after moderate and long term exposure to chronic metabolic stress. The behavioral testing was used to identify if and when phenotypic degeneration could be detected in the mice and its similarity to MS deficits. To this end, the mice were tested for deficits in 3 broadly defined functional groups, physical, emotional and cognitive. For the physical testing the inverted screen test was used in large due to the ease of setting up and running the test and the ability to run the test weekly to allow for increased temporal resolution of phenotypes. Because the inverted screen test uses both movement and grip while inverted to assess motor function, it should either reveal subtle deficits in one attribute or a more pronounced phenotype if both processes fail (Deacon, 2013). The testing for changes to emotion-like pathways in the mice was more complex and subtle as surrogate markers and tests must be used to assess the animals apparent state. In this light, well defined and pharmacologically validated tests were used to asses for an underreported symptom in MS, namely the development of a depression-like endophenotype (Can et al., 2012; Porsolt et al., 1977). Finally, one of the most complex pathways and behaviors in the CNS was

Figure 2.1 - Longitudinal Inverted Screen Testing in the *OBiden* Mouse

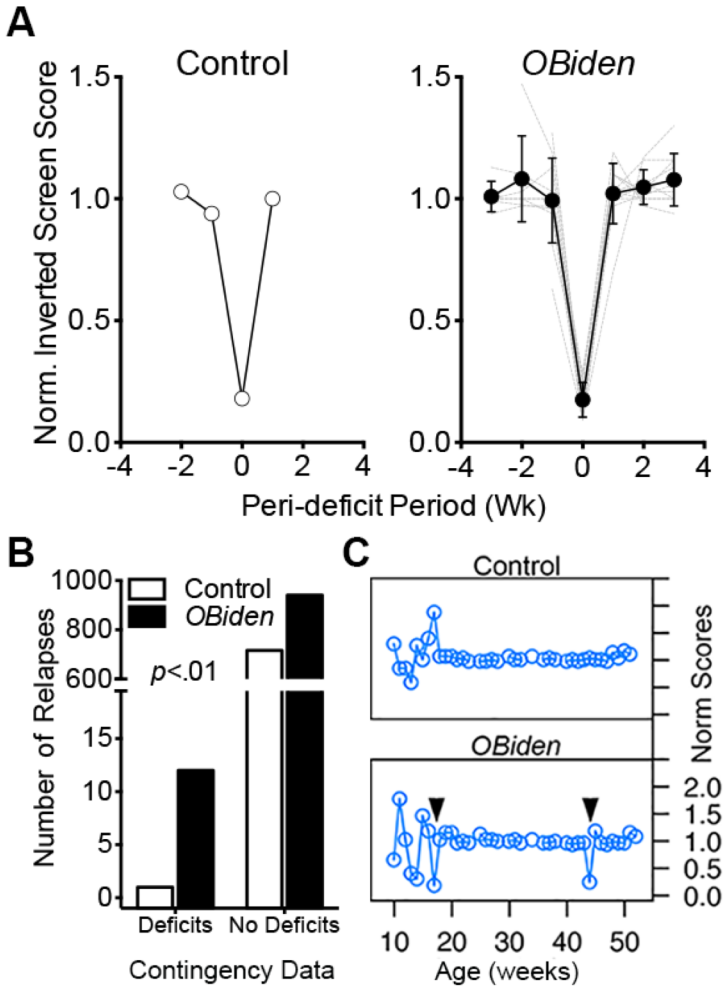

Figure 2.1 – **A**) All examples of 3-fold drop in mean score followed by recovery from control and *OBiden* mice, with the average and SEM plotted as black line over individual gray traces for *OBiden* mice. **B**) Number of weeks with a relapse (drop) and number of weeks without a drop shows a significant increase in the number of deficit weeks in *OBiden* animals compared to controls. **C**) Representative plots from individual mice with arrowheads indicating the weeks of deficit in the *OBiden* animal.

tested, one that is particularly detrimental to MS patients in later stages of the disease, changes to cognition, learning and memory (Kitamura et al., 2015; Llufriu et al., 2014; Pardini et al., 2014). With the complexity of the system, multiple tests are needed to parse out individual functional units to provide a view of exactly where the deficit in the animals might be developing. For this we used a series of tests; spatial memory and Barnes maze for spatial learning and memory, novel object and Win-Shift T-Maze for novel discrimination memory and fear conditioning for negative stimulus and amygdala associated memory (Brown et al., 2000; Chung et al., 2015; Deacon and Rawlins, 2006; Henderson, 1968; Shimai, 1982; Shipton et al., 2014; Şık et al., 2003).

The results for the inverted screen testing of physical ability changes in the mice revealed an interesting, transient phenotype remarkably similar to MS. In MS, patients will often experience transient paralysis or loss of feeling in a limb, or loss of visions only to see the function recover to near-normal levels given enough time. For MS patients they are scored on a scale called the extended disability scoring system (EDSS) where these lesions that develop can appear as an increase in the EDSS (increasing scores represent increasing disability) followed by a recovery. In the mice, our scoring system is inverted where a high score is best and low score is worse, however, we identified the same pattern as seen in MS patients, namely consistent weeks of normalized scores followed by a drop-off for one week, then a subsequent recovery (Figure 2.1A,C). These deficit weeks were observed once across all control animals, but multiple *OBiden* animals at multiple ages displayed the deficit phenotype, indicating the increase is unlikely to be due solely to age, but more to the degenerative nature of the model (Figure 2.1B). In addition, the inverted screen test benefited from our ability to compare a single mouse throughout its experimental lifetime, increasing our power to detect changes and mirroring MS patients as closely as possible.

Depression-Like Endophenotype in OBiden Mice

Next, testing involved running cohorts of mice at key ages to determine if they developed emotional disturbances similar to those reported in MS. The cohorts of mice at each age point

Figure 2.2 - Development of Depression-Like Endophenotype

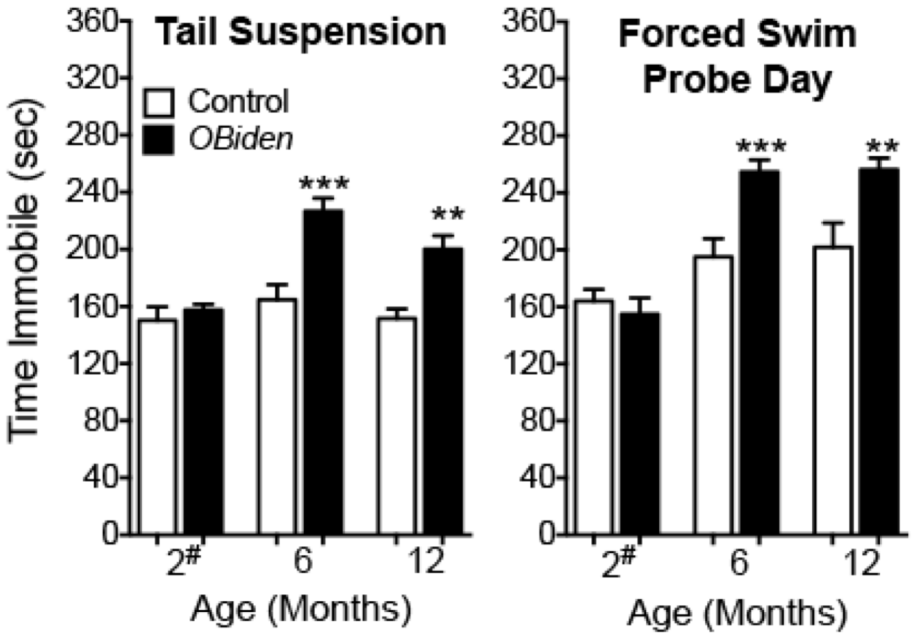

Figure 2.2 – **A**) Tail suspension testing revealed an increased immobility in *OBiden* mice at 6 months maintained through 12 months of age. Controls did not show an increase in immobility across time showing the immobility increase is not age related (# - prior to initial Tamoxifen induction). **B**) Forced swim testing showed a concurrent increase in immobility at 6 months, similar to tail suspension, that was maintained out through 12 months of age.

Table 2.1 - 2-way ANOVA Analysis of Tail Suspension and Forced Swim Tests

Tail Suspension

ANOVA table	SS	DF	MS	F (DFn, DFd)	P value
Interaction	8507	2	4254	F (2, 56) = 5.195	P = 0.0085
Age	19116	2	9558	F (2, 56) = 11.67	P < 0.0001
Genotype	23507	1	23507	F (1, 56) = 28.71	P < 0.0001
Residual	45858	56	818.9		

t-tests	Control - OBiden	Summary	Adjusted P Value
	2#	ns	0.9179
	6	****	< 0.0001
	12	**	0.0021

Forced Swim

ANOVA table	SS	DF	MS	F (DFn, DFd)	P value
Interaction	14384	2	7192	F (2, 52) = 5.935	P = 0.0048
Age	59847	2	29923	F (2, 52) = 24.69	P < 0.0001
Genotype	17621	1	17621	F (1, 52) = 14.54	P = 0.0004
Residual	63010	52	1212		

t-tests	Control - OBiden	Summary	Adjusted P Value
	2#	ns	0.9131
	6	**	0.0015
	12	**	0.0039

Depression-Like Endophenotype Animal Numbers

Tail Suspension (n)	2	6	12
Control	12	10	8
OBiden	12	10	10

Force Swim (n)	2	6	12
Control	10	9	9
OBiden	10	10	10

were different, since tests involving stress to the animals cannot be repeated longitudinally, however, each cohort did undergo both the tail suspension and forced swim test at the same age to minimize the number of animals and for consistency across tests. The *OBiden* mice showed no difference from control animals at baseline testing, prior to gavage, at 2 months of age in either test (Figure 2.2A,B). Therefore, the transgenes in the mice do not effect development or cause a disruption to behavioral processing before the onset of oligodendrocyte metabolic stress. When the tests were run again on a cohort of mice at 6 months of age (i.e. after 4 months of weekly gavage) there was a significant increase in the immobility of the *OBiden* mice compared to controls in both tests (Figure 2.2, Table 2.1). This deficit was maintained out through 12 months of age, indicating the development and maintenance of a depression-like endophenotype in the *OBiden* mice not seen in control animals. An additional comparison was run on the Forced Swim data because the test is run over two days. The forced swim test is also a measure of learned helplessness, a measure of how quickly mice will become immobile when exposed to the same scenario on multiple occasions (Porsolt et al., 1977). To test this, the time the mice spent immobile on Day 1 was also quantified and compared to the Day 2 immobility time within genotypes (Supp. Figure 2.1)(Supp. Table 2.1). Using upaired t-tests between groups, there was a significant increase in immobility on Day 2 in the *OBiden* mice at 6 and 12 months of age (Supp. Figure 2.2). No group at 2 months, prior to gavage, showed a difference and Control mice at 6 and 12 months of age did not show a difference. Together, this shows that only the *OBiden* mice after the induction of metabolic stress are susceptible to learned helplessness, whereas Control mice are not. This is the first indication that there are degenerative changes within the CNS of *OBiden* mice as a result of the oligodendrocyte metabolic stress. However, as depression in humans and the endophenotype in mice can be the result of pathology to numerous pathways or nuclei, further testing was performed to identify specific areas of degeneration.

Recognition and Novel Object Memory Deficits

Arguably one of the most debilitating features of MS, and a pathological feature of many neurodegenerative diseases, is the loss or dysfunction of memory components as the disease progresses. These are often untreatable, irreversible deficits that represent a major burden and intense area of research focus. Therefore, the *OBiden* mice were run through a battery of memory and cognition related tasks to isolate and identify specific areas of deficits. The first set of tasks involved the correct identification and investigation of novel areas or novel objects within the environment of the mouse. This memory pathway primarily involves reciprocal connections between entorhinal and perirhinal cortices and the dorsal hippocampus, so deficits in the testing will indicate specific areas to investigate for pathology.

To begin, the mice were tested using a 1-day novel object paradigm to evaluate their short term working memory and cognition. Initially, the mice are allowed to explore a 61cm X 61cm open field arena for 10min to acclimate themselves to the environment. 30min after the acclimation trial mice were placed back in the box with 2 identical objects for the training trial (Figure 2.3A, Top). Following another 30min interval, the mice were placed back in the box with one object (O-1) replaced with a novel object (N.O.) but one familiar object (O-2) remaining (Figure 2.3A Bottom). For the analysis, total time around both objects was used to create a ratio (preference index) from 0-100, in the case of training trials a score of 0-49 represents a preference for O-1, and 51-100 represents a preference for O-2. There is no difference between control and *OBiden* animals at any age in their preference for O-1 or O-2 indicating the similar objects are indeed similar and the mice will explore them no matter their placement in the arena (Figure 2.3B). When a familiar object was replaced with a novel object, there was no difference in the preference for the novel object between control and *OBiden* mice at 2 or 6 months of age and an example trace is shown in the supplement (Supp. Figure 2.2). However, at 12 months of age there was a significant decrease in the *OBiden* mice preference for the novel object, indicating a likely inability

Figure 2.3 – Longitudinal Novel Object Recognition Testing

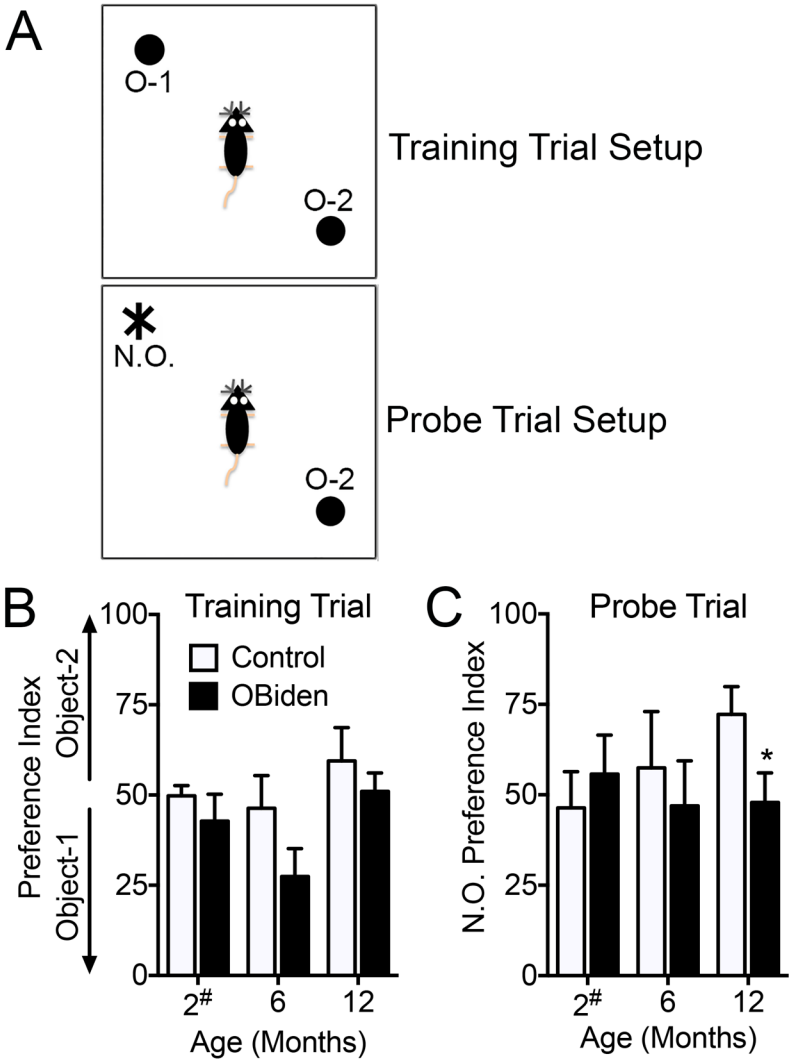

Figure 2.3 – **A**) Schematic of Novel Object training (top) and probe (bottom) trials showing the switch from two identical objects (O-1 and O-2) to a familiar and novel object (N.O. and O-2). **B**) Training trial identical object preference showed no differences at any age point between Control and *OBiden* animals. **C**) On probe day testing there was a significant impairment in the *OBiden* ability to identify the novel object only at 12 months of age (Control and *OBiden* n by age – 2 months = 6, 10; 6 months = 7, 8; 12 months = 8, 9).

Figure 2.4 – Longitudinal Recognition Memory Win-Shift T-Maze Testing

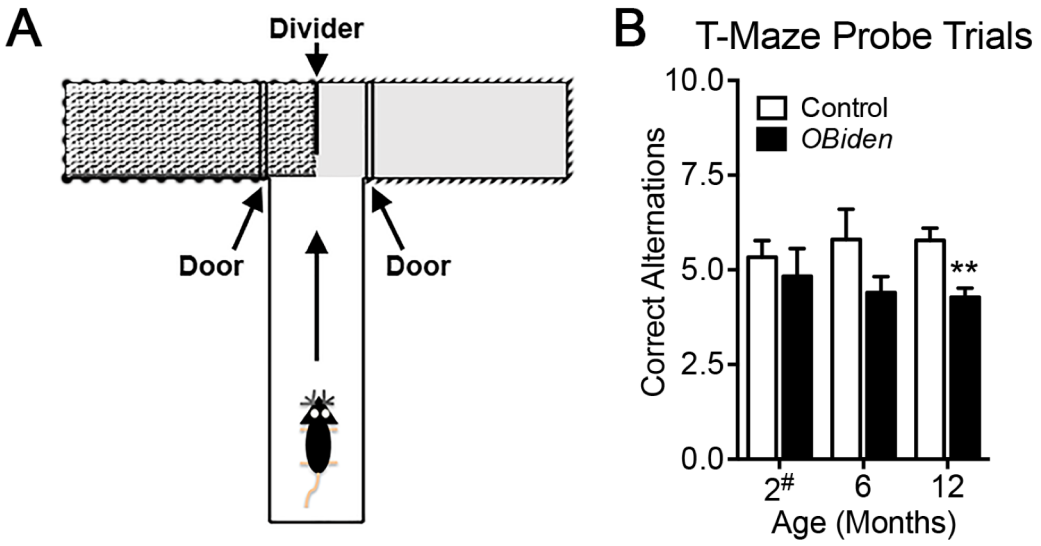

Figure 2.4 – **A**) Schematic diagram of the T-Maze chamber with the start arm for the mouse and two goal arms with guillotine doors, with difference floor textures and wall patterns. **B**) Correct alterations across ages of control and *OBiden* mice showing no differences at 2 or 6 months of age but a significant decrease in performance in *OBiden* mice at 12 months of age compared to controls (Control and *OBiden* n at 2, 6 and 12 months; 2 months = 3, 3; 6 months = 5, 10; 12 months = 9, 9)

Table 2.2 – Longitudinal Recognition Memory Testing Statistics

Novel Object

Age	Significance	P value	*t* ratio	df
2#		0.571	0.579829	14
6		0.602	0.533923	13
12	*	0.048	2.15381	15

Win-Shift T-Maze

2#		0.588	0.588348	4
6		0.109	1.72028	13
12	**	0.002	3.73526	16

to recognize the novel object as novel and a likely deficit in the recognition memory processing pathway (Figure 2.3C).

To confirm the memory deficits seen in novel object testing, an additional test was run to examine the ability of the mice in a foraging-like situation, where they will respond to food cues and enter the most-novel arms of a T-maze on subsequent trials (Figure 2.4A)(Deacon and Rawlins, 2006). After training the mice to alternate arm entrances from one arm to the arm they previously did not enter, and testing their performance at multiple ages, there was a significant deficit in performance of the *OBiden* mice only at 12 months of age, similar to the novel object testing deficit (Figure 2.4B). This indicates a loss of function of the circuits involved with tracking the location of the alternating food rewarding and correctly following the pattern. Although more complex than the novel object testing, both tests rely heavily on an entorhinal cortex to dorsal hippocampus connection that appears to be compromised in the *OBiden* mice.

Stability of Spatial Memory Processing in OBiden Mice

Memory pathways can be subdivided into discreet processing pathways, the recognition/novel object pathway discussed above, and pathways for the identification and location of the animal's location in its environment. This second memory pathway is spatial memory processing, a more visual based memory used to orient the mice within a maze or environment and allowing them to develop strategies to escape the maze or complete set tasks (Harrison et al., 2006; O'Leary et al., 2011). It was important to analyze the spatial memory of the *OBiden* mice to determine if that portion of memory was effected by our primary metabolic stress. And if it was effected, was the change due to visual pathway pathology or pathology to the information processing pathways with the CNS. First, a task called the Barnes Maze was utilized requiring the mice to learn the position of an escape box on a symmetrical elevated platform with room cues for guidance. This test is similar to the Morris Water Maze, but has the advantage of reducing stress and noxious stimuli on the mice by removing the swimming element. There was no difference in latency or errors during training to learn the Barnes maze paradigm, with a fixed

Figure 2.5 - Barnes Maze Analysis of the *OBiden* Mouse

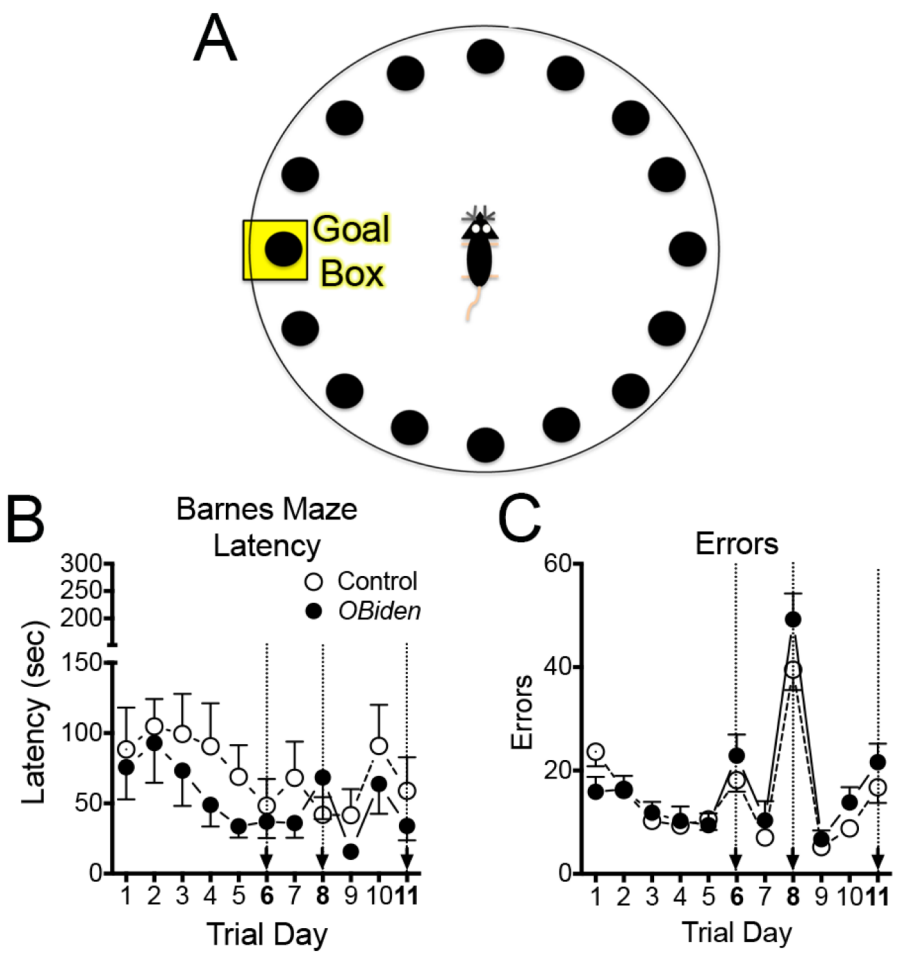

Figure 2.5 – **A**) Diagram of the initial setup of the Barnes maze including mouse placement and location of the goal hole and goal box. **B**) Latency to complete the maze across trials days. The probe day variants are indicated by bolded numbers, arrows and dotted lines (days 6, 8 and 11). **C**) The errors made (wrong hole examined prior to finding goal hole) per trial day across Barnes maze testing (n = 8 per group)

Table 2.3 - Barnes Maze 2-way ANOVA Main Effects

Latency to Complete Maze

ANOVA table	SS	DF	MS	F (DFn, DFd)	P value
Interaction	13407	10	1341	F (10, 140) = 0.6978	P = 0.7253
Test Day	74099	10	7410	F (10, 140) = 3.857	P = 0.0001
Genotype	17998	1	17998	F (1, 14) = 0.8000	P = 0.3862
Subjects (matching)	314976	14	22498	F (14, 140) = 11.71	P < 0.0001
Residual	268990	140	1921		

Errors in Completing Maze

ANOVA table	SS	DF	MS	F (DFn, DFd)	P value
Interaction	787.9	10	78.79	F (10, 140) = 2.137	P = 0.0253
Test Day	17999	10	1800	F (10, 140) = 48.82	P < 0.0001
Genotype	190.9	1	190.9	F (1, 14) = 0.6596	P = 0.4303
Subjects (matching)	4052	14	289.4	F (14, 140) = 7.851	P < 0.0001
Residual	5161	140	36.87		

Table 2.4 – Barnes Maze Post-hoc *t*-tests by Day

Latency in Barnes Maze - post-hoc t-tests per day

Trial Day	Summary	Adjusted P Value
1	ns	> 0.9999
2	ns	> 0.9999
3	ns	0.9963
4	ns	0.884
5	ns	0.9608
6	ns	> 0.9999
7	ns	0.9793
8	ns	0.9957
9	ns	0.9965
10	ns	0.9948
11	ns	0.9974

Errors in Barnes Maze - post-hoc t-tests per day

Trial Day	Summary	Adjusted P Value
1	ns	0.41
2	ns	> 0.9999
3	ns	> 0.9999
4	ns	> 0.9999
5	ns	> 0.9999
6	ns	0.9361
7	ns	0.9959
8	ns	0.1313
9	ns	> 0.9999
10	ns	0.9076
11	ns	0.9245

goal hole, nor were there any differences detected on the various probe days (Figure 2.5B,C)(Table 2.3, 2.4). Probing on day 6 was to account for intra-maze cues the mice may have been utilizing as the maze was shifted 90^{o} but the mice were expected to move quickly to the hole location they had previously associated with ending the maze. Day 8 was a probe to determine if the mice were use extra-maze cues to navigate and if they are, their latency and errors should increase as we blocked their access to peripheral visually cues. This is indeed what we see, that both controls and *OBiden* are using extra-maze cues so their latency and errors increase on day 8 (Figure 2.5B,C). Finally, the mice were re-trained on day 10 to a new goal location 180^{o} away from the original goal hole, this was to test their ability to continue to use maze cues to navigate, but now the navigation is to a new location. When tested on day 11, we again find no difference between control and *OBiden* mice indicating both possess the ability to successfully spatially orient themselves to complete the Barnes maze paradigm (Figure 2.3B,C)(Table 2.4).

In the main effects for the Barnes maze analysis (Table 2.4) there is a significant difference in both latency and errors when looking at the testing day. This difference does not manifest in the post-hoc analysis because all t-test comparisons are within a day between genotypes. It is likely that the main effect difference is due to the spike in latency and errors on day 8 and the differences from the first training day to the fifth training day. Because the main comparisons between genotypes gave no differences, the analysis to determine exactly which comparisons are giving the main effects differences was not run as it was not pertinent given the lack of differences during a specific day across testing.

A second test for spatial memory was used on the *OBiden* mice, one that closely resembled the novel object testing, where a deficit was identified, but relied on a different processing pathway for the mice to successfully complete the task. However, due to an initial test design that was substandard upon subsequent analysis, the spatial memory task was restarted with new cohorts of mice and led to a reduced n across ages. With testing at each age typically utilizing discreet groups, the 12 month age point contains sufficient n's to draw meaningful

Figure 2.6 – Spatial Memory moved object testing in the *OBiden* Mouse

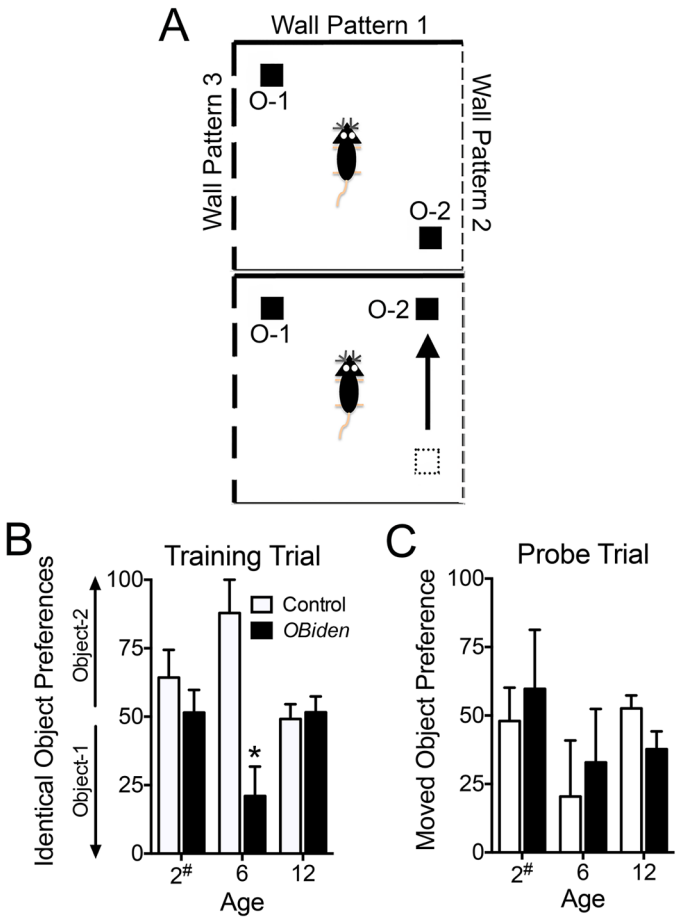

Figure 2.6 – **A**) Diagram of the training trial (top) and probe trial (bottom) of the spatial memory testing. Two identical objects are used for both trials and one object will move relative to the walls and the stationary object and the mice should identify the moved object over the stationary one. **B**) Training trial object preference showed no differences at 2 or 12 months, but at 6 months there was a discrepancy between control and *OBiden* mice in object preference (control n=2, *OBiden* n=3). **C**) No differences were observed at any age during the probe trial with little preference for the moved object over the stationary object (Preference scores > 50) (Control and *OBiden* n per age – 2 months = 6, 4; 6 months = 2, 3; 12 months = 9, 5).

Table 2.5 – Spatial Memory *t*-test Summary

Age	Significance	P value	*t* ratio	df
Spatial Memory Probe Trial				
2#		0.621484	0.513493	8
6		0.701609	0.421745	3
12		0.0869047	1.86438	12
S.M. Training Trial				
2#		0.395085	0.898641	8
6	*	0.0271602	4.04721	3
12		0.775892	0.291171	12

conclusions, especially for comparison with novel object and T-maze tests. As spatial memory relies on external visual cues, the arena for testing had a clear Plexiglas insert to allow the wall patterns to be changed by adding benchcoat paper cut into different patterns between the insert and the black outer wall. This way the mice were trained in an arena with different walls and no objects first, followed by two identical objects in opposite corners, and then during the probe trial one object was moved to an adjacent corner of the maze and the mouse should spend more time with the moved object than the stationary object (Figure 2.6A). During spatial memory training, we saw the appropriate division of time between both objects at 2 and 12 months, however at 6 months of age there was a significant difference in the time spent at objects with the control and *OBiden* mice preferring different starting objects (Figure 2.6B)(Table 2.5). This could be due to low n's at the age point or room conditions we could not account for (i.e. extraneous smells from hallway, slight temperature or olfactory differences within the box) but did not manifest during the probe trial (Figure 2.6C). As with Barnes maze, there were no differences between control and *OBiden* mice in their preference for the moved object within their environment. This could point to one of two explanations, either there are unaccounted variables in our spatial memory testing, or that the mice do not suffer significant deficits to spatial memory processing out to 12 months of age in out paradigm.

Exogenous Stress induced memory and retrieval at 12 months of age

In addition to passive memory tasks such as novel object, T-maze and Barnes maze, there are more active tasks involving conditioning and stimulation of the mice. These tests can use negative or positive reinforcement, with the negative reinforcement often eliciting stronger responses and using a discreet, well defined pathway (Henderson, 1968; Seo et al., 2016). The primary components of this pathway, most generalized sensory and information processing, are the basolateral amygdala and the prefrontal cortex. These regions are discreet from those analyzed previously and allowed us to further analyze the *OBiden* mice for central processing

defects as well as sensory defects as their respond to noxious stimuli may be different if peripheral signal processing is disrupted.

The *OBiden* mice were run through a cue based fear conditioning where a sound and light cue combination is used preceding a mild foot shock delivered through the wire mesh flooring. The mice learn to associated the white noise at light as preceding the shock over 2 days of trials and then a number of extinction days are run to determine how quickly the mice relearn that the light/sound cue pair is no longer associated with a negative electric shock (Figure 2.7A). During the first 120sec the mice are in the chamber on the extinction days we measure their freezing as a percentage of the total time during this acclimation phase to get the contextual fear the animals have towards the chamber itself. In optimal settings, this contextual fear will be low since the mice should have little fear directed toward the chamber because they have been trained to associate the cue pair with the noxious stimulus, not the box itself. Both the *OBiden* and control mice show low percentage of freezing when initially placed in the box for extinction trials, as expected for our paradigm (Figure 2.7B). During the cue presentation without stimulus during extinction days, both *OBiden* and control animals started with high level of freezing in the times succeeding the cue presentation, but the freezing reduced over the days, as expected (Figure 2.7C). There was no difference in the rate of extinction between genotypes, no matter how the freezing trials were segregated or broken down, indicating that the *OBiden* and control mice re-learn that the cues are no longer paired to a noxious stimulus at the same rate. This also indicates that there is no major pathology in amygdala or frontal cortex at 12 months of age, although because fear conditioning uses a noxious stimulus to elicit results, it may take increased levels of degeneration to produce a measureable change compared to more sensitive novel object paradigm.

Figure 2.7 – Fear Conditioning in the *OBiden* Mouse

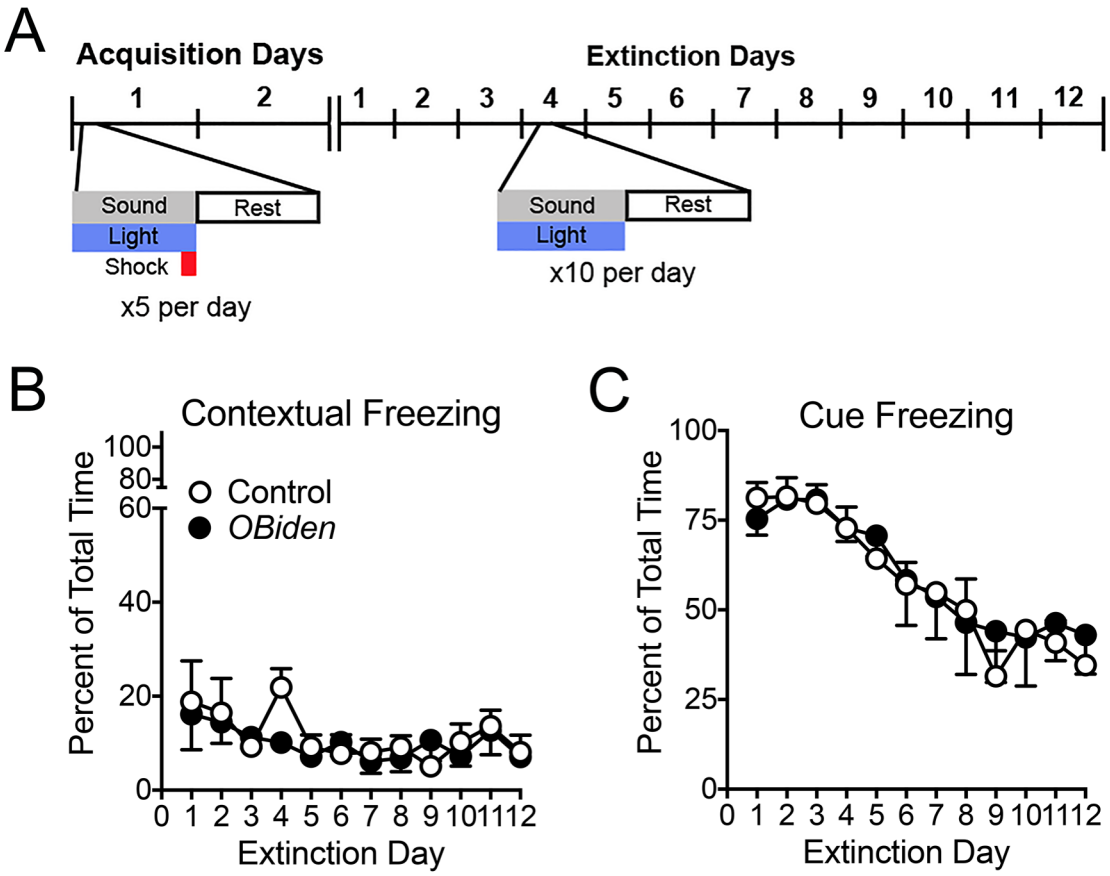

Figure 2.7 – **A**) Timeline of Fear conditioning showing the 10 trials over 2 days of acquisition light/sound with shock pairings and the 12 days of light/shock only during extinction. **B**) Freezing when initially placed in the box (contextual) is measured across all extinction days showing no differences between control and *OBiden.* **C**) Freezing due to cue presentation decreases over time with no differences between control and *OBiden* animals (n = 4 per group)

Table 2.6 – Fear Conditioning Extinction Days 2-way ANOVA Main Effects

Contextual Fear

ANOVA table	SS	DF	MS	F (DFn, DFd)	P value
Interaction	375.1	11	34.1	F (11, 66) = 0.8179	P = 0.6224
Extinction Day	1238	11	112.6	F (11, 66) = 2.700	P = 0.0062
Genotype	51.33	1	51.33	F (1, 6) = 0.1551	P = 0.7074
Subjects (matching)	1986	6	331.1	F (6, 66) = 7.941	P < 0.0001
Residual	2752	66	41.69		

Cue Freezing

ANOVA table	SS	DF	MS	F (DFn, DFd)	P value
Interaction	630.5	11	57.32	F (11, 66) = 0.4414	P = 0.9313
Extinction Day	24459	11	2224	F (11, 66) = 17.12	P < 0.0001
Genotype	79.35	1	79.35	F (1, 6) = 0.04499	P = 0.8390
Subjects (matching)	10583	6	1764	F (6, 66) = 13.58	P < 0.0001
Residual	8571	66	129.9		

Table 2.7 – Fear Conditioning Extinction Day *t*-tests

Contextual Fear

Control - *OBiden*	Summary	Adjusted P Value
Day 1	ns	> 0.9999
Day 2	ns	> 0.9999
Day 3	ns	> 0.9999
Day 4	ns	0.4216
Day 5	ns	> 0.9999
Day 6	ns	> 0.9999
Day 7	ns	> 0.9999
Day 8	ns	> 0.9999
Day 9	ns	0.9927
Day 10	ns	> 0.9999
Day 11	ns	> 0.9999
Day 12	ns	> 0.9999

Cue Freezing

Control - *OBiden*	Summary	Adjusted P Value
Day 1	ns	> 0.9999
Day 2	ns	> 0.9999
Day 3	ns	> 0.9999
Day 4	ns	> 0.9999
Day 5	ns	> 0.9999
Day 6	ns	> 0.9999
Day 7	ns	> 0.9999
Day 8	ns	> 0.9999
Day 9	ns	0.98
Day 10	ns	> 0.9999
Day 11	ns	> 0.9999
Day 12	ns	0.9995

Discussion

Behavioral testing in animal models of disease has been utilized for years but continues to gain more importance as behaviors can be subdivide anatomically and experimentally to give more reliable and detailed results. This allows for *in vivo* analysis of animal models to identify areas of pathology, but also provides a framework for future drug or treatment testing to hone treatment strategies before they reach patients. This is especially true for MS, where years of research has focused on the physical disability associated with overt lesion development, but there has only recently been increased investigation into the detrimental gray matter lesions and neurodegeneration occurring in patients. Additionally, the most common MS model, EAE, is only useful for behavioral testing during a small window before significant pathological development and as the EAE phenotype worsens, mice are incapable of performing most behavioral tests(Acharjee et al., 2013).

The *OBiden* model develops, at worst, a transient physical phenotype that manifests as a one-week dip in performance on the inverted screen test for strength but remains physically capable through the end of our testing at 12 months of age. This resembles aspects of MS, in that many patients will go months or years without a physical attack, but that does not preclude the continuation of subtler neurodegeneration that will only manifest later and by then treatments and therapies can be largely ineffective (Llufriu et al., 2014). Similar to patients, the *OBiden* mice develop cognitive disturbances beginning at 6 months of age in the manifestation of a depression-like endophenotype that persists out through 12 months of age. Although this matches with increased rates of depression seen in MS patients, depression in patients and the endophenotype in mice is often the result of widespread, low levels of pathology throughout the CNS and cannot always be attributed to specific nuclei. However, when we investigated further using more sophisticated tests to evaluate differential memory pathways, we found that the *OBiden* mice develop a recognition memory deficit at 12 months of age. The inability to recognize novel objects and the lack of ability to identify more novel arms of the T-maze and correctly alternate show that

the *OBiden* mice are likely developing pathology in the dorsal hippocampus, entorhinal cortices or associated white matter pathways and these pathologies are affecting their cognitively ability.

Although the *OBiden* mice develop one memory deficit they do not suffer from a generalized failing of all subtypes of memory. This is important because the normal functioning of spatial memory and cue-based fear memory narrowed the list of possible CNS locations that are most strongly effected in our model. It also could point to regional susceptibility within the CNS of the mice, that not only allows us to focus on specific areas for pathology, but also to correlate with MS and determine if patients also display regional susceptibility. This feature of the *OBiden* mice not only opens up additional possibilities into the pathophysiology of MS, but also allows the mice to be monitored for extended periods of time *in vivo* to better characterize deficits and the temporal and physical distribution. Finally, there is the possibility of increasing the level of primary metabolic stress in the mice and evaluating the mice to see a decreased time to deficit onset, increased pathology across more pathways or the development of new deficits outside of those already identified.

The behavioral changes in the *OBiden* model are of particular use when studying the neurodegenerative aspects of MS. Compared to the traditional adaptive immune mediate model, EAE, *OBiden* undergoes much less physical pathology allowing for reliable cognitive testing. Additionally, the current *OBiden* pathology can be identified as part of an established connection system between the entorhinal cortex and hippocampus (Igarashi et al., 2014). This allows us to test particular cell populations in gray and white matter areas and attempt to follow and identify degenerative footprints and it directs some future experiments by pointing towards connectome electrical disturbances as another symptom of the *OBiden* mouse. Possibly of paramount importance, though, is the fact that from primary metabolic stress in oligodendrocytes there can be a myriad of behavioral symptoms, indicating the importance of synthesizing and maintaining proper myelin throughout life to maintain normal cognitive functions and avoid degenerative changes.

CHAPTER 3 – MAGNETIC RESONANCE IMAGING IN THE *OBIDEN* MOUSE

Introduction

For any disease it is critical to have accurate information about its extend and progression and in the case of treatment, how efficacious and the extent of treatment effectiveness. In neurodegenerative diseases this information can sometimes be difficult to obtain because the CNS is not amenable to biopsy and unless lesions or degeneration are substantial enough, the built in redundancies in the CNS may not cause overt manifestation of symptoms (Adams and Kubik, 1952; Bjartmar and Trapp, 2001, 2003; Fischer et al., 2013; Trapp et al., 1999). Historically, the diagnosis and interpretation of MS phenotype relied on physical symptoms in patients. However, because sub-clinical lesions could not be detected, and until the disease reached the more progressive phase it would be difficult to track the progress and disability of patients (Lorscheider et al., 2016; Polman et al., 2011; Schumacher et al., 1965).

The analysis of MS, as well as other neurodegenerative diseases, has greatly improved over the last 30 years with the advent and improvement of magnetic resonance (MR) imaging techniques. MR is based on the fact that different ions within molecules contain electrons spinning at various frequencies and that these electrons are susceptible to external magnetic fields. With the addition of a radio frequency coil sensitive to the directional field induced by the ionic spins, the internal structure of physical bodies could be analyzed for structure based on water content in the most common form of MR imaging (Scherzinger and Hendee, 1985). The ability to analyze water content in tissues is based on the susceptibility of the spin fields around hydrogen (H^1) atoms in water molecules and because all tissues have various concentrations and distribution of water molecules, H^1 MR as the differentiation of tissues.

These structural scans, given sufficient field strength power of the magnet of the MR scanner, are invaluable at detecting lesions that might not otherwise manifest as a physical disability. In fact, the success of structural MR scans at identifying the dissemination of white

matter lesions in the CNS of MS patients caused a change in the diagnostic criteria of MS from more clinical judgement to include MR lesions as well as clinical evaluation (Polman et al., 2011). This introduced new lines of research on correlating the MR signatures to pathological features in the CNS. For example, hyper-intensities in T2 weighted spin-echo scans were often associated with active, inactive or remyelinating lesions in the white matter as they are associated with an increase in water density that shows up as increasing white intensity on T2 scans. Conversely, T1 scans suppress the signal of water and give the same lesions, and additional gray matter lesions, as hypo-intensities sometimes referred to as 'black holes' (Kilsdonk et al., 2016). As the power of scanners and the sensitivity of the receivers increased, greater and greater detail was resolved about these pathological feature *in vivo* and additionally the components were miniaturized sufficiently to allow for experimentation on small animal models.

The additional power and sensitivity as the MR technology progressed also allowed for the development of novel sequences to investigate functional as well as structural aspects of the CNS. These included fMRI that analyzed oxygenated versus de-oxygenated blood to local areas as a marker of neuronal activity; MRS (spectroscopy) to look at metabolite concentrations across the CNS for disruptions due to disease states, and DTI (diffusion tensor imaging) at method of looking at the directional flow of water that highlights dense, parallel fiber tracks in the CNS (Benveniste et al., 2000; Filippi, 2001). These techniques have opened powerful windows into the brain in living patients and model organisms. As MR techniques are part of the current diagnostic criteria for MS, they were applied to the *OBiden* mouse in an attempt to identify *in vivo* pathology detectable at a gross level from our primary metabolic stress.

Materials and Methods

Magnetic Resonance Imaging (MRI) – All MR images were acquired on a Bruker 7T Clinscan magnet connected to Siemens Syngo MR B15 software platform using a dual coil mouse brain surface coil from Bruker. For structural T2 scans the following parameters were used for

spin echo (SE) sequences: TR = 1200ms, TE = 61ms, TA = 41:58, FoV = 16mm X 16mm, Echo Train (Turbo Factor) = 22, 180° flip angle, 125μm X 125μm in plane resolution, 3D acquisition, averages = 2. Scans were triggered by exhalation from the animals, who were maintained at 70-90 breaths/min under a 1.5-3.0% isoflurane-medical air mixture delivered at 1 liter/min. Animal temperature was maintained through the plastic animal holder which was warmed to 30-34^{C} through circulating water. After acquisition, DICOM files were output and transferred to OsiriX image analysis software for volumetric analysis and image reconstruction. For ventricular volumes, the lateral and third ventricles were traced by hand by a trained rater, and the forebrain (rostral to inferior colliculus) and hindbrain (caudal to inferior colliculus) volumes were also obtained through manual segmentation and then forebrain and hindbrain volumes were combined to obtain the total brain volume. All ventricle measurements were normalized intra-mouse to total brain volume. The aqueduct connecting the lateral and third ventricles was excluded from analysis, as was the aqueduct connecting the lateral and fourth ventricles (non analyzed).

Diffusion Tensor Imaging – DTI image acquisition was performed with the same isoflurane, heating and gating setup as structural MRI. Image parameters for DTI acquisition were: TR = 2500ms, TE = 30ms, 6 diffusion directions, 2D, average=1, 90° flip angle, FoV=46mm X 68mm, 5 simultaneous slices at 500μm thick, 1.2mm spacing. Two sets of scans were obtained; the second set was offset 500μm caudally compared to the first set of scans to obtain images across more of the forebrain region. Raw images were output to OsiriX and reconstructed using the DTI Map plugin to obtain 2D intensity images of: FA values, Eigen vectors 1 ($\lambda 1$), 2 ($\lambda 2$) and 3 ($\lambda 3$), and color coded DTI directionality map. For analysis, we obtained each Eigen value for at least 8 pixels across these regions: genu, mid and splenium of corpus collosum (2 slices each), left and right external capsule (3 slices each), left and right internal capsule (2 slices each). FA was calculated from Eigen vectors as described:

$$FA = \sqrt{1/2} * \frac{\sqrt{(\lambda 1-\lambda 2)^2+(\lambda 2-\lambda 3)^2+(\lambda 3-\lambda 1)^2}}{\sqrt{\lambda 1^2+\lambda 2^2+\lambda 3^2}}.$$

The FAs across 8-10 pixels were averaged per region to get an FA average per slice, and these were averaged across slices to get an FA value for a given white matter region. Color coded images were generated from the DTI Map plugin in OsiriX and trimmed manually using OsiriX viewer and trimming tools.

Results

Longitudinal Structural MRI in OBiden Mice

To analyze the *OBiden* mice, mice were run at 2, 6 and 12 months through a battery of MR sequences. The first set, performed longitudinally when possible, was a series of structural T2 and T1 weighted spin-echo scans to probe the structure of the *OBiden* brain. Specifically, the scans were analyzed for lesion development in white or gray matter and the volume of the ventricular system was obtained from T2 scans. In T2 scans, the greater the concentration of water, the brighter the signal will appear because T2 scans use a relatively long echo time. This echo time (TE) directs when the receiver will analyze for spins from the tissue and the more residual magnetic excitement remaining in the tissue at the time of analysis, the brighter the signal. Our scans were based on hydrogen excitation, and if the hydrogen atoms are in densely packed molecular locations surrounded by non-excitable atoms, such as within plasma membranes or intracellular fluid filled with protein structures and lipids, the hydrogen atoms give off their spin energy quickly. This causes the signal to fade faster than in location where there are more hydrogen atoms and less non-excitable atoms, such as the CSF filled lateral ventricles (Benveniste et al., 2000; Scherzinger and Hendee, 1985). Example slices of a T2* weighted scan is shown in Figure 3.1A and B in the insets, where the ventricles appear as bright white and the surrounding tissue is varying shades of gray. The ventricular system is useful as a proxy for overall degeneration in the CNS. As the brain degenerates, the ventricles will expand from within the brain to keep the shape of the CNS roughly stable over time, rather than allowing the brain to collapse inward during neurodegeneration. Therefore, we segmented out the largest and most

Figure 3.1 – Segmentation of the *OBiden* Mouse Ventricular System

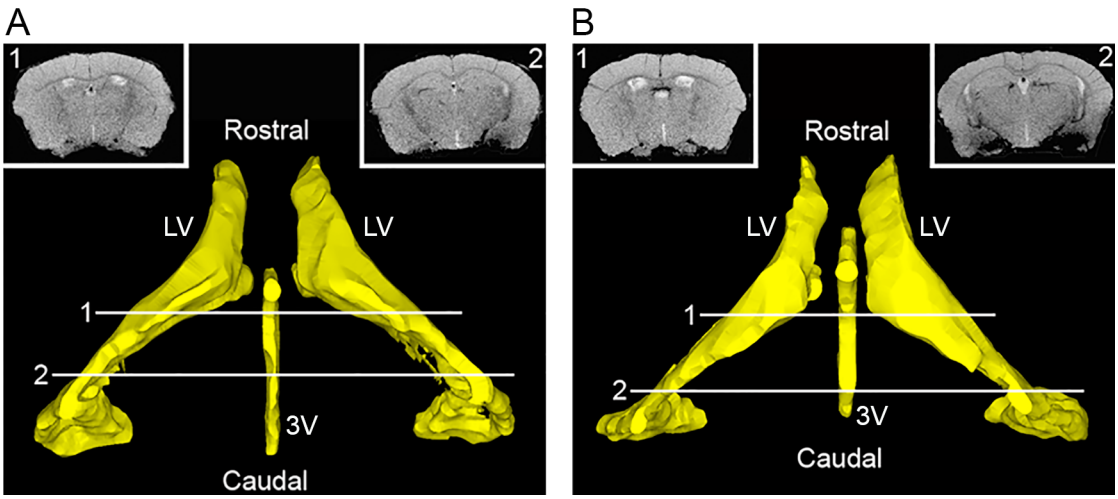

Figure 3.1 – **A**) Segmentation of a control mouse lateral ventricles (LV) and third ventricle (3V) at 12 months of age. Insets 1 and 2 correspond to the white lines through the ventricles representing the location of the slices from T2* scans see in the insets. **B**) Segmentation of the ventricle system in a 12 month *OBiden* animal.

well defined pieces of the ventricular system in mice, the lateral ventricles (LV) and third ventricle (3V) to obtain the volume of the ventricular system at 2, 6 and 12 months of age (Figure 3.1A,B). There is no reliable automated segmentation tool for mouse brain MRI as of yet, so all the ventricles were segmented manually to assure accuracy and reliability as multiple raters would obtain volumes with ±5% of one another. In addition to the ventricles, the total volume of the brain was obtained by manually segmenting around the outer circumference of the brain from the olfactory bulbs to the forman magnum. This way the ventricle volumes could be normalized to total brain volume (TBV) to account for inter-mouse variability and standardize the measurements. The volumes were also normalized to the 2 month, pre-gavage value for each group resulting in a value of 1 at 2 months, and then changing values as the mice aged. There was no difference in the TBV values at any age point, after normalizing to the 2 month values, indicating that the overall volume of the mouse brains did not change as a result of age or our induction of primary metabolic stress (Figure 3.2A). When the lateral ventricles were analyzed, there was an increase in volume as the mice aged in both control and *OBiden* animals and no difference between the two genotypes (Figure 3.2B). This indicates that any expansion we are seeing is likely a result of normal aging or development processes in the mice, since we would anticipate an accelerated increase in volume if there was additional degeneration in the *OBiden* mice. Finally, the third ventricle was analyzed, and as was the case with the lateral ventricles, we did not see a significant difference between the control and *OBiden* mice at any age point indicating no accelerated degeneration (Figure 3.2C). Segmentation of specific gray matter structures was attempted, such as the hippocampus and thalamus, however our scans were of insufficient detail to allow for accurate volumetric analysis and obtaining detailed scans was temporal prohibitive as each scan for a mouse would run for 3+ hours. Due to the lower resolution, it did not appear that any focal lesions could be detected, even though those lesions did develop as will be discussed in later chapters. Overall, there was no detectable difference in generalized degeneration using the volume of the ventricular system as a surrogate marker for degeneration *in vivo*.

Figure 3.2 – Longitudinal Ventricle Volumes in the *OBiden* Mouse

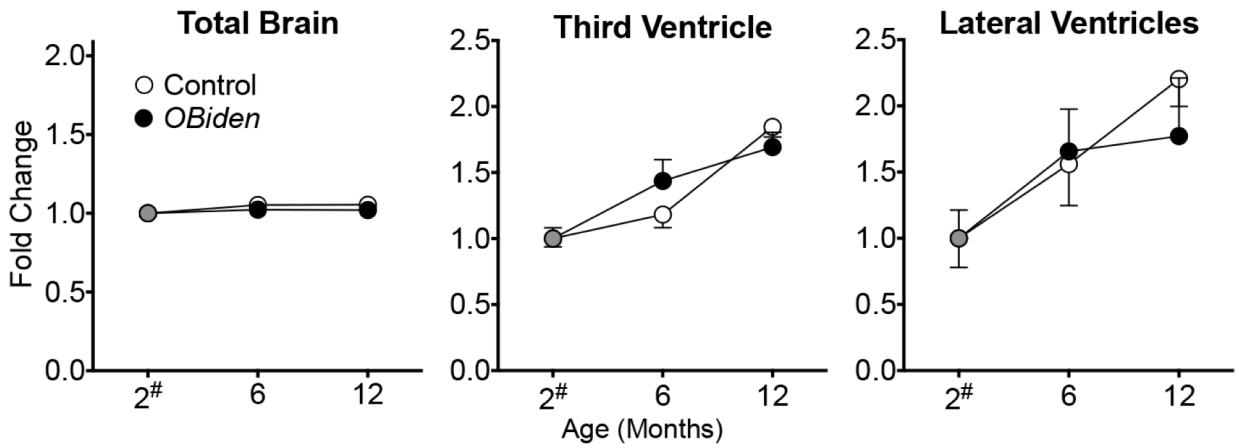

Figure 3.2 – **A**) Normalized total brain volumes (TBV) from control and *OBiden* mice at 2, 6 and 12 months of age with no differences between genotypes. **B**) Lateral ventricle (LV) normalized volume across ages with no differences between genotypes. **C**) Normalized third ventricle volumes across ages showing no differences between genotypes (Control and *OBiden* n per age – 2 months = 7, 7; 6 months = 7, 7; 12 months = 7, 5).

Table 3.1 – Longitudinal Ventricle Volumes 2-way ANOVA Main Effects

Total Brain Volume

ANOVA table	SS	DF	MS	F (DFn, DFd)	P value
Interaction	0.002443	2	0.001221	F (2, 36) = 0.3256	P = 0.7242
Age	0.01313	2	0.006564	F (2, 36) = 1.750	P = 0.1883
Genotype	0.004821	1	0.004821	F (1, 36) = 1.285	P = 0.2644
Residual	0.1351	36	0.003752		

Lateral Ventricles

ANOVA table	SS	DF	MS	F (DFn, DFd)	P value
Interaction	0.4676	2	0.2338	F (2, 33) = 0.4414	P = 0.6469
Age	6.251	2	3.126	F (2, 33) = 5.901	P = 0.0064
Genotype	0.1187	1	0.1187	F (1, 33) = 0.2241	P = 0.6390
Residual	17.48	33	0.5297		

Third Ventricle

ANOVA table	SS	DF	MS	F (DFn, DFd)	P value
Interaction	0.2972	2	0.1486	F (2, 36) = 1.974	P = 0.1536
Age	4.199	2	2.099	F (2, 36) = 27.89	P < 0.0001
Genotype	0.0119	1	0.0119	F (1, 36) = 0.1581	P = 0.6933
Residual	2.71	36	0.07528		

Table 3.2 – Longitudinal Ventricle Volume Post-hoc *t*-tests

Total Brain Volume - Sidak's Comparison

Control-*OBiden*	Summary	Adjusted P Value
2#	ns	> 0.9999
6	ns	0.7447
12	ns	0.6599

Lateral Ventricles - Sidak's Comparison

Control-*OBiden*	Summary	Adjusted P Value
2#	ns	> 0.9999
6	ns	0.9925
12	ns	0.7064

Third Ventricle - Sidak's Comparison

Control-*OBiden*	Summary	Adjusted P Value
2#	ns	> 0.9999
6	ns	0.2497
12	ns	0.66

DTI Characterization of OBiden Mice at 12 months

Although there was no observable degeneration through T2 structural MRI analysis, that technique has its limitations and only gives a general picture of tissue integrity throughout the CNS. As the *OBiden* model primarily affects white matter, there are other MR techniques that focus more on the structure and stability of dense fiber tracts, many myelinated, in the CNS. The main technique to date for white matter analysis is diffusion tensor imaging (DTI). DTI is also based on utilizing and controlling the spin of hydrogen atoms, but instead of looking mainly at the local environment through spin-loss of the atoms, it analyzes for movement of the atoms in different directions.

DTI scans work by magnetizing hydrogen atoms within the magnetic field and tracking the movement of the hydrogen atoms, mostly those in water molecules, as they diffuse through their local environment (Aung et al., 2013). By adjusting the timing of the scan, it can suppress the signal obtain from freely diffusing molecules in the ventricles or blood vessels and focus on more confined diffusion, especially in intracellular compartments. This is particularly beneficial when looking at axon bundles and myelinated tracts as there are a large number of directional axons moving in parallel that will give similar signals upon DTI stimulation. By analyzing the direction of movement in three main directions (eigen vectors) a map can be obtained of the diffusivity of water, and importantly the more tightly organized and intact tracts are the more directional the signal. As degeneration occurs and tracts lose their integrity or lose axons to degeneration, the signal will be altered and picked up upon scanning. This directionality is referred to as the fractional anisotropy (FA) of the tissue and the ranges from 0 -1, with 1 representing movement restricted to only one direction and 0 means freely diffusing water in all directions. The FA values are then converted to a 3D matrix for color coding to represent direction and intensity of color to show the value of the FA (Figure 3.3A).

Upon quantification of the FA intensity at 12 months of age, there was no difference between control and *OBiden* animals across the corpus collosum (CC) (Figure 3.3B). Multiple

Figure 3.3 – DTI of Neocortical White Matter Tracts in the *OBiden* Mouse

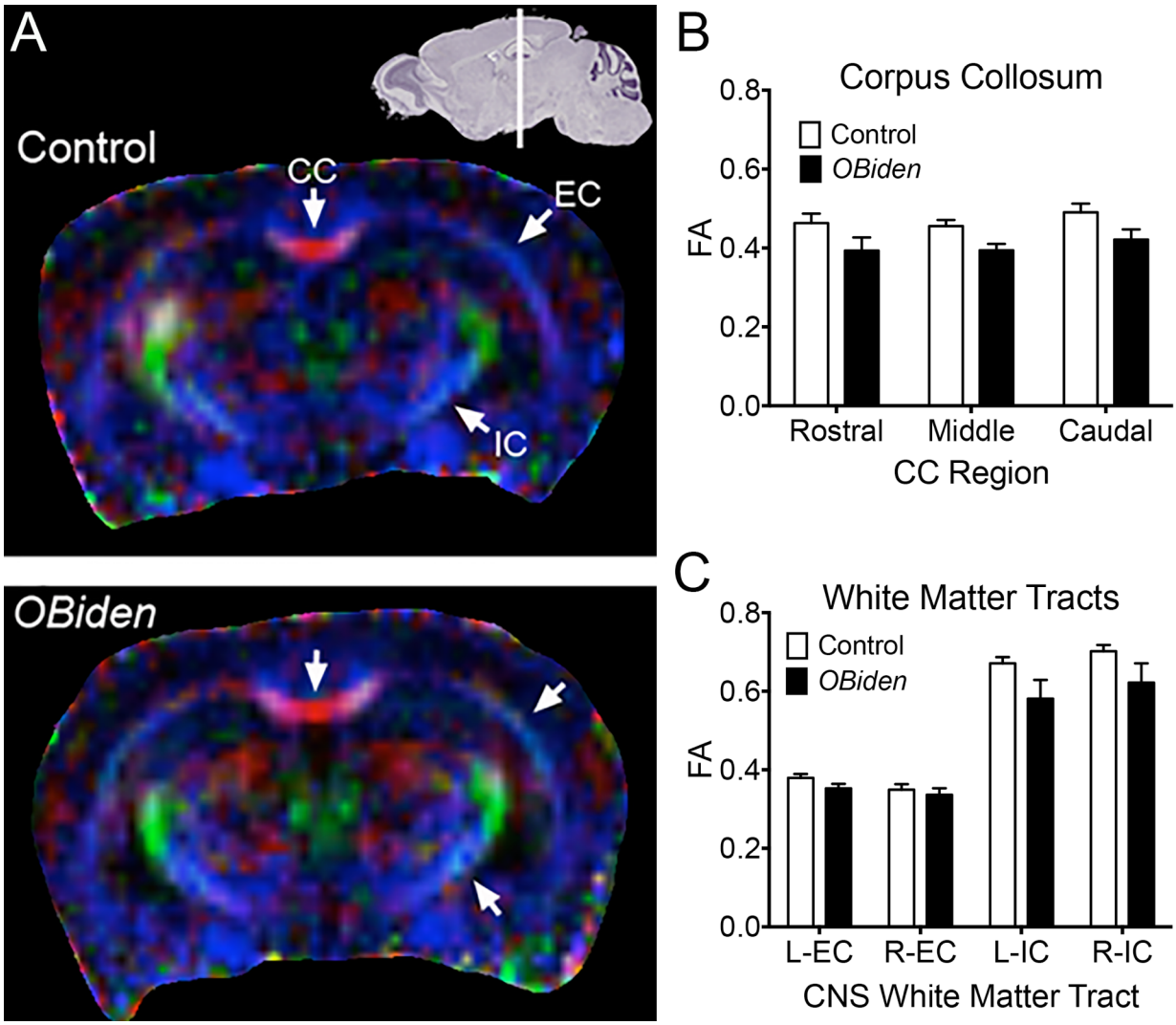

Figure 3.3 – **A**) Representative color-coded slices from DTI of 12 month control (Top) and *OBiden* (Bottom) mice. Position and thickness of slice is indicated on the sagittal brain atlas picture at the top right. Arrows indicate the white matter tracts used for analysis; corpus collosum (CC), external capsule (EC) and internal capsule (IC). **B**) FA values from various regions of the CC show no difference in between control and *OBiden* animals (n = 7,9). **C**) FA values from bilateral white matter tracts of the EC and IC show no differences at 12 months between control and *OBiden* mice (n = 7,7).

Table 3.3 – Corpus Collosum DTI Statistics

CC DTI Main Effects

ANOVA table	SS	DF	MS	F (DFn, DFd)	P value
Interaction	0.0001714	2	8.568E-05	F (2, 42) = 0.01773	P = 0.9824
CC Location	0.009049	2	0.004525	F (2, 42) = 0.9363	P = 0.4001
Genotype	0.05274	1	0.05274	F (1, 42) = 10.91	P = 0.0020
Residual	0.203	42	0.004832		

CC DTI - Sidak's Comparison

Control-*OBiden*	Summary	Adjusted P Value
Rostral	ns	0.1494
Middle	ns	0.2382
Caudal	ns	0.1565

Table 3.4 – External and Internal Capsule DTI Statistics

EC and IC DTI Main Effects

ANOVA table	SS	DF	MS	F (DFn, DFd)	P value
Interaction	0.01534	3	0.005112	F (3, 48) = 0.9913	P = 0.4049
CNS Tract	1.187	3	0.3955	F (3, 48) = 76.71	P < 0.0001
Genotype	0.03833	1	0.03833	F (1, 48) = 7.432	P = 0.0089
Residual	0.2475	48	0.005157		

EC and IC DTI - Sidak's Comparison

Control-*OBiden*	Summary	Adjusted P Value
L-EC	ns	0.9327
R-EC	ns	0.9953
L-IC	ns	0.0902
R-IC	ns	0.161

regions of the CC were used because there is heterogeneity across the CC in terms of fiber diameter and therefore extend of myelination. However, even after 10 months of metabolic stress induction there was no change to the overall FA's in any region. Further, additional white matter tracts were analyzed to determine if there were regional differences between white matter tracts. The external capsule (EC) and internal capsule (IC) were analyzed because they were easily identifiable on the DTI scans, and because together with the CC, they carry many of the neuronal projections running between hemispheres and nuclei in the CNS. Even with the extended analysis, there was no difference between genotypes when analyzing identical tracts in the CNS. However, there was a difference in the FA between the EC and IC, but that is due to the structure and size of the tracts with the IC being larger and more densely packed than the EC and therefore giving a larger FA with our scan technique (Figure 3.3C).

Although there were no observable changes with DTI, that does not necessarily indicate a lack of pathology. For one, the MR system used for this study did not have the power to acquire more complex DTI data that may have resolved micro-lesions that developed but were unobservable at the current resolution. Also, there is evidence that even in MS patients, degeneration and lesions can be difficult to detect with DTI and that either reliable longitudinal studies or higher magnetic field strengths are critical for obtaining informative data (Aung et al., 2013; Filippi, 2001).

Atlas Generation from in vivo MRI

Another use for the MRI that originated as an attempted quantitative study but ended as a more qualitative and visually appealing study, was the segmentation of nuclei within the CNS. Originally, the idea was to analyze the volume of various structures throughout the brain, however due to limited resolution and poorly defined borders, especially in cortical regions, it was not feasible to complete the study. However, the segmentation proved valuable in other avenues, especially as a visualization tool for mapping back regions of confirmed pathology and understanding the anatomical relationship to each other in 3D space. The MRI analysis software

Figure 3.4 – Segmentation of MRI Derived from the *OBiden* Mouse Brain

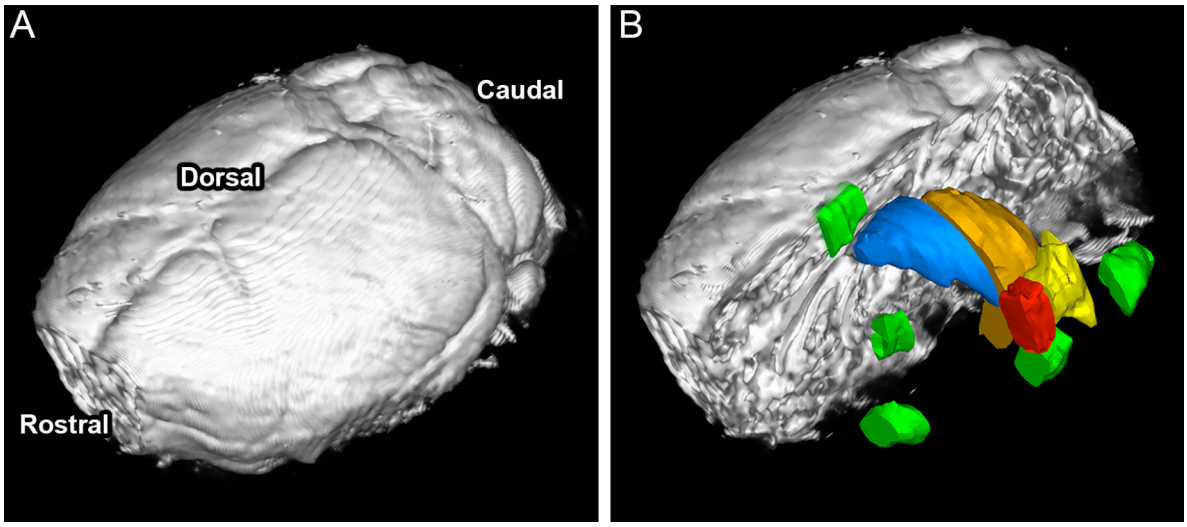

Figure 3.4 – **A**) Whole segmented mouse brain after skull stripping. The rostral, caudal and dorsal surfaces of the brain are indicated and the ventral surface is below the brain, out of the picture image. **B**) Various brain ROIs are highlighted within the mouse brain. Green nuclei are those of less interest to the current studies and from rostral to caudal position are: rostral piriform cortex, reticular thalamus, cingulate cortex, caudal piriform cortex and flocculus. Colored brain regions of future to the study are: blue – dorsal hippocampus, orange – ventral hippocampus, red – rostral entorhinal/perirhinal cortex, yellow – entorhinal cortex.

used allowed an individual mouse brain to be stripped of the skull to isolate the neocortex and create a basic brain template (Figure 3.4A). On the original scans, regions of interest (ROIs) can then be drawn over any region or multiple regions to highlight approximate areas of cortex, thalamus or any brain region to be displayed and visualized in three dimensions (Figure 3.4B). This allows the distance between ROIs to be visualized, their anatomical relationship to each other and other intermediate ROIs that could be of interest in future studies.

The atlas has the additional benefit of use in future studies using *in vivo* MR spectroscopy (MRS) studies. The MRS studies involve analyzing the CNS for the concentration of various metabolites within the CNS and also requires placing specific ROIs over the brain to confine the analysis to specific brain nuclei. As certain regions of the brain will express specific metabolites, for example ventral tegmental area (VTA) produces dopamine in high concentration and amygdala produces GABA at levels above other nuclei, it is important to isolate specific regions to reduce contamination from surrounding structures.

Discussion

Unlike diseases of many peripheral organs or systems such as liver, kidney, or gastro intestinal as examples, the brain and neurodegenerative diseases are not amenable to biopsy, surgical evaluation or peripheral sampling. Because, to an extent, the CNS is isolated form the periphery of the body it can be difficult to analyze neurodegenerative disease *in vivo*, for diagnostic or treatment tracking purposes.

With the translation of imaging techniques from the analytical realm to the clinical and research realm, new avenues of research and comparison between models of disease and patients have opened up. These techniques, such as MR imaging, were first established for their usefulness in the clinic. However, as technology allowed for miniaturization and increased sensitivity, it became evident that the same techniques could be applied to research models to

track the progress of disease *in vivo*, and to correlate the findings with observations from patient populations.

In the *OBiden* model, MR techniques were utilized to analyze the mice as they aged to develop the techniques for the lab, and to attempt to identify comparable pathologies to MS patients. Also, these techniques were very useful in obtaining data from within the CNS without sacrificing the mice and allowing for continued testing with behavior tests and general monitoring of the mice as they aged. Although there were not significant differences between the control and *OBiden* mice in terms of ventricular volume or DTI analysis of fiber tracts, this does not rule out the possibility of harnessing new techniques as they become available, or fine tuning they techniques available to optimize our data. Even studies of MS patients are finding that much of the pathology that can be identified through post-mortem histological and immunocytochemical studies is still lost to MR techniques (Kilsdonk et al., 2016). Continuing our studies on the *OBiden* model and relating it to our observed pathology, as well as patient pathology could identify novel pathologies or novel methodologies for evaluating pathology, which would benefit patients as well as the research into MS models.

Currently, one of the benefits obtained from some of our imaging studies is the development of our own 3D atlas of the brain and areas of pathology. For many neuroscientists, they are familiar with human and often animal brain structures, so the model becomes a tool to concisely display the data we accumulate to better convey our results. However, for non-scientists or those outside the neuroscience field, it represents a display technique that can more easily convey our message across fields and outside the scientific community as a way of increasing the knowledge and collaboration within and outside the research community.

CHAPTER 4 – HISTOLOGICAL AND IMMUNOCYTOCHEMICAL ANALYSIS OF THE *OBIDEN* MOUSE AND MS TISSUE

Introduction

The characterization and investigation into the pathology of MS was first accomplished through the use of histological methods that were later supplemented with molecular staining and blotting techniques. However, because of the established nature, detail and previous characterization of MS pathophysiology through histology it remains and important technique in evaluating MS post mortem samples and any developed models of the disease.

Histopathological methods are still used in the diagnosis and post-mortem identification of diseases in patients because of their reliability, relative ease to perform and relative sensitivity to changes in tissue composition. These techniques are often basic or acidic plant derivatives that bind to nuclei acids or proteins depending on their distribution in the tissue. For neuropathology, the most famous stains are the silver impregnation techniques adapted from early photography that stained different components of the neural architecture depending on the modification, preparation and length of the stain (Garven and Gairns, 1952). These techniques were not only critical for Golgi, Cajal and Brodmann to describe and setup fundamental understandings of the arrangement and architecture of the nervous system, they are still valuable in giving high contrast and detailed images for the analysis of cellular and sub-cellular pathologies within the CNS (Conel, 1953; Funkhouser, 1915).

The *OBiden* mouse had not been evaluated prior to this study and therefore it was not only necessary but expedient to use a number of histopathological techniques to describe pathology in the mice and compare the model to MS tissue. This included the use of silver techniques and specifically a modification called the modified Bielschowsky stain that is used to highlight neurofibrillary tangles and axons throughout the CNS (Yamamoto and Hirano, 1986). By staining for axons, we could identify areas of axonal loss, axonal spheroids and transections or

other pathologies in the *OBiden* and MS tissue, regardless of the preservation or preparation of the tissue given the robustness of the technique.

In addition to the silver staining of neurons, staining myelin was important, especially considering the effect the *OBiden* mouse should be having on the myelin of the CNS. To detect myelin, a stain based on the interaction of a dye with the phospholipid dense myelin sheaths was utilized called Luxol Fast Blue (LFB) (Snodgress et al., 1961). LFB is specific for CNS myelin, it will not work as efficiently on PNS myelin, and has the additional benefit of losing specificity for degenerating myelin. This means that it can be used to differentiate between intact CNS myelin and myelin that has undergone substantial degeneration but may still stain with myelin proteins. LFB then is particularly useful as a stain for identifying primary myelin pathology, whether it is in the *OBiden* mouse or in MS patients were active, inactive and chronic lesions can all have differential staining patterns when analyzed histopathologically.

While the histopathological stains are important historically and for comparing the *OBiden* mouse to MS tissue, the development and refinement of antibody staining techniques has allowed for additional analysis of tissue and the cellular and molecular composition. By staining for surface or intracellular markers we can determine, semi-quantitatively, the abundance of various cell types as well as their general health and state. For example, the endogenous immune cells of the CNS, microglia, are nominally at rest but upon sensing debris or changes to their environment can alter their expression profiles. They upregulate lysosomes for degeneration and change their phenotype as they phagocytose surrounding tissue (Bennett et al., 2016; Kuhlmann et al., 2017). Changes can also occur in the oligodendrocyte, astrocyte and neuronal populations that may be detectable with various markers.

Together, the idea is to compile a broader view of the scope, location, extent and severity of degenerative phenotypes in the *OBiden* mouse. Because, unlike models such as EAE, it has not been characterized to date and because, so far, overt physical phenotypes have not developed that would allow us to pinpoint pathology it is necessary to undergo a survey to

understand the model better. To this end, histopathological and immunocytochemical techniques were brought to bear on first 6 month and then 12 month *OBiden* mice as the analysis was extended. Although gross level pathologies were not present, many instances of regional, focal and discrete pathology developed throughout the CNS of the mice. More importantly, many of these pathologies showed similarities to known MS pathologies given a molecular credence to the *OBiden* model as a potential new tool for investigating and understanding MS disease course.

Materials and Methods

Luxol Fast Blue

The stock solutions can be made in advance and stored, covered from light, until use. The Luxol Fast Blue (LFB) solution is made by mixing 995ml of 95% ethanol is 5ml of 10% acetic acid (final concentration is .01% acetic acid), then adding 1g Solvent Blue 38 (Sigma S-3382) mixing, and then filtering with 0.45μm filter. 0.1% (w/v) Lithium carbonate ($LiCO_3$ - Arcos 554-13-2) is made in filtered water, and 1% Eosin-Y stock is made by dissolving 1g Eosin-Y (Sigma E511-25) in 100ml of 95% ethanol and mixing then filtering. For staining, 10μm frozen cryostat sections are thawed in 1xPBS for 10min, washed in filtered water, and then taken up through the ethanol series (50%→70%→80%→90%→95%→95%) for 2min at each step and then into xylene washed 2 times for 2min each. Slides are washed twice for 2min in 95% ethanol then placed in LFB solution and placed in a heating oven at 70^C for 6-8hours. The slides are then removed and allowed to cool to room temperature over 30min, then excess stain is removed by washing in 95% ethanol for 1min. Next, slides are washed twice for 5min each in distilled water to prepare for differentiation. The slides are placed in 0.1% $LiCO_3$ for 20-30sec, moved to an 80% ethanol wash for 15-20sec with constant agitation and then dipped into distilled water followed by a distilled water wash for 5min. Once all slides are finished differentiating, they are placed in Hematoxylin solution (Gill's No.1, Sigma GHS-132) for 5min, followed by washed with tap water until the water from the slides runs clear. While the slides are in tap water, 1% Eosin-Y is made into its working solution by

diluting it to 0.25% with 100% ethanol and then adding 500µl acetic acid for every 100ml of Eosin-Y solution (solution should go from opaque green/orange to bright and clear orange). Add slides to 0.25% Eosin-Y working solution for 20-30sec, and then wash with tap water until the water runs clear. Next, wash slides in a shortened ethanol series of 70%→90%→95%→95% washes for 1min each, followed by 2, 2min xylene washed. Remove slides from xylene, tap off the excess then add Cytoseal-60 (Richard Allan Scientific – 8310-16) and coverslip.

Bielschowsky Modified Silver Stain

This silver stain is modified to highlight axons and axonal pathologies opposed to traditional silver stains (i.e. Golgi staining) which highlight some neuronal cell bodies, dendrites and axons. The solutions for the Bielschowsky stain were made the day of staining, and acid washed glassware was always used for any reagents or staining steps that involved silver solutions. Solutions: 10% silver nitrate ($AgNO_3$) in distilled water, 10% ammonium $AgNO_3$ (to stirring 10% silver solution, ammonium hydroxide (NH_4OH) was added dropwise until the silver solution oxidized, then re-cleared), Developer Stock Solution (80ml distilled water+20ml 37.5% formaldehyde+0.5g citric acid+2 drops of 14N nitric acid with stirring), Working Developer Solution (to 100ml distilled water add 16 drops Developer Stock Solution and 16 drops ammonium hydroxide), 5% (w/v) sodium thiosulfate in distilled water, Ammonium water (for every 100ml distilled water add 16 drops ammonium hydroxide). Preheat the 10% $AgNO_3$ and 10% ammonium $AgNO_3$ in acid washed glassware at 40^C. Thaw frozen slides in 1xPBS then wash in distilled water followed by ethanol series (as in LFB) to xylene washes, and then back down the ethanol series to distilled water in acid washed glassware. Place the slides in 10% $AgNO_3$ for 15min at 40^C. Wash the slides in distilled water for 5min, and while washing add ammonium hydroxide to the 10% $AgNO_3$ until the solution oxidizes and clears, place the slides back into the just made 10% ammonium-silver for 10min at 40^C. Wash the slides in distilled water, and place in the original 10% ammonium-silver that was heating at 40^C and stain slides for 10min. Remove the slides from heat

and place in the Working Developer Solution at room temperature and watch for differentiation. Fiber tracks will turn brown then black and once black fibers in gray matter are just visible (anywhere from 5-20min) wash the slides in ammonium water 3 times for 2min each wash. Next, wash in distilled water for 3 washes of 1min each, then wash in sodium thiosulfate for 5min to remove residual metal ions. Counterstain if desired for 5min with hematoxylin, then wash slides, go through the ethanol series to xylene and add Cytoseal-60 with a coverslip.

Immunocytochemistry and Primary Antibodies

For ICC procedures see Chapter 2.

Table 4.1 – Primary Antibodies to Characterize the *OBiden* Mouse

Antigen	Isotype	Name	Cell/Structure	ICC Dilution	Permeabolization	Company	Product#
Alzheimer Precursor Protein	Ms IgG1	APP	neurons	1:100	MeOH	Millipore	MAB348
Oligodendrocyte Transcription Factor 2	Rb	Olig 2	dividing/mature oligos	1:500	MeOH	Millipore	AB9610
Oligodendrocyte Transcription Factor 1	Ms IgG2b	Olig 1	dividing/mature oligos	1:3000	Triton	Millipore	MAB5540
Adenomatus Polyposis Coli (APC)	Ms IgG2b	CC-1	mature oligos	1:100	MeOH	Calbiochem	OP80
Proteolipid Protein 1	Rt	AA3	myelin/stress oligos	1:300	MeOH	Hybridoma	
Myelin Basic Protein	Ms IgG2b	SMI99	myelin	1:500	MeOH	Covance/Biolegend	808401
Myelin Basic Protein	Ms IgG1	SMI94	myelin	1:1000	MeOH	Covance	SMI-94R
2', 3'-cyclic nucleotide 3'-phosphodiesterase (CNPase)	Ms IgG1	SMI91	myelin	1:1000	MeOH	Covance	SMI91-R
Glial Fibrilary Acidic Protein	Ms IgG1	GFAP	astrocytes	1:1000	Triton	Neuromics	MO22136
Neurofilament Light Chain	Rb	NF-L	neurons	1:100	MeOH	Cell Signalling	2837
Phophorylated Neurofilament Heavy Chain (P-NF-H)	Ms IgG1	SMI31	neurons	1:1000	Triton/MeOH	Covance	SMI-31P
Nonphosphorylated Neurofilament Heavy Chain (NF-H)	Ms IgG1	SMI32	neurons	1:1000	MeOH	Convance	SMI-32P
Casper (NCP)	Gp	Casper	paranode	1:1000	MeOH	Open Biosystems	D2683-4007
Neurofascin 186	Rb	NF186	nodes	1:500	MeOH	Open Biosystems	B7946
4'6' Diamidino-2-phenylindole		DAPI	nuclei/chromatin	1:1000	Any	Sigma	D9542
Cluster of Differentiation 68	Rt IgG2a	CD68	lysosomes in microglia	1:500	No Perm	AbD	MCA1957
Ionized Calcium Binding-Adaptor 1	Rb	IBA-1	microglia	1:1000	Triton/MeOH	Wako	019-19741
Vesicular GABA Transporter	Gp	VGAT	Pre-synaptic GABA Vesicles	?	Triton/MeOH	Synaptic Sysytems	224 104
COUP-TF Interacting Protein 2	Rt IgG2a	Ctip2	Post-Mitotic Pyramidal Cells	1:300-1:500	Triton/PBTGS	Abcam	ab18465 (clone 25B6)
NeuN	Ms IgG1	NeuN	Neurons	1:1000	Any	Millipore	MAB377

ICC Cell Counting and Analysis

For Iba-1 and GFAP cell counts, cells with either GFAP+/DAPI+ or Iba-1+/DAPI+ cell bodies and nuclei were counted from across the entire corpus collosum (defined as the white matter region from cingulum to cingulum spanning the midline), the external capsule (white matter from the cingulum to the medial to the piriform cortex) and the internal capsule (from the ventral surface of the lateral ventricles through the mid-thalamus). GFAP+ astrocytes were either present or absent, no other phenotypic metric was used. Iba-1+ microglia were sub divided into inactive cells (thin cytoplasmic wrap of the nucleus, multiple long, branching processes) or active cell

(enlarge cytoplasm (3x inactive size), retraction and thickening of processes and/or bipolar or amoeboid morphology). Total white matter volume analyzed was calculated by outlining the white matter tracts to obtain an area and multiplying by tissue thickness, or cells were presented as a percentage of the total cell population.

Results

Histopathological Characteristics of MS Tissue

The first step in the analysis of all the tissue was to develop and confirm that the histology stains such as LFB and the modified Bielshowsky stain worked on MS tissue and historical staining could be reproduced. In addition, this had the benefit of screening the tissue for lesions or pathology that may have been overlooked during the neuropathology report. This was especially important so that we could determine if the post-mortem tissue in our possession was indeed normal appearing tissue or if it had subtle underlying pathologies that would need to be taken into account. The first stain was LFB to test procedures, including staining times, temperatures and differentiation procedures, as well as evaluate the white matter integrity of the tissue. In Figure 4.1A, a low magnification image of healthy control human tissue shows that typical staining pattern for LFB stain with intact myelin stained a dark blue and indicated by the arrowhead, with gray matter showing a more dispersed staining pattern from radiating myelin fibers (Figure 4.1A,B). Also, the tissue has a pink background and upon higher magnification, purple nuclei can be discerned in the section. This is the result of counter staining with the common hematoxylin and eosin (H+E) counter stain to highlight the general tissue (pink) and dense nuclei acids (purple). The circular holes in the tissue are a result of the tissue punches obtained from the sections for later molecular analysis and are not the result of pathology or processing.

Interestingly, in this patient-MS pair, LFB revealed the presence of two lesions in this small piece of normal appearing tissue. An active white matter lesion stripped of intact myelin and with

Figure 4.1 – LFB Staining of Control and MS Tissue

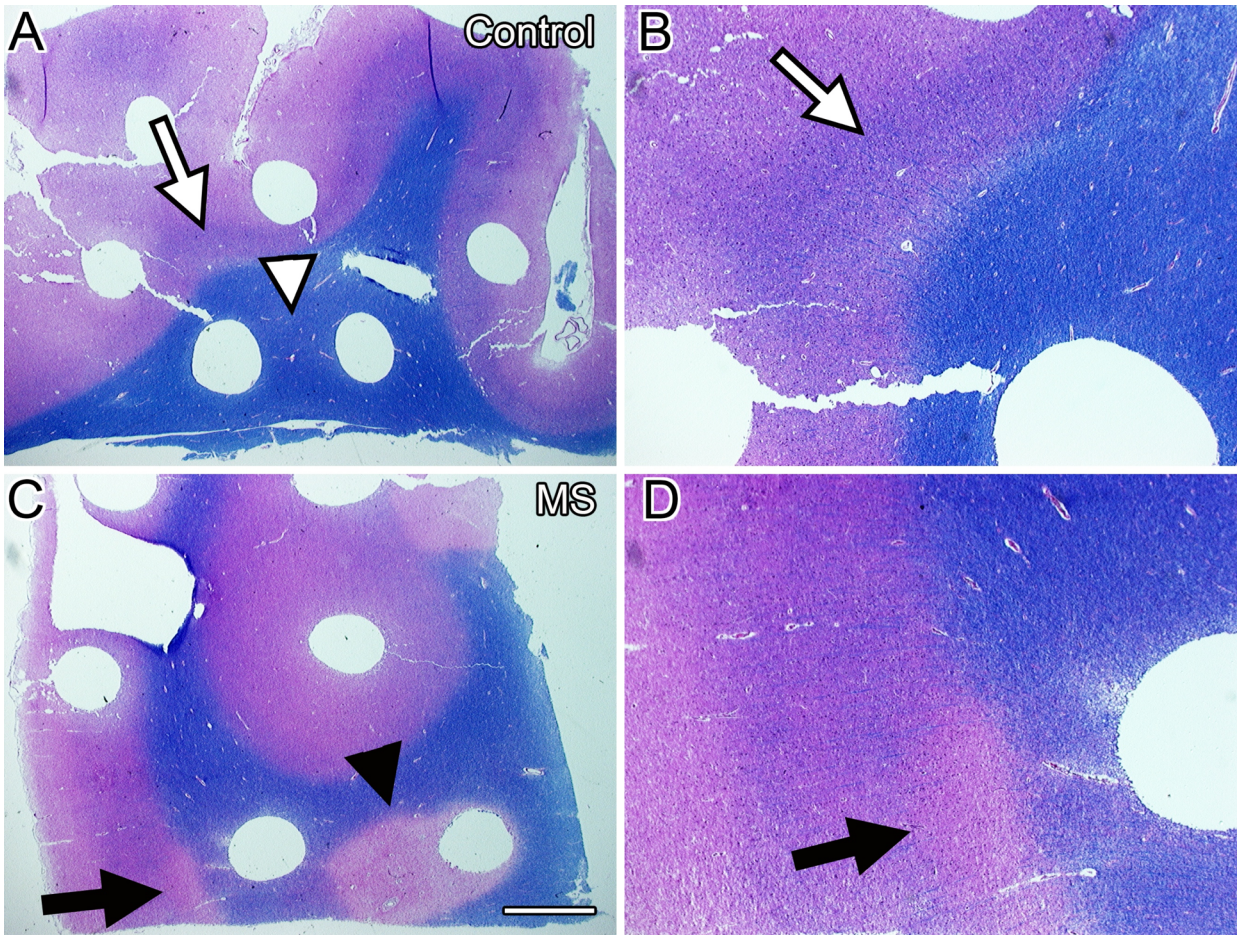

Figure 4.1 – **A**) LFB staining (blue) and H+E counter stain (pink and purple) in the cortex of a healthy control patient post-mortem sample**. B**) Enlarged portion of the control tissue indicated by the white arrow in **A** showing staining in deep gray matter with radiating myelinated fibers. **C**) LFB staining of MS tissue again showing intact myelin but also the presence of two micro lesions, one in the gray matter (black arrow) and one in the white matter (black arrowhead). **D**) Enlarged portion of the cortex indicated by the arrow in **C** from the MS tissue. It shows an area of pink, eosin only staining deep in the cortex and surrounded by intact myelin. Scale bar = **A**+**C** = 200μm, **B**+**D** = 75μm.

Figure 4.2 – Bielschowsky Silver Stain of MS Tissue

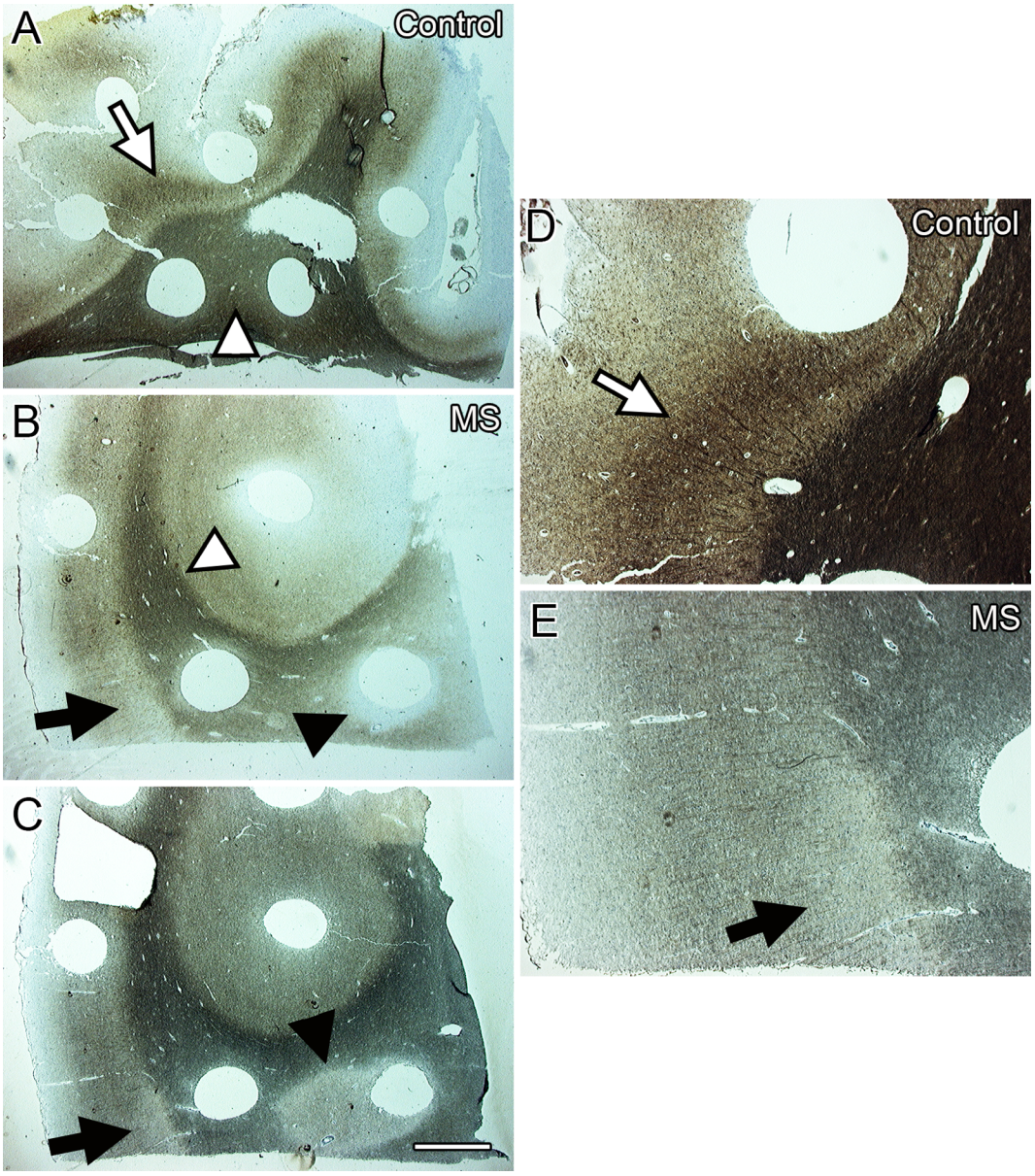

Figure 4.2 – **A**) Silver staining of control patient tissue showing dark axonal silver stain in myelinated areas (white arrowhead) and radiating fibers in gray matter (white arrow) that is enlarged in **D**. **B**) MS patient silver staining showing much of the same pattern as **A**, with the addition of potential lesions in white matter (black arrowhead) and gray matter (black arrow). **C**) Section matching LFB stain from Figure 4.1 showing definite white (arrowhead) and gray (arrow) matter lesions matching the locations in Figure 4.1 with gray matter enlarged in **E**.

classical feature of MS lesions such as perivascular cuffing and apparent immune infiltrates. Also, a deep gray matter lesion that was subtler, but nevertheless evident from the lack of LFB staining on the border of the deep blue gray matter, and surrounded on all sides by dispersed myelinated fibers in the cortex (Figure 4.1C,D). Compared to the control deep gray matter (Figure 4.1A,B, white arrow), there is a noticeable difference in the MS tissue. The remaining MS patients analyzed did not show evidence of lesion activity in the tissue for this analysis. However, this does show that the LFB technique is robust and sensitive to white and gray matter lesions of myelin, and that there is pathology occurring throughout the CNS of patients that is continually going undetected, indicating the need for better diagnostic criteria and a better understand of the disease process.

Next, the analysis was extended to include the modified-Bielschowsky silver stain for axons in the MS tissue. Unlike the original Golgi stain, the Bielschowsky modification is a shorter silver impregnation and fixing (7-14 days vs. 1 hour) and can be completed in one day with tissue mounted to slides rather than larger tissue blocks. Instead of filling certain neurons in the CNS, Bielschowsky silver appears to stain in a similar pattern to neurofilaments where cell bodies can be identified but the stain is more diffuse and can appear spindly, while axons appear as dense, dark brown or black structures. Slides adjacent to those used in Figure 4.1 were utilized for silver staining to test two points: first, do the lesions seen in Figure 4.1C and D all cause an alteration in silver staining and second, do the lesions change or disappear from adjacent slides as they should if the lesion is real and not an artifact of staining. In control tissue, there is consistent, dark silver staining throughout the white matter, similar to the dark LFB staining previously seen, indicating intact white matter (Figure 4.2A,D). There are also radiating fibers from the white matter into the deep gray matter that thin as they move into shallower cortical areas as predictive if the silver stain highlights axons where many of the largest will be located in the deep cortical regions (Figure 4.2A,D).

Figure 4.3 – End Stage LFB Histopathology in the *OBiden* Mouse

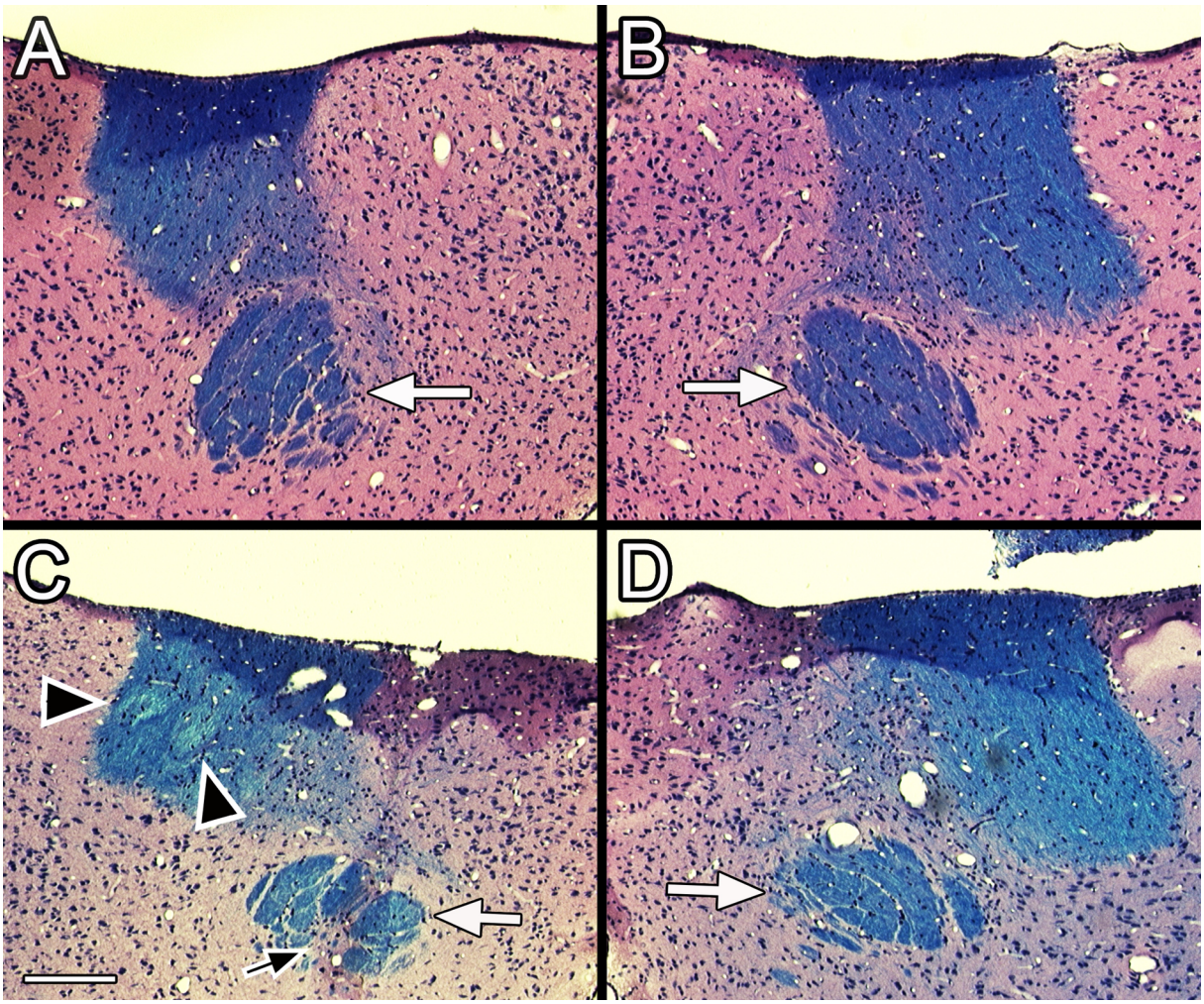

Figure 4.3 – **A**) LFB staining of the left stria medullaris in control mice. White arrow indicates an area of intact myelin stain. **B**) LFB staining of the right stria medullaris in control mice. **C**) LFB staining in the left stria medullaris of end stage *OBiden* mouse. Two areas of subtle demyelination are indicated by black arrowheads. An area of apparent myelin loss is indicated by the black arrow. **D**) LFB staining in the right stria medullaris of *OBiden* shows intact, normal appearing myelin compared to the contralateral side in **C**. Scale bar = 200μm.

Staining in the MS tissue showed many of the same patterns seen in control tissue, intact dark white matter staining and radiating gray matter fibers (Figure 4.2B,C,E). The stain also highlighted the changing shape of the gray and white matter lesions. When a slide was chosen adjacent to the lesion identified in Figure 4.1, there was a dramatic decrease in the size of the unstained white matter lesion area (Figure 4.2B, black arrowhead). Also, the gray matter lesion appeared larger and more diffuse in an adjacent slide, but changed to the deep, focal lesion when tissue immediate succeed the LFB tissue was stained (Figure 4.2B,C,E). The white matter lesion also expanded and was clearly evident in the silver stain, showing the same ovoid shape as in LFB staining. This indicates that both histological stains are appropriate to use on intact, control tissue and show robust staining patterns. In disease states, the stains are very susceptible to tissue integrity and their binding will be effected even by small disturbances, such as the deep gray matter lesion seen in Figures 4.1 and 4.2.

Histopathological Survey of OBiden Mice

The histopathological analysis of tissue was tested and extended to the *OBiden* mice. Given the robust nature of histological techniques, additional testing and optimization were not required to obtained good staining results. First, LFB series were completed on 6 and 12 month *OBiden* tissue to identify any detectable pathology in the tissue and similarities or differences to the human tissue (Figure 4.3). One issue that was encountered was the fact that the white matter tracts, especially in the neocortical area, are much smaller in mice than in humans so many pathologies are smaller than more focal than in MS. An example of the pathologies identified was in the stria medullaris, a white matter tract connecting the habenula with forebrain structures. In the control, there was consistent LFB staining in this tract similar to that see in the control patients (Figure 4.3A,B). In the *OBiden* animal the presence of unilateral, focal lesions was detected only in the left stria medullaris (Figure 4.3C,D). The pathologies included the presence of two hypomyelinated areas, either as a result of active demyelination or partial remyelination and the dropout of stain in a fiber bundle just ventral to the stria medullaris (Figure 4.3C,D). The presence

Figure 4.4 – Astrocytes and Microglia in White Matter of the *OBiden* Mouse

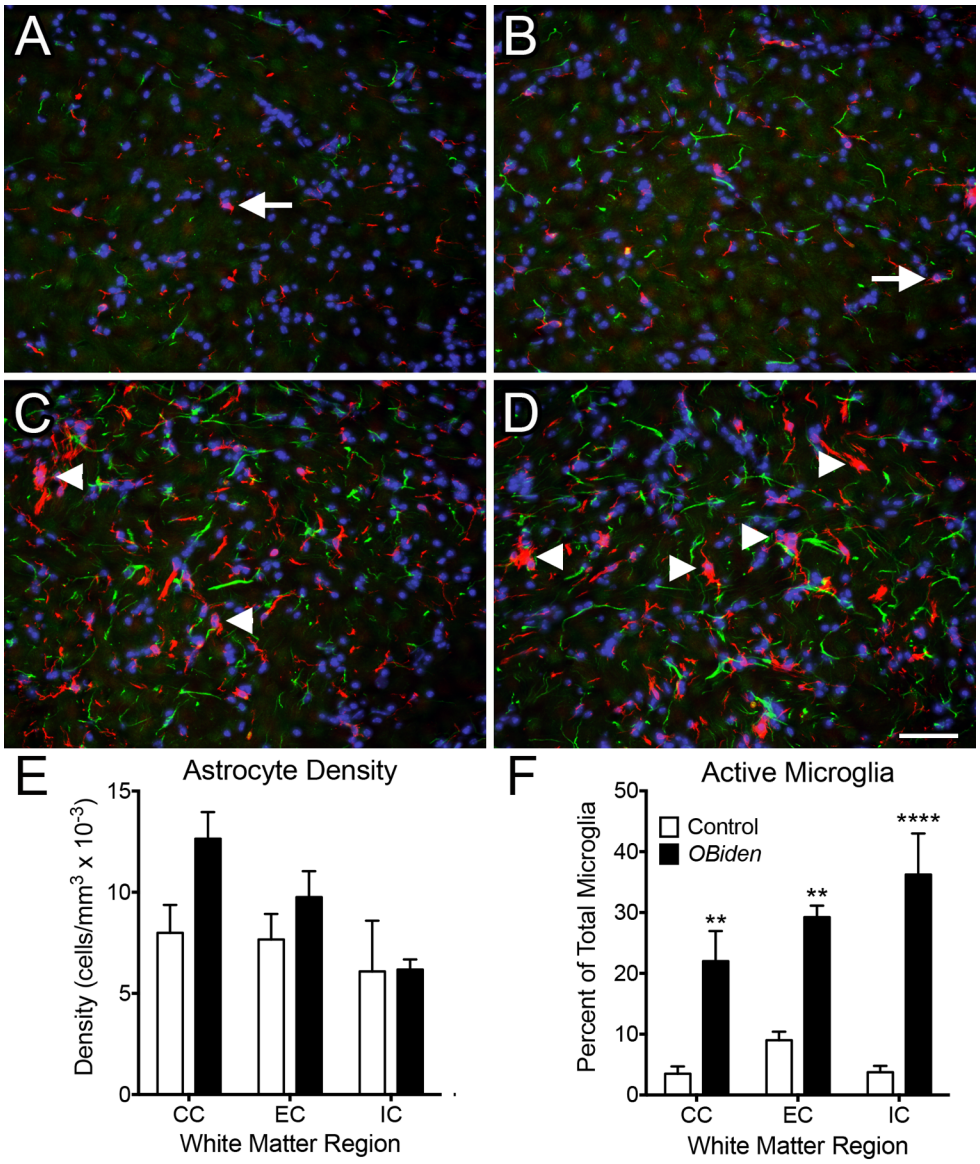

Figure 4.3 – **A**) Left and **B**) right control internal capsule. **C**) left and **D**) right *OBiden* internal capsule. **E**) Quantification of astrocyte cell density in white matter tracts; CC – corpus collosum, EC – external capsule, IC – internal capsule, showing no change in density. **F**) Percent total microglia with active morphology is increased in all white matter tracts in *OBiden* mice. Green = GFAP, Red = Iba-1, Scale bar = 25μm (n = 4 animals per group, 3 slides per animal).

Table 4.1 – White Matter Astrocyte and Microglia Statistics

Astrocytes in White Matter

ANOVA table	SS	DF	MS	F (DFn, DFd)	P value
Interaction	20.87	2	10.44	F (2, 18) = 1.169	P = 0.3331
WM Area	71.43	2	35.72	F (2, 18) = 4.001	P = 0.0365
Genotype	31.17	1	31.17	F (1, 18) = 3.492	P = 0.0780
Residual	160.7	18	8.926		

Control - *OBiden*	Summary	Adjusted P Value
CC	ns	0.1181
EC	ns	0.7052
IC	ns	> 0.9999

Active Microglia in White Matter

ANOVA table	SS	DF	MS	F (DFn, DFd)	P value
Interaction	15.65	2	7.823	F (2, 18) = 0.3421	P = 0.7148
WM Area	8.771	2	4.385	F (2, 18) = 0.1918	P = 0.8271
Genotype	858	1	858	F (1, 18) = 37.53	P < 0.0001
Residual	411.6	18	22.86		

Control - *OBiden*	Summary	Adjusted P Value
CC	**	0.0095
EC	*	0.0214
IC	**	0.0017

of unilateral lesions is encouraging as MS is not a symmetrical disease and can disproportionately affect the CNS, in addition, both the lesions show no signs of peripheral infiltrates indicating that oligodendrocytes stress can cause MS lesion-like damage.

As in the patient samples, *OBiden* tissue was run through silver staining and a number of pathologies were identified throughout the CNS (Supplemental Figure 4.1). In the brainstem pons nucleus there was a swollen neuron with evident buildup of silver staining at the axon hillock compared to control neurons in the area (Supp. Figure 4.1A,B). Moving to the cerebellum of one mouse, there was a cluster of axonal spheroids in the white matter of the flocculus (Supp. Figure 4.1C,D). In the control white matter, dark axons can be seen traversing the picture and look even in texture and diameter. However, in the *OBiden* animals, numerous black spheroids can be seen with axons exiting from one point of the spheroid (Supp. Figure 4.1D). These are swellings along the axon and a hallmark of neurodegenerative diseases, including MS (Adams and Kubik, 1952; Kornek and Lassmann, 1999). Finally, evidence of mild axonal pathology or loss was found in the external capsule in the neocortex (Supp. Figure 4.1E,F). Both the left and right external capsule showed evidence of decreased silver stain in the *OBiden* mouse, but only the left external capsule is shown. The control mouse as strong dark brown or black staining throughout the white matter, but in the *OBiden* mouse, there is a noticeable lightening of the stain similar to the gray matter lesion in the MS patients. Overall, the *OBiden* CNS looks similar to control and many of the pathologies are detectable at microscopic levels (Supp. Figure 4.2). This shows that although we are generating pathology, it is not the wholesale change or degeneration seen in other mouse models of disease.

Secondary Gliosis in the OBiden Mouse

The next analysis of the *OBiden* mouse was to determine the cellular reaction to these apparent disturbances in white and gray matter identified through histopathology. Specifically, the reaction of two types of glial cells, astrocytes and microglia, to the primary metabolic stress and whether this reaction is similar to those described in MS. The particular phenotype of interest is

the change of microglia from an inactive to an activated state, which occurs when the cells encounter cellular debris or injury in their local environment and work to remove the debris. Astrocytes and microglia were stained for using antibodies against glial fibrillary acid protein (GFAP) and Iba-1 (Calcium channel) and total cells of each type were counted, as well as the percentage of microglia that displayed and active vs. Inactive phenotype. The differential phenotype was defined by a thin cytoplasm and long, branching processes for inactive cells, and 3x enlarged cytoplasm, a bipolar or amoeboid shape and ramified processes for the active state.

First, the density of GFAP+ astrocytes was determined across all white matter regions in the neo cortex at the level of the dorsal hippocampus. There was no difference in astrocyte density between control and *OBiden* mice at 12 months of age (Figure 4.4A,B,E). There was also no apparent overall increase in GFAP immunoreactivity away from cell bodies that would indicate areas of astrocyte differentiate, migration or phenotypic alterations (Figure 4.4A,B,C,D). This eliminated the more structurally and metabolically supportive astrocytes from gross disturbances in the white matter of *OBiden* mice.

Second, the number of microglia was determined and what subset of the microglia displayed an activated instead of an inactive, resting morphology. There was a significant increase in the proportion of activated microglia in the *OBiden* mice in all white matter tracts (Figure 4.4A,B,C,D,F). As indicated by the arrowheads in Figure 4.4, the activated microglia appear more pronounced with Iba-1 staining because of the enlargement of their cytoplasm where the Iba-1 protein is located. The glial activation in the *OBiden* mouse is also more focal than in other degenerative diseases, with only a few cells activated in a patch rather than all cells throughout the white matter. This could be related to the lower level of stress that requires long term accumulation to manifest the more canonical signs of neurodegenerative disease. A secondary confirmation of the activation of the microglia was obtained by staining with the marker CD68, a lysosomal protein expressed in microglia and highly upregulated when

microglia are actively phagocytosing debris. Numerous examples of CD68+/Iba-1+ cells were found in the *OBiden* mice with high levels of CD68 staining throughout the cell (Supp. Figure 4.3B,D,F). In the control, most Iba-1+ cells did not express CD68, and in the few instances they did it was low expression and confined to a small portion of one branching process (Supp. Figure 4.3A,C,E). These changes indicate and increased prevalence of activated microglia in the *OBiden* CNS compared to controls.

Additional Phenotypic Observations

The gross pathological features of the *OBiden* mouse and their similarities to MS are an important connection to make. Further, there are subtler and microscopic pathologies that appear in the *OBiden* animals that are less frequent, yet still match disease phenotypes. One of these pathologies is axonal spheroids. They are enlargements and swellings along an axon that precede neuronal transection and can be transported along axons and cleared, but are prevalent in neurodegenerative diseases and one marker of neuronal stress. Because the diameter of axons is tightly regulated and is relatively invariable, compared to dendrites that can swell and contract depending on osmotic pressure, spheroids are a useful marker of neuronal injury.

In the *OBiden* mice, two different antibodies were used to detect spheroids in 6 month old animals in a preliminary study. The first set of experiments was a co-stain with neurofilament light chain (NF-L) and synaptophysin (SYP). NF-L is a structural protein in axons and should be abundant especially in white matter regions where axons are densely packed. SYP is a synaptic transmembrane protein that is transported along axons as an mRNA for translation at the synapse or a protein that has been synthesized in the soma. In Figure 4.5, an example of a SYP+ spheroid in the external capsule of the *OBiden* mouse is shown. There is a clear buildup of SYP that colocalizes with NF-L in the axon extending from one side of the spheroid (Figure 4.5, arrow). In the surrounding axons there is little to no SYP staining as would be expected if neuronal function and transport were not impaired and the protein was being moved efficiently in the anterograde direction.

Figure 4.5 – Synaptophysin Spheroid in White Matter of the *OBiden* Mouse

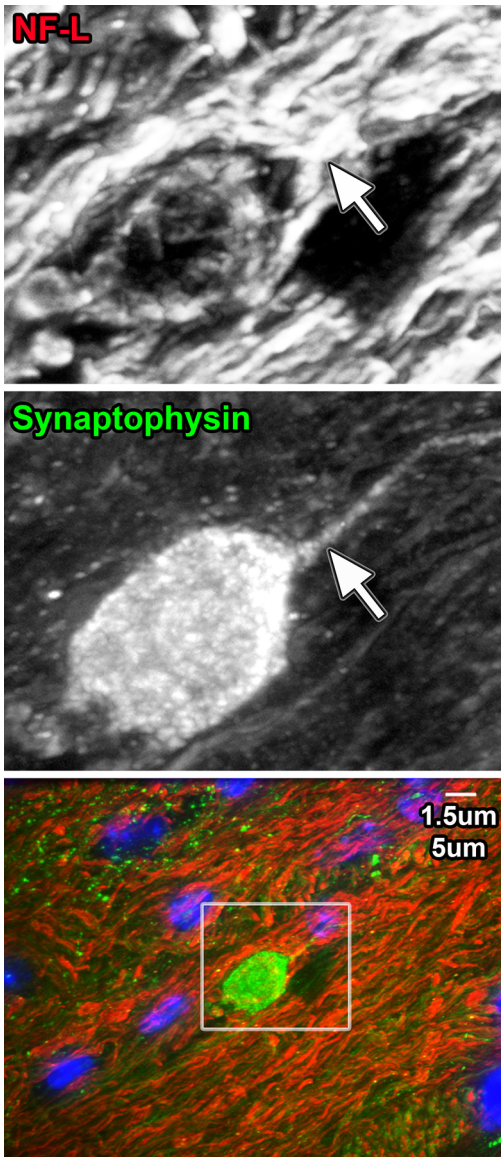

Figure 4.5 – Staining from 6 month old *OBiden* external capsule (white matter) showing the development of a synaptophysin (SYP)+ spheroid (green). The section was co-stained for NF-L to highlight the majority of axons. The spheroid has a clear buildup of SYP in the axon proximal to the spheroid (arrow) as well as the spheroid itself. An axon was only found on one side of the spheroid indicating a possible transection.

Figure 4.6 – Gray Matter Spheroid in the cortex of the *OBiden* Mouse

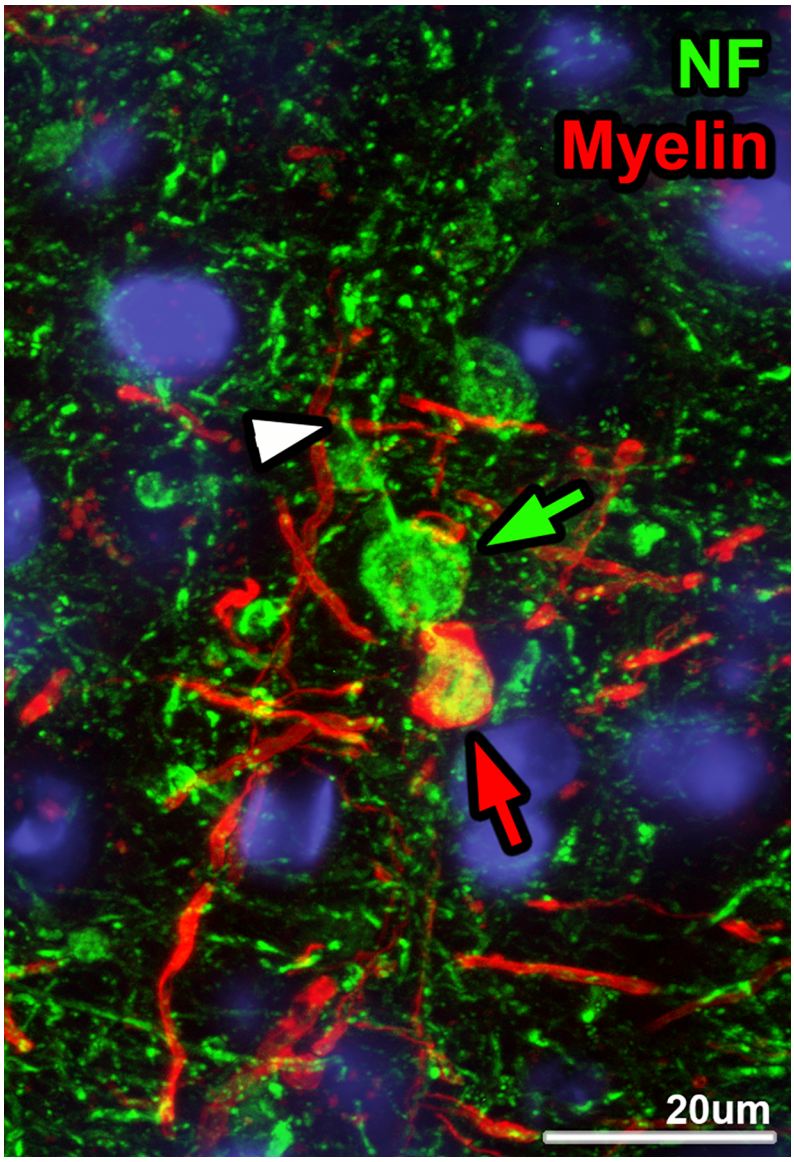

Figure 4.6 – Staining of an example axon in the cortex of an *OBiden* mouse showing the development of multiple neurofilament medium/heavy (NF-green) spheroids (arrows). The green arrow indicates a spheroid occurring at an unmyelinated portion of the axon. The red arrow shows a spheroid occurring underneath a myelin internode. The white arrow is the normal axon entering the spheroids.

In addition to white matter spheroids, gray matter spheroids also develop in the *OBiden* model, as well as MS. Figure 4.6 shows an example of a cortical spheroid in the *OBiden* mice. In these animals, the myelin of oligodendrocytes expression mutant protein is labelled with eGFP (false colored to red in the figure) and the antibody SMI32 (neurofilament heavy and medium chain) is used to counter stain axons. The figure shows an intact axon that developed two spheroids in close succession, one in an unmyelinated region and one developing underneath a myelinated internode (Figure 4.6). The development of the spheroids in a different CNS region is an indicator of the extent of secondary pathology in the CNS. Also, a spheroid developing under an internode is important as it shows axonal pathology can develop while myelin is still present. It does not require demyelination to result in pathology, and shows the usefulness of a model with a well-defined primary etiology and the ability to study the secondary effects of that pathology.

Discussion

The characterization of the *OBiden* tissue to MS post-mortem samples allowed for a number of facets of the model to be evaluated. The extent, location, and distribution of pathology was investigated and compared to the changes seen in the CNS of patients. This showed that in MS NAGM and NAWM, as well as lesioned areas, the *OBiden* mice showed similar pathologies including decreased LFB staining and alterations to silver stained axons. Possibly of greater importance, thought, was that some of the pathologies were focal and even unilateral within the CNS. MS can be a heterogeneous disease with intra and inter patient variability of the location, extent and type of pathology. Although this does introduce a degree of difficult if the *OBiden* pathology mirrors the MS pathology in its variable generation, it will allow for the identification of consistently affected areas, as well as possibly leading insights into why there is such variability in the first place.

Part of the variability may be due to secondary factors such as the local glial environment of astrocytes and microglia in the vicinity of effected oligodendrocytes. These cells will react to

changes in their local environment including retraction and alteration of processes and the upregulations of phagocytic markers in the case of microglia. These are well known phenotypes in MS patients, especially within and around white matter lesions. The *OBiden* mice also develop this phenotype and interestingly it is more pronounced than the lesions detected through histological techniques. This may lead to interesting future observations as it could mean that before there is overt demyelination, there are significant changes to oligodendrocyte structure or function that surrounding astrocytes and microglia react to. Although this is not a new concept, the *OBiden* model may be well suited to study the interactions between the cells given its relatively mild level of pathology compared to models with more overt demyelination.

The interest in microglia and astrocytes lies in the possibility of modulating these cells and creating a neuro/oligo protective environment to delay or alter the courses of disease. Evidence exists that these cells are critically important in the normal functioning of the CNS and therefore changes to their state or functioning could be contributing to disease (Chen et al., 2010; Tang and Le, 2016; Trapp et al., 1999). Specifically, microglia are sensitive to changes within the CNS either through their surveillance of synapsis or clearing debris from stressed or dying cells. Loss of microglia causes dramatic phenotypic changes and alterations to behavior, highlighting their importance to the stability and functioning of the CNS (Chen et al., 2010).

In addition to the above pathologies, it is important to document secondary neuronal pathologies in line with MS. One of the characteristics of MS, and many neurodegenerative diseases, is the development of axonal spheroids and swellings. The *OBiden* mouse indeed develops these pathologies, evident in both the white and gray matter of the mice.

Although these features have been noted for years in diseases, the cause of spheroids and their effect on neuronal soma remains incompletely understood. There is evidence of synaptic, axonal and soma proteins within spheroids, indicating that retrograde and anterograde transport may be effected as well as remodeling of resident neuronal proteins. The *OBiden* model could offer interesting insights into the development of this pathology and its time course. Pathology

could be directly related to trophic support and release of metabolites or exosomes from oligodendrocytes to axons, or if it could be more related to structural support (Acharjee et al., 2013; Oluich et al., 2012; Southwood et al., 2013).

CHAPTER 5 – SECONDARY NEURODEGENERATIVE CHANGES IN THE *OBIDEN* MOUSE AND SIMILARITIES TO MS TISSUE

Introduction

Many models of CNS diseases achieve changes through sudden, massive stresses, alterations to protein expression or massive protein overexpression to trigger degeneration (Brockschnieder et al., 2006; Hampton et al., 2013; Traka et al., 2016). There are advantages in these models including short time courses and rapid disease development. However, they are often limited by the intensity of the pathology hampering physical or behavioral testing of animals and the systemic, acute nature of the pathology only reproduces a subset of the pathologies seen in patients. This has opened to door for the development of more chronic, longitudinal models that may recapitulate more of the underlying degeneration of disease, like MS, that are most debilitating to patients and, so far, lack reliable efficacious treatments.

The *OBiden* model is a disease model designed to use a known endogenous stressor to the CNS to initiate disease progression. These mice develop behavioral and cognitive deficits over time as a result of the chronic, primary metabolic stress that is present even at end stage ages in the mice. In addition they develop prototypic pathologies seen in neurodegenerative diseases, such as focal lesions, secondary gliosis and axonal spheroids that are all characteristic secondary reactions in many diseases including MS (Adams and Kubik, 1952; Staugaitis et al., 2012).

However, many of those pathologies are general, found throughout the tissue and especially it active, chronic or inactive lesion areas in MS. As the *OBiden* mouse appeared grossly normal, it became apparent that comparing it to MS tissue should involve an area of subtler pathology. This meant utilizing what is referred to as Normal Appearing Gray Matter (NAGM), areas that appear grossly normal upon neuropathological examination. Recent evidence has indicated that this is a simplistic view and the NAGM, and NAWM (white matter), can show signs

of degeneration at a molecular level, before it reaches the point of developing into macroscopic lesions (Kearney et al., 2015; Llufriu et al., 2014; Seewann et al., 2009).

One aspect of lesion development is alterations to the neurofilament profile in neurons. Whether it is changing the phosphorylation state or the amount of neurofilaments detectable by western blotting, either light, medium or heavy chain neurofilaments, and these alterations are detectable before lesions develop (Hares et al., 2016; Huizinga et al., 2008). In MS in particular, lesions and neurodegeneration can result in the release of neurofilaments into interstitial fluid eventually leading to the detection of neurofilaments within the CSF (Bacioglu et al., 2016). Identifying and monitoring changes to neurofilament populations within the *OBiden* mouse would allow for correlations with MS tissue and confirming that the primary oligodendrocyte stress is capable of recreating similar neuronal dysfunction as seen in the human disease.

Interestingly, the neurofilament genes are of variable importance for axon integrity and stability. Neurofilament heavy chain (NF-H), for example, is necessary for creating axons of large calibers, but is not necessary for expression or correct arrangement of neurofilament medium (NF-M) or light chain (NF-L) or microtubules (Elder et al., 1998b). However, NF-M is important not only for the expression of NF-L but also correct trafficking of the protein from the soma to the axonal compartment (Elder et al., 1998a; Jacomy et al., 1999). Although the exact nature of neurofilament interactions and how they affect each other and their importance to neuronal architecture are still debated, changes to neurofilament populations do affect neuronal function and are a potential indicator that more severe pathology may develop.

Following the general neurofilament changes, more specific alterations to neuronal structure were investigated to identify novel pathologies in the *OBiden* mouse, their correlation to MS and to open areas of investigation into the function significance of those pathological changes. The more specific pathology identified in *OBiden* mice was found to relate to the axon initial segment (AIS). This is a substructure of the neuron in the proximal axon, but distal to the axon hillock, that contains high concentrations of sodium, potassium and calcium channels to initiate

individual or trains of action potentials (Kole and Stuart, 2012; Rasband, 2010). Additionally, recent evidence has implicated the AIS in the setup and maintenance of neuronal polarity, filtering of axonal cargo and a target of injury in neurodegenerative diseases (Kole and Stuart, 2012; Rasband, 2010; Schafer et al., 2009). These functions make the AIS a critically important component of the neuron and neuronal function and disruptions to its structure or function are likely to have significant downstream consequences.

The AIS is a rigorously organized structure with a periodic arrangement of scaffolding proteins β4-spectrin and Ankyrin-G (AnkG) working to organize sodium channel variants such as $Na_v1.2$ and 1.6 and potassium channels $K_v4.1$-4.4 and $K_v7.1$-7.3 (Inda et al., 2006; Kuba et al., 2015; Trimmer, 2015). Through the distribution and organization of these channels, as well as their proximity or distance to the soma, the AIS is the location for control of the tone, threshold and hyperpolarization of the action potential. The influence on the AIS is not only driven by the proximal soma but also by extensive axo-axonic synaptic connections arising from interneurons and contralateral cortical connections (Fish et al., 2013; Wefelmeyer et al., 2015). Due partly to this complexity of channels, inputs and structure, the AIS is susceptible to changes of neuronal state, input signals and changes to downstream targets and the can alter its state and composition in turn (Kuba et al., 2014).

Important to the *OBiden* project is the scaffolding protein AnkG and the potassium channel variant $K_v7.2$. AnkG is specifically located at the AIS, and Nodes of Ranvier, because it has an actin interacting domain, spectrin interacting domain as well as binding properties to ion channels (Ho et al., 2014; Susuki and Rasband, 2008). Also, AnkG is critical for the formation of the AIS and establishing neuronal polarity, although interestingly, it is not necessary once the AIS has been established in maintaining neuronal polarity and AIS function (Song et al., 2009). AnkG is then useful as a marker for the location, size and proximity to the soma of the AIS, and is currently the marker used to define its limits.

The main ion channel of interest is the potassium channel variant $K_v7.2$, a fast-activating, slow-inactivating voltage gated ion channel that is critical for setting the tone of the neuron by modulating the M-current (Hernandez et al., 2008; Ikeda and Kammermeier, 2002). The M-current is a prolonged current influx that maintains the AIS below threshold potential to prevent firing of additional action potentials. This allows for long term modulation of neuronal tone and prevents aberrant firing of action potentials or propagation of a spreading potential as is found in the epilepsy patients harboring $K_v7.2$ mutations (Delmas and Brown, 2005; Kuba et al., 2015). This makes the channel critical for correct neuronal function and alterations to its abundance, location or distribution could cause changes to neuronal function, animal behavior and even offer predictions as to the likely electrophysiological changes that would be observed.

Materials and Methods

Tissue Collection

Mice were anesthetized with 375mg/kg of a 2.5X dose of 2-2-2 tribromoethanol (TBE) made in 2-methyl-2-butanol at 40X and diluted in 1X PBS with vortexing to the working concentration. The thoracic cavity was opened on the mice and a catheter was inserted into the left ventricle while a small cut was made in the right atrium. Next, 4% paraformaldehyde (PFA) dissolved in 0.1M Phosphate Buffer pH 7.2 was allowed to flow through the catheter by means of gravity for 15min until the mouse was ridged and fixed. Brains were dissected by removing the skull from the body, removing the lower mandible and making a vertical cut through the hard palate. Next, the ventral skull was broken away until the optic chiasm was revealed and the optic nerves were cut rostral to the optic chiasm followed by an incision along the midline of the skull moving rostral from the forman magnum to the olfactory bulbs. The skull was then removed, the brain extracted and tissue of interest placed in 12.5% sucrose in1X PBS for 6-8 hours followed by placing the tissue in 25% sucrose overnight. Finally, tissue was placed in tissue molds, covered with OCT embedding media and frozen by slowly submerging in dry-ice cooled 2-methyl butane.

Frozen tissue sections were cut between -18°C and -20°C and attached to Fisher Superfrost Slides and immediately stored in a slide box on dry ice. Slides were maintained at -20°C until use, at which time they were thawed in three, 10min washes of 1x Phosphate Buffer Saline (PBS) pH 7.5. Following washes, one of four permeabolization/blocking steps were used to remove lipids and create holes in the tissue for a more thorough and consistent infiltration by primary antibodies.

Staining Protocol

Phosphate Buffer/Goat Serum/Triton X-100 – (Adpated from Ho, et al, 2014) Pap pen is applied around tissue that has been thawed in 1xPBS. The permeabolization and blocking steps are combined into one step by adding a solution of: 0.1M Phosphate Buffer, 0.3% Triton X-100, and 10% Goat Serum (PBTGS) for one hour while the slides are horizontal and not rocking. For the addition of primary antibodies, the old PBTGS is removed and antibodies are diluted in fresh PBTGS and added to sections. The sections must be maintained horizontal and cannot rock as rocking will cause the high Trinton X-100 content to dissolve the Pap pen and potentially allowing the solution to leak off the tissue sections.

Primary Antibodies – Primary antibodies are diluted in either TBSGBA-2%Gts or PBTGS, depending on the blocking solution, and up to three antibodies are diluted in one solution. 100-150µl of diluted antibodies is placed on each tissue section and for TBSGBA-2%Gts the sections are rocked overnight, but for PBTGS staining the slides are left in the damp chamber on the bench top overnight as rocking can cause the Triton to remove the pap pen and cause antibody run off from the sections. Sections from control and experimental animals were also taken for no primary controls to test the non-specific secondary staining, and in these cases the tissue received only blocking solution with no antibodies for overnight incubation. After staining, slides are washed three times for 5-10min in 1x PBS.

Secondary Antibodies – Isotype specific antibodies were used against primary antibodies, and all secondary antibodies are diluted at 1:1000 in TBSGBA-2%Gts. The most common fluorophores conjugated to secondary antibodies are Alexa488 (green), Alexa568 (red) and Alexa647 (infrared), as well as the addition of DAPI at 1:1000 to all secondary antibody mixes. Secondary antibodies were added to sections for 3 hours, with rocking, then washed in 1x PBS, 3 times for 5-10mintes each. Following washes, the pap pen was removed with a Q-tip dipped in chloroform, and then a drop of Vectashield to prolong fluorescence was added to each slide before the addition of the coverslips. Coverslips were allowed to settle overnight on the slides while at 4^{C} before excess Vectashield was vacuumed off and coverslips sealed to the slides with nail polish. Slides were stored at 4^{C} to prolong fluorescence before image acquisition.

Table 5.1 – Axon Initial Segment Related Primary Antibodies

Antigen	Isotype	Name	Cell/Structure	ICC Dilution	Permeabolize	Company	Product#
Parvalbumin	Ms IgG1	PARV	interneurons	1:2000	MeOH	Sigma	P 3088
Ankyrin-G	Ms IgG2a	ANK-G	axon initial segment	1:300	Triton/PBTGS	NeuroMab	75-146
Phophorylated Neurofilament Heavy Chain (P-NF-H)	Ms IgG1	SMI31	neurons	1:1000	MeOH/Triton	Covance	SMI-31P
Nonphosphorylated Neurofilament Heavy Chain (NF-H)	Ms IgG1	SMI32	neurons	1:1000	MeOH	Convance	SMI-32P
Pan Sodium Channels	MS IgG1	Na Channel	nodes/AIS	1:100	MeOH	Sigma	S8809
Sodium Channel Variant 1.2	Ms IgG2a	Nav1.2	Sodium Channels	1:100	MeOH/Triton	Antibodies Inc.	73-024
Sodium Channel Variant 1.6	Ms IgG1	Nav1.6	Sodium Channels	1:100	MeOH/Triton	Antibodies Inc.	75-026
Potassium Channel Variant 7.2	Ms IgG1	Kv7.2	Potassium Channels	1:10	Triton/PBTGS	Antibodies Inc.	73-079
COUP-TF Interacting Protein 2	Rt IgG2a	Ctip2	Post-Mitotic Pyramidal Neurons	1:300-1:500	Triton/PBTGS	Abcam	ab18465 (clone 25B6)
NeuN	Ms IgG1	NeuN	Neurons	1:1000	All	Millipore	MAB377

AIS Analysis

AIS Length Analysis – Confocal pictures were taken on a Leica microscope with Orca R2 camera and Melles-Girot Spinning Disk laser. Picture stacks were taken of 10um thick cryostat sections at 0.3um step size with 25-30 pictures taken per stack. Stacks were flattened to produce a maximum intensity projection image, which was used for subsequent analysis. Each color channel (RGB) was imported into FIJI for ImageJ, automatically brightness/contrast adjusted and then color combine into an RGB image. The line tool was then selected and changed from a straight to freehand line to account for curves in the AIS. Next, the image was zoomed in 2x to make the AIS easier to identify, where the proximal end identified by the end of the ankyrin-G

staining closest to the NeuN+ cell body. The ankyrin-G staining also had to form railroad track-like pattern (e.g. ||) before it terminated to be used for analysis and the distal end was considered valid when it tapered to a point below the resolving power of the microscope and was not truncated where a square end could easily be identified. When the AIS met the above criteria, a line was drawn from the proximal to the distal end and the length measured, at least 5 AIS lengths were measured per picture at 40x magnification (213um x 163um picture dimensions). 6 images were analyzed per animal, 3 from matched left and right cortices, and the all AIS lengths for each animal were plotted as a cumulative frequency with bins of 2um, starting at length 0 and ending at 40um. This gave a roughly sigmoid curve for each animal, and the curves were averaged together within genotypes to get the average cumulative frequency, and then a Gaussian distribution was fit to the curves and the analyzed to determine if the shape, rise, or amplitude of the curves were different.

Hippocampus AIS analysis – 40x pictures were taken of CA1 layer in dorsal (DHC) and ventral (VHC) hippocampus. The CA1 layer as defined as the cell dense layer either dorsal to the dentate gyrus and CA3 in DHC, or lateral to those structures in VHC and an area roughly halfway along the length of the CA1 layer was chosen as being representative and to avoid contamination from CA2. Image stacks were taken through ~8um of the 10um tissue slice, and combined into single images in Metamorph imaging software. The combined images were moved into FIJI where black and white images were color merged to obtain RGB images with DAPI=blue, Kv7.2=green and Ankyrin-G=red. For the analysis, a rectangle 50 pixels wide (~8um, or one cell body) and 700 pixels long (~110um) and was centered over CA1 to account for AIS that exited from either direction of CA1, even though CA1 axons should exit the same direction. The analysis always began on the medial or dorsal part of CA1 and then moved laterally or ventrally, with the box placed, measured to stamp its location that the color profile obtained for each line of pixels along the length of the analysis box. This gave us RGB output graphs where intensity in each channel could be plotted for each portion of CA1. At least 10 analysis boxes were used per image and 3

Figure 5.1 – Gray Matter Neurofilament and Structural Western Blot

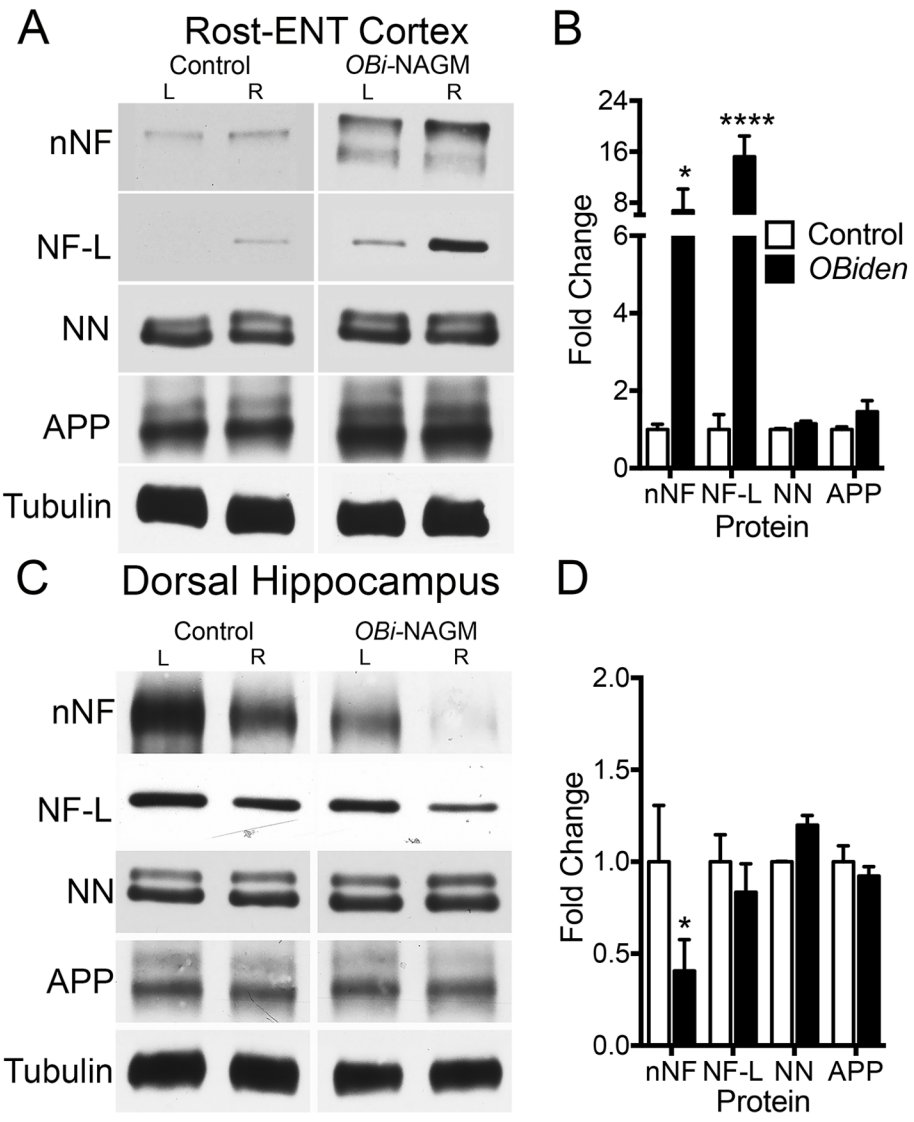

Figure 5.1 – **A**) Representative bilateral western blots from a control and *OBiden* animal taken from the rostral entorhinal cortex. **B**) Quantification of normalized western blot signals showing an increase in nNF and NF-L without an increase in neuronal NeuN or synaptic APP. **C**) Representative bilateral western blots from dorsal hippocampus of control and *OBiden* mice. **D**) Quantification of normalized western blot signals showing a decrease in nNF in *OBiden* mice without changes to NF-L, NeuN or APP (n= 4 per group)

Table 5.2 – Gray Matter Neurofilament Related Western Blot Statistics

Rost-ENT Cortex

ANOVA table	SS	DF	MS	F (DFn, DFd)	P value
Interaction	323.3	3	107.8	F (3, 43) = 9.549	P < 0.0001
Protein	323.3	3	107.8	F (3, 43) = 9.549	P < 0.0001
Genotype	307.6	1	307.6	F (1, 43) = 27.26	P < 0.0001
Residual	485.3	43	11.29		

Control - OBiden	Summary	Adjusted P Value
nNF	*	0.0281
NF-L	****	< 0.0001
NN	ns	> 0.9999
APP	ns	0.998

Dorsal Hippocampus

ANOVA table	SS	DF	MS	F (DFn, DFd)	P value
Interaction	0.4318	3	0.1439	F (3, 16) = 2.438	P = 0.1022
Protein	0.4318	3	0.1439	F (3, 16) = 2.438	P = 0.1022
Genotype	0.1356	1	0.1356	F (1, 16) = 2.296	P = 0.1492
Residual	0.9446	16	0.05904		

Control - OBiden	Summary	Adjusted P Value
nNF	*	0.0482
NF-L	ns	0.9038
NN	ns	0.8305
APP	ns	0.9936

left and right images were analyzed per mouse. All left and right images were averaged separately to give a left and right average for each animal in case of side bias or slightly unmatched sections, as hippocampal structure can change quickly in the rostral-caudal direction we were cutting slides. When each average curve was obtained, they were integrated without smoothing to obtain a curve giving the change in intensity across CA1, where regions of higher intensity would give greater integral changes and a larger subsequent area under the curve (AUC). AUCs were calculated for each stain, in each animal, bilaterally and then averaged together to get composite AUCs for each genotype.

Results

Gray Matter Neurofilament Changes in OBiden and MS

Aged *OBiden* mice at 12 months old were sacrificed and 1.5mm tissue punches were obtained and immediately frozen. Various gray matter regions were analyzed, through western blotting, to determine the overall integrity of the tissue and to identify any general changes to neurofilament proteins as a sign of degeneration. To control for the state of the tissue markers for neurons, NeuN, and synapses, amyloid precursor protein (APP), were utilized as well as loading control of α-Tubulin (Figure 5.1A,C). In two gray matter regions, the rostral entorhinal cortex (Rost-ENT) and dorsal hippocampus, there were no differences in NeuN or APP signal after accounting for loading and comparing control and *OBiden* mice (Figure 5.1 B,D)(Table 5.2-5.3). This shows that what appeared grossly normal under MR and visual evaluation at the time of dissection is molecular normal at least at the level of the abundance of neuronal and synaptic markers. However, when analyzing the neurofilament profile obtained from non-phosphorylated neurofilament (nNF) and neurofilament light chain (NF-L), there were differences between the control and *OBiden* groups. In the Rost-ENT cortex, there was a significant increase in the amount of nNF and NF-L in the *OBiden* cortex compared to controls (Figure 5.1A,B). In addition, there was an increase in the NF-L signal, indicating an area of potential neurofilament buildup. The

dorsal hippocampus showed a different, although still altered, signature with a decrease in the nNF signal, without changes to any other proteins including NeuN or APP (Figure 5.1C,D). The changes in the dorsal hippocampus could the result of the beginning of trimming neuronal processes, or neurons in the region have already undergone a buildup of neurofilament proteins and have since released some giving the decrease detected on western blots. Together, they show that the *OBiden* mice have alterations to their neurofilament profile, as detected across neurodegenerative disease.

In order to confirm that the *OBiden* mice look like MS, samples of normal appearing gray matter (NAGM) without gross neuropathological lesions, were punched in gray and white matter and the gray matter punches were used for the same analysis as *OBiden* mice. As with the *OBiden* mice, there was no change to the overall level of NeuN or APP proteins, indicating that what appeared as NAGM physically, showed no difference between control and MS patients on a molecular level (Figure 5.2). Similar to the *OBiden* cortical tissue, the MS cortical punches showed a significant increase in the amount of nNF present in the cortex (Figure 5.2). This confirmed two ideas, first, the MS and *OBiden* cortical tissue share similar molecular changes and second, that so-called NAGM, is not always normal, and there are potential underlying pathologies that are currently undetected until autopsy.

In addition to the entorhinal cortex and hippocampus, another cortical area called the piriform cortex was analyzed in *OBiden* mice for signs of changes. The piriform cortex receives much of its input from the olfactory tract and outputs to the entorhinal cortex and amygdala to control memory and response to odorant stimuli (Wang and Sun, 2012). Part of the piriform cortex was used to test antibodies, but the results showed similarities to the other cortical tissue tested from *OBiden* mice and MS patients. There was an increase in the mean nNF signal in the piriform cortex, however, because of increased variability in the tissue samples, this change was not statistically different (Supp. Figure 5.1). The change, though, was in the direction of other cortical

Figure 5.2 – MS Patient Cortical Neurofilament Western Blot

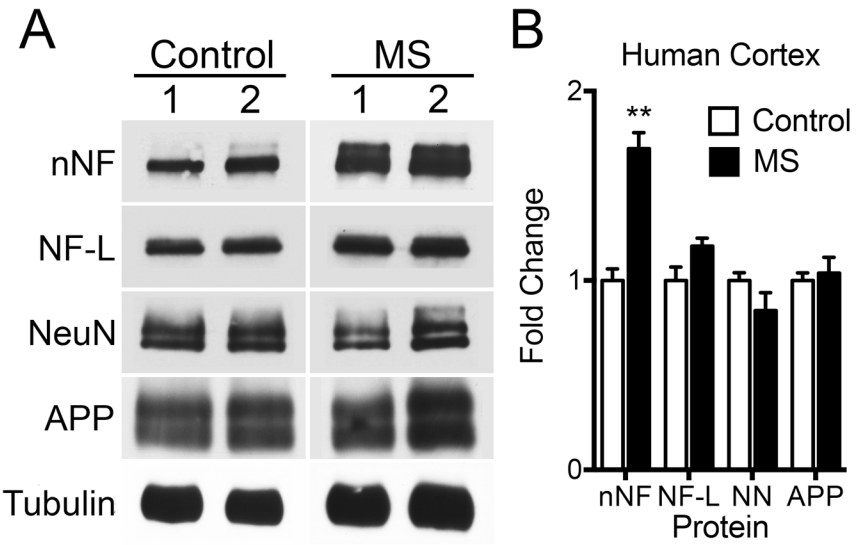

Figure 5.2 – **A**) Representative blots from two control and two MS patients' cortical gray matter blotted against neurofilament (nNF, NF-L) proteins and neuronal and synaptic parkers (NeuN and APP, respectively). **B**) Quantification of neurofilament western blots showed an increase in the nNF signal and no changes in any other protein analyzed including normal levels of NeuN and APP (n = 5 per goup)

Table 5.3 – MS Patient Western Blot Statistics

MS Normal Appearring Gray Matter

ANOVA table	SS	DF	MS	F (DFn, DFd)	P value
Interaction	0.8001	3	0.2667	F (3, 24) = 14.44	P < 0.0001
Protein	0.8001	3	0.2667	F (3, 24) = 14.44	P < 0.0001
Genotype	0.2827	1	0.2827	F (1, 24) = 15.31	P = 0.0007
Residual	0.4432	24	0.01847		

Control - OBiden	Summary	Adjusted P Value
nNF	****	< 0.0001
NF-L	ns	0.2625
NN	ns	0.3711
APP	ns	0.992

areas and could be a sign that the piriform cortex is at an earlier stage of degeneration and has not undergone sufficient pathological changes to be significantly different from controls.

Axon Initial Segment in the OBiden Mice

Neurofilament changes are an indication of pathological mechanisms at work in the *OBiden* and MS tissue, however, they are a more generalized pathology. To identify if the *OBiden* mice developed any novel pathologies, or specific secondary neuronal changes, a more in-depth analysis of neuronal structures was performed. For the beginning analysis, the concentration of NeuN+ neurons in comparable cortical areas showed no difference between control and *OBiden* mice (Figure 5.3A,B). This analysis was to determine if the overall number of NeuN+ neurons has changed between comparably regions of control and *OBiden.* A loss of neurons in *OBiden* mice would have been another confirmation of a secondary degenerative phenotype in response to primary oligodendrocytes stress, and could have implied the remaining neurons have substantial increases in intracellular neurofilament as detected from western blotting in Figure 5.1A. As an additional control, the percentage of NeuN+ cells with an intact, normal appearing DAPI+ nucleus was determined to confirm they were cells and none of the nuclei appeared to be blebbing, fractured, or exhibiting any signs of apoptosis (Figure 5.3C).

After confirming the presence of intact neuronal cells, the focus was shifted to specific subdomains within the neurons. The analysis began by staining for the AIS of neurons in the cortex, specifically those in layer 5 and 6, the deep cortical output layers. These neurons should represent the final output from of processing through neocortical areas and therefore disruptions to signal processing or transmission should manifest in these cells (Glasser et al., 2016; Zingg et al., 2014). First, the number of NeuN+ cells with an AnkG+ segment was computed for the same cortical areas analyzed in Figure 5.3 (Figure 5.4A,B). This showed that a similar proportion of NeuN+ cells had easily identifiable AnkG+ segments associated with their cell body. Although most neuronal cell types have an AnkG+ AIS, those from interneurons can be more difficult to detect because they are shorter and smaller diameter. By showing that the cortical areas under

Figure 5.3 – General Characterization of the *OBiden* Mouse Cortex

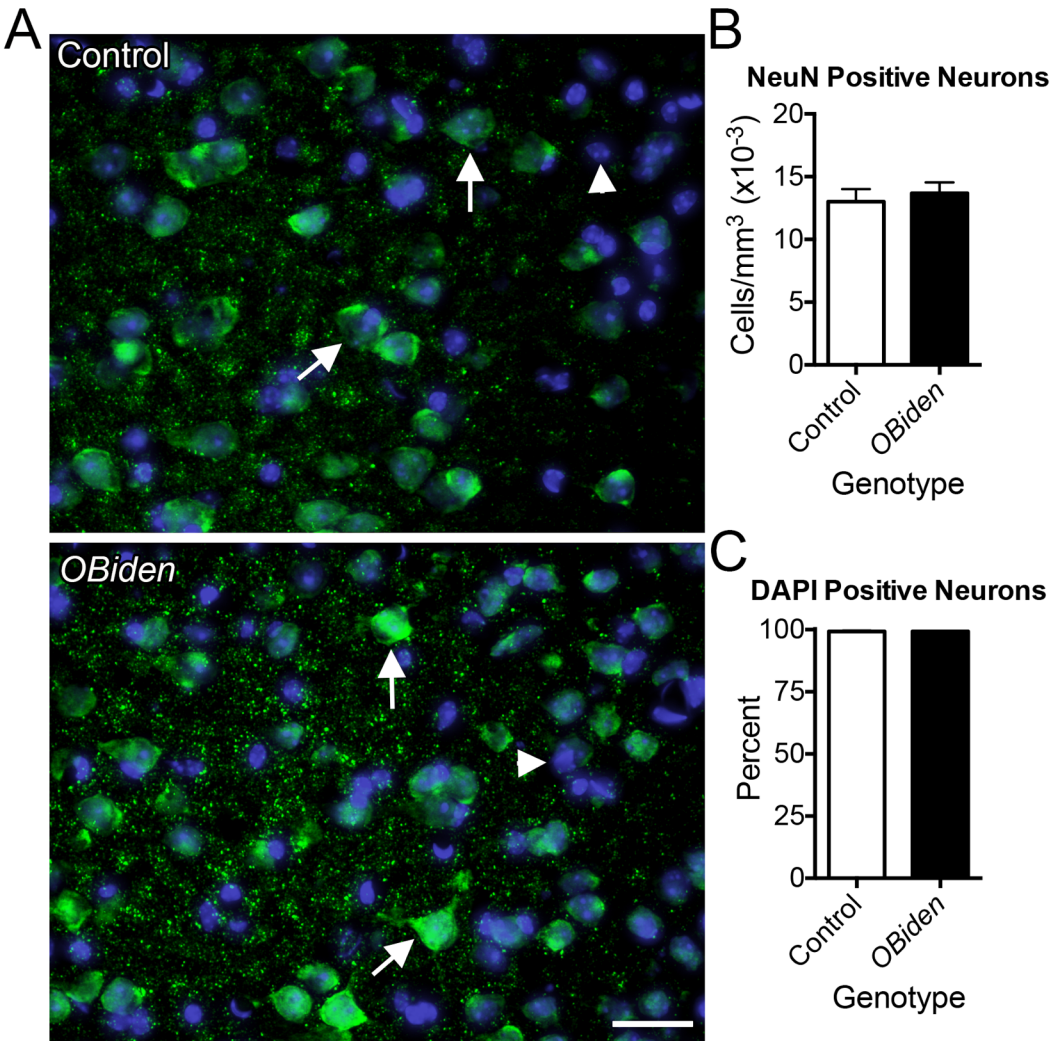

Figure 5.3 – **A**) Representative pictures from Control and *OBiden* cortex stained for the neuronal marker NeuN and nuclear chromatin with DAPI. NeuN+/DAPI+ cells are evident in both and spaced throughout the section (arrows) and there are NeuN-/DAPI+ non-neuronal cells that were no used for the analysis (arrowheads). **B**) There was no difference in the density of NeuN+ cells in the cortex between Control and *OBiden.* **C**) Virtually all NeuN+ cells had an identifiable DAPI nucleus, indicating no overall degeneration (n = 5 animals per group, 3 slides per animal).

Figure 5.4 – Axon Initial Segment Length in Rostral Entorhinal Cortex

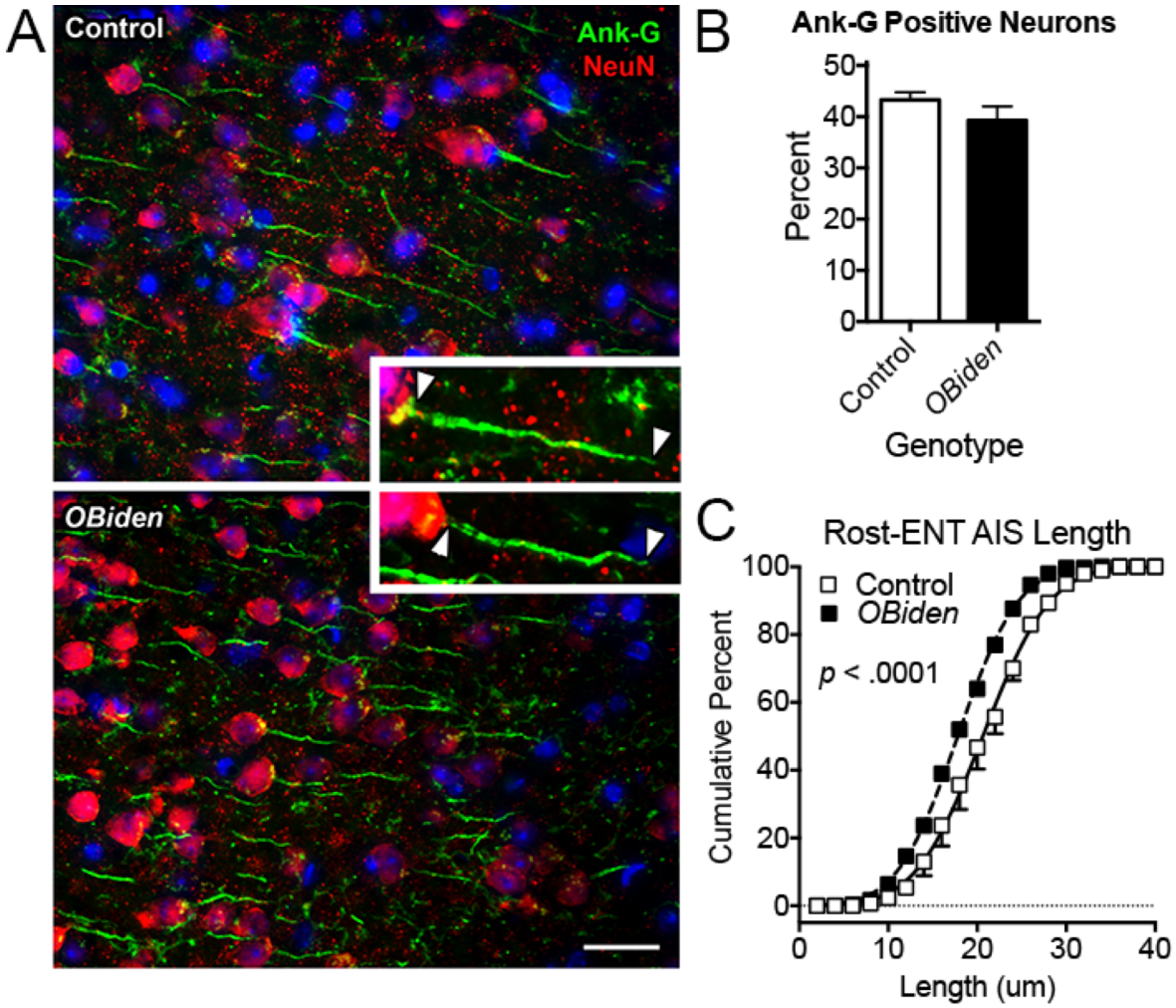

Figure 5.4 – **A**) Representative rostral entorhinal cortex layer 5 staining highlighting NeuN cell bodies (red) and AnkG+ AIS segments (green). Insets – Enlarged pictures of single AIS segments with arrowheads indicating the beginning and end of the AIS used for length measurements. Scale bar = 25 and 8.5μm. **B**) The proportion of AnkG+ neurons is unchanged between control and *OBiden* mice. **C**) Plot of the cumulative percent of AIS segments of various lengths. There is a significant left-shift in the curve as the AIS segments in the *OBiden* cortex are shorter than in the control cortex (n = 5 animals per group, 3 slides per animal, >30 AIS segments per slide)

Table 5.4 – Axon Initial Segment Statistics in Rostral Entorhinal Cortex

AnkG+ Neurons; Control vs. *OBiden*

Unpaired t test

P value	0.2678
P value summary	ns
Significance (P < 0.05)	No
One- or two-tailed?	Two-tailed
t, df	t=1.286 df=4

Comparison of Fits

Null hypothesis	One curve for all data sets
Alternative hypothesis	Different curve for each data set
P value	< 0.0001
Preferred model	Different curve for each data set
F (DFn, DFd)	125.0 (2,116)

Best-fit values	**Control**	***OBiden***
Mean	20.62	17.81
SD	5.959	5.372

analysis have equivalent numbers of AIS segments, it demonstrates a similar area for analysis. Next, the length of each AIS associated with an identified NeuN+ cell body was measured by hand. This was done with a line following the exact path of the AIS to account for curves and turns deflecting the AIS off a straight line. The lengths of the AIS segments were binned into 1μm bins and averaged across bilateral cortical areas to obtain a distribution for each of the mice analyze. When plotted as a cumulative distribution and averaged across mice, there was a significant left-shift in the length curve for *OBiden* mice indicating a move towards shorter AIS segments (Figure 5.4A,C). The AIS is known to be a plastic structure and ca vary its location from the soma and length as input and reciprocal feedback changes (Kuba et al., 2014; Kuba et al., 2015). This change, then, shows primary oligodendrocyte stress is affecting functional components of cortical neurons, which in turn could be leading to the behavioral changes observed in Chapter 2.

The AnkG protein is a critical part of the AIS, but it is only one of a number of structural components and does not give information on the functional ion channels at the AIS. One of the other structural components is β4-spectrin (β4-spec) that associates with AnkG and the microtubule structure in the AIS. Then there are the functional ion channels represented by $Na_v1.2$ and $K_v7.2$ that contribute to the rising phase of the action potential and the after-hyperpolarization and tone of the neuron, respectively. Finally, as the analysis has focused on the neurons in deep cortical layers 5 and 6 the transcription factor Ctip2 (known as BCL11B (B-cell lymphoma/leukemia 11B)) was used to identify post-mitotic pyramidal neurons and determine if there was a change to that specific population of cells (Chen et al., 2008). To test for the presence and abundance of each of these proteins, tissue punches taken from gray matter regions were analyzed for their protein content.

Western blots from the rostral entorhinal cortex and the more caudal, canonical, portion of the entorhinal cortex were analyzed for protein changes related to the AIS (Figure 5.5). Punches encompassing most of the cortex from layer 1 to layer 6 were homogenized and run to

Figure 5.5 – Entorhinal Cortex Axon Initial Segment Western Blot

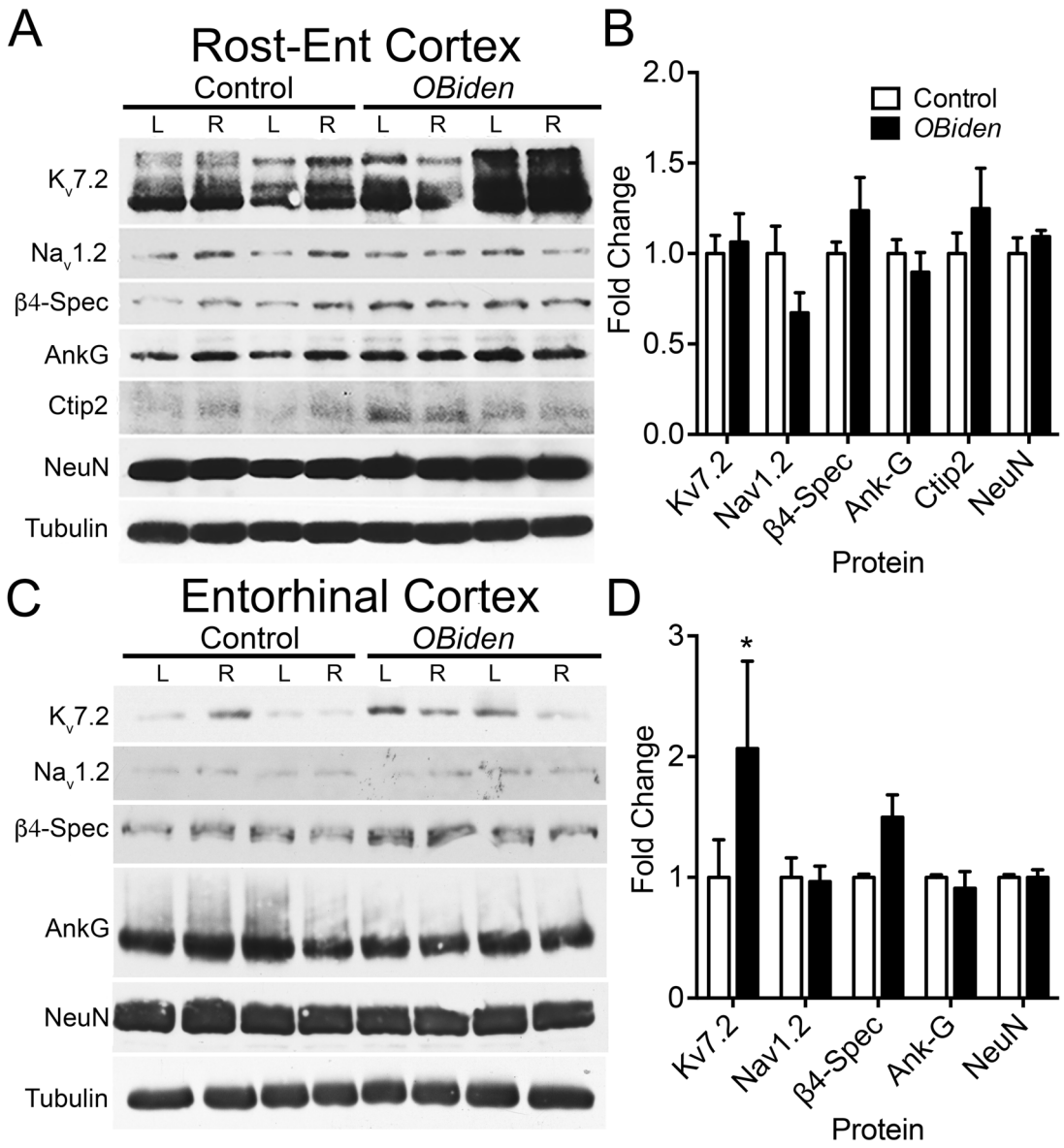

Figure 5.5 – **A**) Representative bilateral western blots from the rostral portion of the entorhinal cortex for major AIS related proteins. **B**) Quantification and normalization to control signals of the blots in **A** showing no significant changes. **C**) Representative bilateral western blots from the caudal portion of the entorhinal cortex. **D**) Quantification and normalization of the western blots from **C**, where there is a significant increase in $K_v7.2$ signal in *OBiden* mice. (n = 4 per group)

separate AIS proteins onto the same, or at most, 2 gels for consistency of analysis. Also, bilateral punches were run rather than pooling punches for a single animal. This was to determine if there was a left-right bias in the regions analyzed and increase our ability to detect unilateral lesions or pathology. In the rostral entorhinal cortex, there is some variability in proteins such as $K_v7.2$ between mice, however the relative signal within bilateral punches of a single mouse is relatively consistent (Figure 5.5A). This could be due to variable experiences of the mice or developmental differences or possibly the result of significant pathology in one mouse. When the average signals across animals were compared though, there was no difference between control and *OBiden* mice in any of the analyzed proteins (Figure 5.5B). Interestingly, although there was a shortening of the AIS in layer 5 of the rostral entorhinal cortex, there was no change in AnkG levels measured by western blotting. A primary reason for this discrepancy could be that while ICC staining focused on a specific layer and region of cortex, the punches encompass a volume ~3000x larger than the volume used for staining analysis. This introduces more cells with possible AIS segments, and more AnkG protein, and the additional cells may have normal levels of AnkG, hence burying the signal from the shortened AIS in layer 5.

Next, the analysis was continued into the caudal entorhinal cortex, and there a significant difference was detected via an increase in $K_v7.2$ protein in the *OBiden* mice (Figure 5.5C,D). This change occurred without increases to the sodium channels or the structural proteins AnkG and β4-spec. Together, these results could indicate an increased concentration of the $K_v7.2$ ion channel at the distal portion of the AIS, or a spreading of the $K_v7.2$ channel towards more soma proximal regions of the AIS. However, the $K_v7.2$ antibody did not work on many regions of the CNS for staining with ICC, as will be discussed later, and made confirmation of which pathology is causing the increased signal in the entorhinal cortex difficult to determine. As an additional check, though, the length of the AIS segments in layer 5 was analyzed the same way as those in the rostral entorhinal cortex in Figure 5.4C to determine if there were generalized changes to AIS length in the output pyramidal neurons (Supplemental Figure 5.2).

Next, the analysis of the AIS was extended to the hippocampus. Because of the behavioral deficits in memory identified in Chapter 2, and the intricate relationship between behavior and signaling between the entorhinal cortex and hippocampus, it was a logical area to analyze for deficits. As in the cortex, ICC staining was performed and in this region both AnkG and $K_v7.2$ will stain the AIS and as in the cortex the analysis was confined to the main cell output layer prior to the subiculum, namely the CA1 layer of the hippocampus (Witter, 2006). However, CA1 AIS segments are all oriented dorsal-ventrally and are relatively dense thereby creating a cellular layer with DAPI+ CA1 cell nuclei, then an AnkG/$K_v7.2$+ AIS layer with those two layers flanked by DAPI/AnkG/$K_v7.2$ negative regions. By drawing 10μm wide boxes across the CA1 region and analyzing the staining intensity, an estimate of the abundance of each stain can be obtained giving valuable information regarding the AIS integrity and composition (Figure 5.6A, yellow rectangles).

Dorsal Hippocampus CA1 Axon Initial Segment Analysis

The analysis began in the dorsal hippocampus (DHC) CA1 layer, where the left and right CA1 layers were analyzed across multiple mice to give intensity profiles of stains for AnkG, $K_v7.2$ and DAPI (Figure 5.6A-C). In Figure 5.6A, a dotted yellow box represents the size of one of the measurements taken in the CA1 region and at least 10 measurements were obtained across a single CA1 area for each animal, bilaterally. These gave intensity profiles for the staining seen in Figure 5.6B and C, where the mean profile from the control and *OBiden* left and right CA1 areas is displayed. These traces show a characteristic peak in blue from the DAPI channel representing the dense CA1 nuclear layer. Also, they show an increase in AnkG intensity towards the strata oriens (S. oriens) side of CA1 where the AIS segments from the majority of the resident cells are projecting (Figure 5.6B,C, red traces). Finally, there are the green traces from the $K_v7.2$ signal that also are greatest on the S. oriens side of CA1 and for controls show a consistent pattern of reaching their highest expression level after AnkG peaks. However, in the *OBiden* mice, there is

Figure 5.6 – Dorsal Hippocampus CA1 Axon Initial Segment Staining

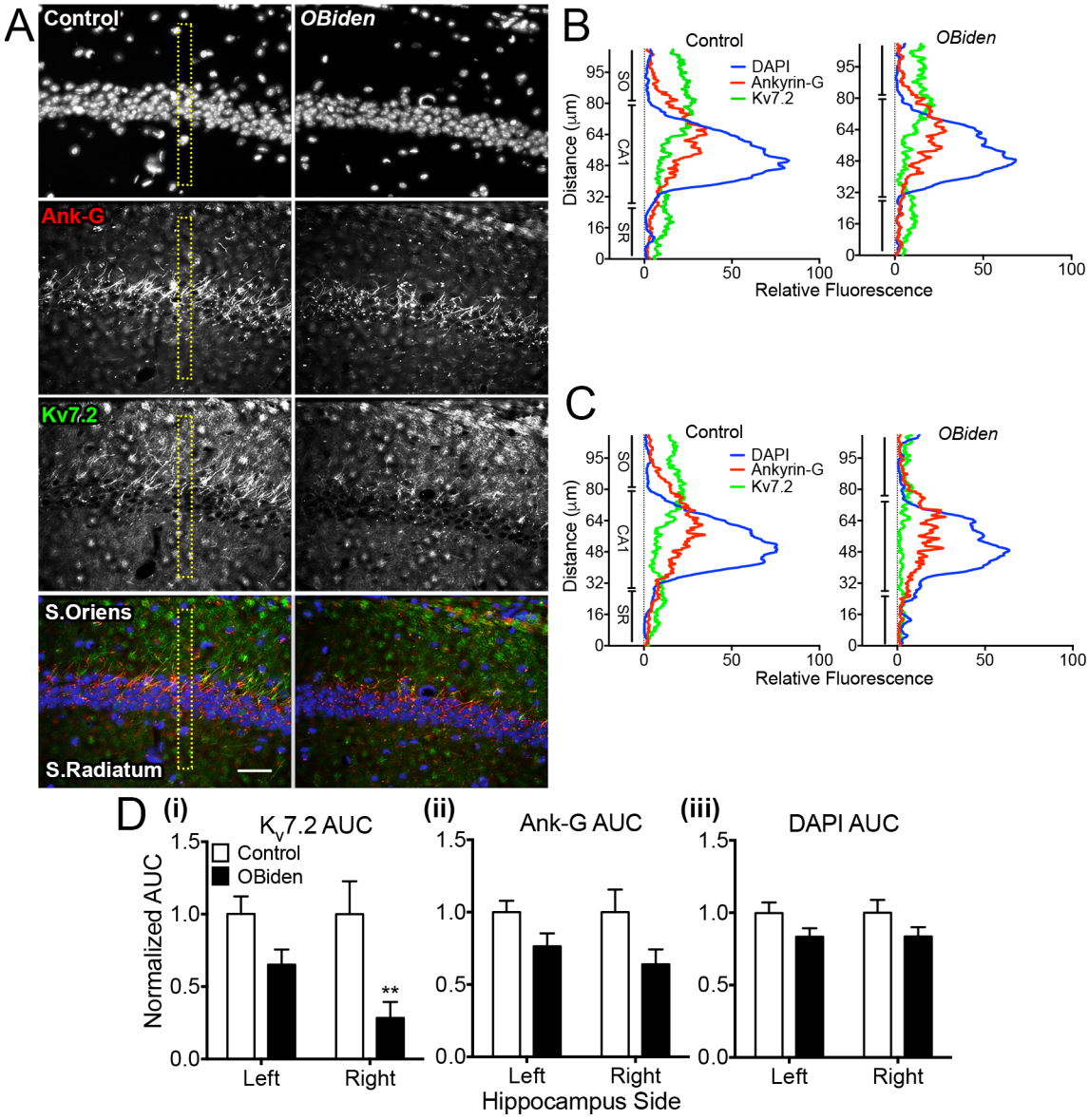

Figure 5.6 – **A**) Representative staining images from the right CA1 layer of the DHC in control and *OBiden* mice with a single analysis box shown in dashed yellow. **B**) Left CA1 DHC plots of staining intensity, similar between genotypes. **C**) Right CA1 DHC plots of staining intensity with an apparent loss of intensity in $K_v7.2$ staining of *OBiden* mice. **D**) Normalized AUC graphs obtained from the integrals of the plots in **B** and **C** confirming the loss of $K_v7.2$ signal in the right CA1 of *OBiden* mice (n = 4 animals per group, 3-5 slides per animal).

Table 5.6 – Dorsal Hippocampus CA1 Area Under the Curve Statistics

	ANOVA table	SS	DF	MS	F (DFn, DFd)	P value
DAPI	Interaction	1.665E-16	1	1.665E-16	F (1, 16) = 6.440e-015	P > 0.9999
	Side	0.00002	1	0.00002	F (1, 16) = 0.0007735	P = 0.9782
	Genotype	0.1345	1	0.1345	F (1, 16) = 5.201	P = 0.0366
	Residual	0.4137	16	0.02586		
AnkG	Interaction	0.01922	1	0.01922	F (1, 16) = 0.3132	P = 0.5835
	Side	0.01922	1	0.01922	F (1, 16) = 0.3132	P = 0.5835
	Genotype	0.444	1	0.444	F (1, 16) = 7.235	P = 0.0161
	Residual	0.9819	16	0.06137		
Kv7.2	Interaction	0.1674	1	0.1674	F (1, 16) = 1.508	P = 0.2372
	Side	0.1711	1	0.1711	F (1, 16) = 1.541	P = 0.2323
	Genotype	1.42	1	1.42	F (1, 16) = 12.79	P = 0.0025
	Residual	1.777	16	0.111		

	Control - OBiden	Summary	Adjusted P Value
DAPI	Left	ns	0.2368
	Right	ns	0.2368
AnkG	Left	ns	0.28
	Right	ns	0.0696
Kv7.2	Left	ns	0.219
	Right	**	0.0073

a noticeable absence of $K_v7.2$ signal that is particularly noticeable on the right side where the $K_v7.2$ trace remains near zero across the entire region (Figure 5.6C, right graph).

The next step was to confirm that the apparent loss of staining in the DHC CA1 layer of *OBiden* mice was indeed a significant loss of signal. Therefore, the intensity plots from Figure 5.6B and C were integrated to give a continuously rising function, and then the area under the curve (AUC) was calculated for each animal bilaterally, then averaged together across genotypes. There was a significant reduction in the AUC for the right DHC CA1 in *OBiden* mice compared to controls, only for $K_v7.2$ staining, matching the visual results obtained from ICC (Figure 5.6D(i)). In addition, there was no change to either AnkG or DAPI staining, indicating that the loss of $K_v7.2$ is independent of AIS loss or cell loss in the CA1 (Figure 5.6D). The change to ion channels without loss of AIS structural proteins is not unusual as others have noted alterations to ion channel staining location or abundance as a result of neuronal stresses (Hamada and Kole, 2015; Kuba et al., 2015; Yamada and Kuba, 2016). This could be a likely explanation for the alteration to the $K_v7.2$ profile seen in the DHC, that the CA1 neurons have undergone a physical or electrical stress and to compensate, the potassium channel distribution along the AIS has been altered.

A quantification was then made of AIS proteins from punches encompassing the dentate gyrus (DG), CA2 and CA3 layers and the molecular portions of the dorsal hippocampus. The westerns showed a significant decrease in AnkG signal from the entire hippocampus of the *OBiden* mice, when normalized to the NeuN signal (Supp. Figure 5.3). NeuN was used because the α-Tubulin blot was damaged and did not develop, however throughout the *OBiden* experiments the NeuN signals between control and *OBiden* animals were usually within 5% of each other. Therefore, normalizing to NeuN should give an accurate picture of the tissue and loading. In addition to significantly less AnkG, there was a decrease in the mean $K_v7.2$ signal that did not reach significance, however given the unilateral reduction in staining intensity seen in Figure 5.6 this could be reflected in the variability and lack of significance in the western blot as one side of the dorsal hippocampus is more strongly affected than the other.

Ventral Hippocampus AIS Analysis

The AIS analysis in the hippocampus was extended to the ventral hippocampus CA1 layer to determine if there were similar changes to the staining profiles of the AIS from VHC. Similar to the DHC, regions of interest were drawn medial-laterally to encompass the CA1 layer and the surrounding molecular layers. The staining intensities were computer, plotted and averaged across both genotypes (Figure 5.7). In the VHC, the CA1 changes position so that the main cell layer is oriented dorsal-ventrally rather than medial laterally. Also, the cell layer is less condensed in the VHC, possibly reflecting the differential information processing that occurs in the VHC compared to the DHC. The intensity profiles from the VHC CA1 are more variable than those obtained from the DHC, again likely due to the de-condensation of the cell layer in the VHC. However, there appears to be no major loss of staining from DAPI, AnkG or $K_v7.2$ in the *OBiden* mouse on either left or right side, unlike the change seen in DHC (Figure 5.7B). When the intensity plots are quantified to obtain the AUC, no differences were detected between control and *OBiden* mice in the CA1 region of VHC. As with the DHC, punches were obtained from the VHC encompassing all layers of the hippocampus and analyzed by western blotting for major AIS related proteins (Supp. Figure 5.4).

From the western blots of whole VHC, a significant decrease in $K_v7.2$ was detected in *OBiden* mice compared to controls (Supp. Figure 5.4B). This result differed from the intensity analysis as no loss of $K_v7.2$ was detected specifically in the CA1 layer. Therefore, it would seem there is a dropout of $K_v7.2$ in one of the other cellular areas of the VHC that accounts for the consistent drop in signal seen on western blots. The VHC is involved in much of the information processing relating to fear, anxiety and social memory in rodents, but as seen earlier there was no apparent deficit in fear conditioning in the *OBiden* mice at 12 months of age (Padilla-Coreano et al., 2016). Social and anxiety stressors were not tested at 12 months of age, but the change in $K_v7.2$ level in the VHC would imply one of those processing pathways may also be perturbed in the *OBiden* animals.

Figure 5.7 – Ventral Hippocampus CA1 Axon Initial Segment Staining Analysis

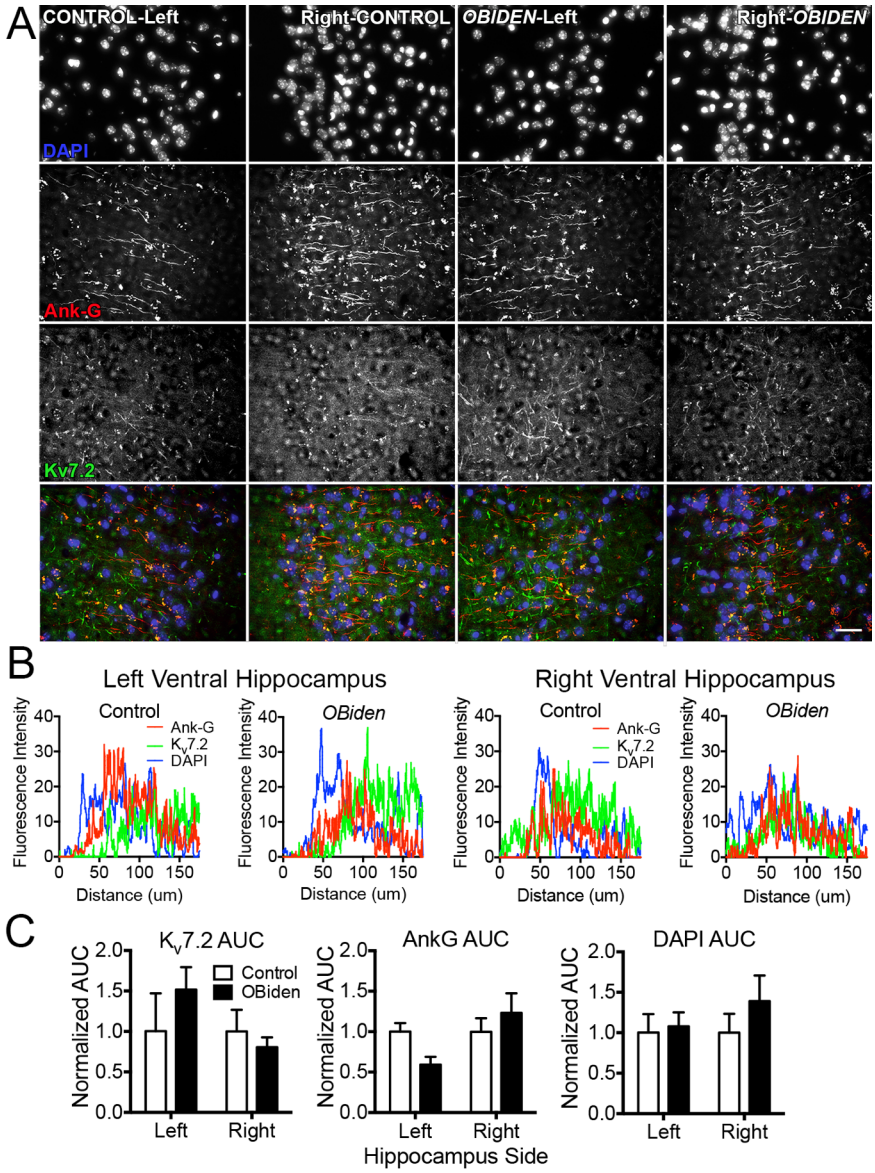

Figure 5.7 – **A**) Representative staining images from left and right VHC CA1 layer of control and *OBiden* mice. **B**) Intensity profile plots obtained from VHC CA1 layer showing no apparent differences between genotypes. **C**) Area under the curve measurements for all stains, bilaterally, in the VHC show no differences between control and *OBiden* mice (n = 4 animals per group, 3-5 slides per animal).

MS Cortex AIS Analysis

As the *OBiden* model is meant to replicate the degenerative aspects of MS disease model, it was important to test MS and healthy cortical tissue to determine if AIS proteins could be detected after variable post-mortem intervals and if there were differences between groups. MS tissue was obtained from the Human Brain and Spinal Fluid Resource Center (HBSFRC) at UCLA from five MS patients and 5 patients whose cause of death was non-neurological. The tissue was taken from the frontal cortex, mainly from the inferior portion bordering the temporal lobe, however, the tissue was not from identical cortical areas. All MS tissue was confirmed to have neuropathological lesions as determined by a pathologist at UCLA, meaning that the tissue was considered NAGM for our analysis, similar to the state of *OBiden* cortical tissue that appears grossly normal.

Tissue punches were obtained by gently thawing the tissue and taking punches from multiple white and gray matter areas from each patient. Given that human cortical tissue is much larger than mice, the gray matter punches encompassed multiple or single layers of cortical tissue with some crossing layers as they approached gyri or sulci in the brain. Therefore, the protein Ctip2 was also blotted for because it is expressed at higher levels in layers 5 and 6 than in any other layers of cortex as shown in mouse cortex (Supp. Figure 5.5). After blotting, the human cortical tissue showed no differences between healthy control patients and MS patients (Figure 5.8A). Across the gray matter punches from the four patients analyzed, only AnkG and Ctip2 showed even a possible change in expression levels, however neither protein was statistically significant so across these patients they did not change (Figure 5.8B). Because there was an increase in the mean of Ctip2 in MS patient samples compared to controls, this could indicate that the punches were taken from a slightly different cortical region than controls. To determine if compensating for Ctip2 would affect the results, the western blot signals were normalized to Ctip2 for comparison (Figure 5.8C). Although there is an apparent drop in the mean for AIS proteins such as AnkG and $K_v7.2$, the values did not reach significance when run through a 2-way ANOVA

Figure 5.8 – Human Cortical Axon Initial Segment Western Blot

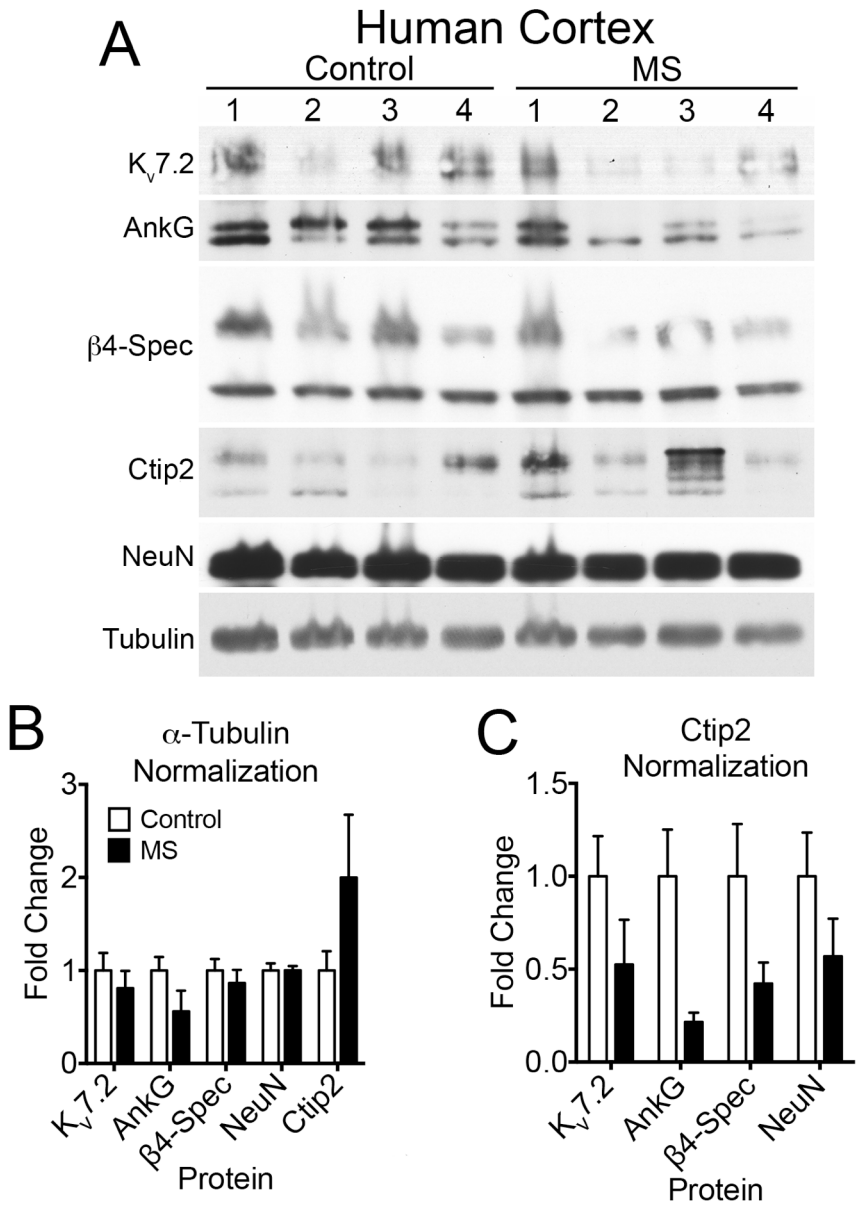

Figure 5.8 – **A**) Western blots from four healthy control and MS patients for AIS and neuronal related proteins. **B**) Quantification of signals when normalized to α-Tubulin as a loading control showing no changes in expression level. **C**) Quantification of signals after double normalization to α-Tubulin, then to Ctip2 to account for layer 5/6 neurons. No differences were detected, likely due to the variability between patient samples.

Table 5.7 – Human Cortical Axon Initial Segment Statistics

2-way ANOVA Main effects

ANOVA table	SS	DF	MS	F (DFn, DFd)	P value
Interaction	2.467	4	0.6168	F (4, 30) = 2.257	P = 0.0863
Protein	2.467	4	0.6168	F (4, 30) = 2.257	P = 0.0863
Disease Status	0.02176	1	0.02176	F (1, 30) = 0.07965	P = 0.7797
Residual	8.197	30	0.2732		

Post-hoc t-tests

Control - MS	Summary	Adjusted P Value
Kv7.2	ns	0.9908
AnkG	ns	0.7532
β4-Spec	ns	0.9981
NeuN	ns	> 0.9999
Ctip2	ns	0.055

analysis. This could be due in part to the low number of n, as many studies with human samples need n>7 to achieve sufficient power to detect changes, and the lack of difference is also due to the variability between samples. However, the decrease in the mean signal of AIS proteins when normalized to Ctip2 indicates that increasing the number of patient samples may reduce the variability and allow us to detect changes between groups.

Discussion

In previous chapters of this work, the focus has been on the primary pathological changes in *OBiden* mice and the development of secondary behavioral changes evident in the mice. However, even though myelin and oligodendrocytes are critical to CNS function, they do not work alone and as the *OBiden* model relies on a stress to myelin rather than the destruction of myelin, it is important to evaluate what are historically considered the important cells in the CNS, the neurons. The gray matter and neurons represent the major information processing centers of the CNS and do much to shape the behavior and physiology of the animals. Also, in MS the gray matter pathology has been overlooked for years even through in the progressive phases of the diseases it is likely the major contributor to dysfunction and cognitive issues in patients. Therefore, it was critical to understand the gray matter and neuronal pathology in the *OBiden* mice and its correlation to MS.

The *OBiden* mice were evaluated for one of the pathologies identified in MS, as well as other neurological diseases affecting neurons, changes to the neurofilament profile in gray matter regions. There were significant changes to the neurofilament profile in multiple, cognitively related regions of gray matter including entorhinal cortex and dorsal hippocampus. Both areas are involved in the pathways responsible for an animal's ability to correlate perform identification tasks such as T-Maze and Novel object, both of which the *OBiden* mice are deficient in. Critically, MS post-mortem tissue from normal appearing cortex shows the same neurofilament increase as the *OBiden* mouse cortex and initial indication that the primary metabolic stress in oligodendrocytes

can lead to similar secondary gray matter pathology. This result begins to establish the molecular links between the *OBiden* model and MS, especially in the area of NAGM, which is often abnormal and understanding the early molecular changes in gray matter before overt lesions may help to establish new treatment paradigms for patients.

Although the scope of this work did not encompass the exact changes to the neurofilament population, there is past evidence that the alteration to neurofilament pools affects neuronal structure and functions. Specifically, the diameter of axons can be altered as neurofilament heavy-chain proteins change and for neurofilament light-chain alterations axonal transport and structure can be significantly altered (Elder et al., 1998a; Elder et al., 1998b; Jacomy et al., 1999; Lee et al., 1994; Liu et al., 2013). These effects could be evident if a technique such as electron microscopy to analyze exact axon diameters and subcellular structures. There could also be more gross effects that could be detected over larger areas of the cortex through the use of simpler staining or blotting techniques, which was the path pursued for the next stage of the *OBiden* project.

The analysis then focused on the AIS as alterations to neuronal transport, diameter and functional connectivity could all manifest as disruptions to the action potential generating AIS. Because the AIS is regularly organized and relatively confined <50μm from the soma, alterations to the location or structure are readily detectable and can lead to valuable information regarding the state of the neuron. The investigation into the *OBiden* mice revealed two main changes, both related to the AIS. First, there was a shortening of cortical AIS segments in the entorhinal cortex as measure by AnkG. By altering the AIS length it changes the location of the ion channels relative to the soma, potentially altering two aspects of the action potential generation. One is that the voltage necessary at the soma decreases making action potentials easier to fire as the ion channels are located closer to the soma and the second is that back propagation of charge from the AIS to the soma. These changes could result in altered action potential timing, frequency and

bursting all of which could affect the downstream target of the neuron creating a cascading change within the CNS.

Along with structural proteins like AnkG, select ion channels were analyzed in the *OBiden* mouse to determine if their abundance was altered due to ongoing pathology. Between the sodium and potassium channels we analyzed, which are the major ion channels responsible for shaping the action potential and affecting tone, all the differences we detected revolved around the $K_v7.2$ channel. $K_v7.2$ is a six-pass transmembrane protein that can form a heterotetramer with $K_v7.3$ as one of the main fast-activating and slow-inactivating channels at the AIS. Because of their slow inactivation, they are responsible for shaping part of the after-hyperpolarization of the action potential and setting the tone at which a neuron can fire. Alterations to the $K_v7.2$ channel can have two different effects; if the protein is upregulated it will decrease the tone of the neuron and if it is downregulated it should allow for an increased tone and burst firing (Battefeld et al., 2014). To confirm the hypothesis would require patch clamping or brain slice electrophysiology, which could become part of future work on *OBiden.*

Finally, human cortical tissue was analyzed for the presence of AIS proteins and their abundance. Although the proteins were detectable on western blots, there were no differences between healthy controls and MS patients when normalizing with tubulin or with tubulin and Ctip2. The second normalization was meant to account for the location of the punches, as some may have encompassed more superficial layers while others the deep layers, and Ctip2 is highly expressed in deep cortical layers 5 and 6 so it was one way to control for the location of punches. However, even controlling for Ctip2 there were no significant differences between control and MS patients, but there were promising changes in the mean in the direction we would predict from the *OBiden* model. Namely, there was a decrease in the mean signal in MS, especially for AnkG, and increasing the n to increase power may allow future experiments to confirm that there are AIS related differences in the cortex of MS patients.

One of the most interesting aspects of the *OBiden* model here is the number and distribution of secondary neuronal changes originating from the primary oligodendrocyte stress. Although there was a thought to look at the communication between oligodendrocytes and neurons in this project, because the communication between the two cell types is largely unknown, it was beyond the scope of this project. However, the model shows that even small perturbations to myelin can result in detectable, long lasting molecular and organismal effects and may provide an interesting aspect for further study in MS.

GENERAL DISCUSSION AND CONCLUSION

General Characteristics of the *OBiden* Mouse

In Chapter 1 of this work, the *OBiden* mouse was shown to develop metabolic stress in oligodendrocytes, even at 12 months of age. The stress was not present in every oligodendrocyte, however the goal of creating chronic stress in a subset of oligodendrocytes was achieved. Importantly, the *OBiden* mice retained normal molecular and functional characteristics in myelinated tracts. This included normal expression levels of major myelin proteins like MBP, PLP1 and CNPase, and no temporal alterations when analyzed using auditory brainstem responses. This shows that the *OBiden* model, therefore, is well suited for chronic study, and any pathologies identified result from primary stress and demyelination of subsets of susceptible oligodendrocytes in the CNS.

Also, the *OBiden* mouse showed that the UPR could be activated in mature, myelinated oligodendrocytes and it was not necessary to affect the cells only during development when they more metabolically active. This idea could be applied to MS as well, because pediatric-MS is more severe, quicker to progress and more difficult to treat than the more common adult MS (Chitnis et al., 2016). Meaning that if we were to activate the *Plp1-i.msd* transcript during development, we would see and accelerated rate of disease in the *OBiden* model. Potentially an interesting future investigation to define the temporal susceptibility of oligodendrocytes *in vivo*.

One aspect of the current study is the low dose of Tamoxifen used to activate metabolic stress, and the resulting mild overt phenotypic changes. Overall, the *OBiden* mice do not manifest overt sensorimotor deficits compared to Controls. And even with an *in vivo* analysis of the CNS through non-invasive MR techniques, as seen in Chapter 3, there is no overt pathological change. In the future, this could be altered by increasing the dose of Tamoxifen from 175mg/kg to the maximum tolerable dose of 450mg/kg as a weekly oral gavage. In theory, this would increase the number of cells undergoing metabolic stress and increase the rate and extent of pathology

development. One of the goals of this updated experiment would be to detect lesions and changes through MR imaging to allow for tracking of pathology and targeted tissue extraction for analysis. Also, it would allow for treatment efficacy in the *OBiden* mouse to be tracked similar to the MR outcome measures used in clinical trials (Calabresi et al., 2014; Lublin et al., 2016).

This work also utilized *ex vivo* histological techniques to compare the *OBiden* mouse to MS tissue. Here, there were distinct similarities between the *OBiden* mouse and MS pathology, most notably is the detection of focal demyelinating lesions in white matter tracts. Because this is one of the hallmark pathologies of MS it was excellent to see similar pathological features in the *OBiden* mouse. It showed that although MS is characterized as an autoimmune disease with peripheral cytotoxic cell infiltration necessary for lesions, similar demyelination can occur through chronic oligodendrocyte stress. This implies that if oligodendrocyte metabolic stress contributes to MS, the disease may be ongoing for years before reaching the clinical threshold. It could also explain the long-term failure of immune-modulatory therapy to prevent MS progression because it is targeting a symptom and not an underlying etiology of the disease (Feinstein et al., 2015; Lublin et al., 2016). However, the second point remains to be proven in relation to the *OBiden* mouse and early metabolic stress in MS patients.

Secondary Behavioral Phenotypes

The pathology and chronic metabolic stress in the *OBiden* mouse is interesting, but without a secondary manifestation affecting neuronal function and cognitive ability of the animals it would not truly resemble MS. In this work, it was established that the *OBiden* mice do development temporal and pathway specific cognitive changes as they age.

The first change is a depression-like endophenotype beginning at 6 months of age and continuing through 12 months of age. This matches increased rates of depression in MS patients, independent of being diagnoses with a terminal disease (Haussleiter et al., 2009). The depression-like endophenotype was the first indication that chronic oligodendrocyte metabolic

stress could result in secondary dysfunctions identifiable *in vivo*. One benefit of the *OBiden* mouse developing this pathology is that the behavioral tests are comparatively simple to run over the long term. This means that neuroprotective or oligo-protective therapies could be tested in the *OBiden* mouse in high throughput to screen multiple candidate therapies.

Temporally, following the depression-like endophenotype, the *OBiden* mouse develops a recognition memory deficit that is evident at 12 months of age. Changes to memory and cognition are especially detrimental in MS, and all neurodegenerative diseases, because of the toll they can take on patients and the limited treatments available to prolong function (Feinstein et al., 2015). Therefore, the *OBiden* mouse displays another aspect of MS important to patients and another behavioral change for future use in treatment trials. The recognition memory change in the *OBiden* mouse was very specific, as it only occurred in tests where the mice had to identify novel objects and novel areas. Deficits did not occur in spatial navigation or the ability to solve the Barnes maze paradigm, nor did changes occur when the mice were place in a noxious test for cue- based fear conditioning. The specific changes indicated a well-defined pathway between entorhinal cortex and dorsal hippocampus was most likely disrupted. These CNS areas are highly involved in recognition memory compared to the other behaviors (Igarashi et al., 2014). Spatial memory and fear condition rely more, but not exclusively, on ventral hippocampus, amygdala and pre-frontal cortex which may degenerate given a longer timeline or increased metabolic stress.

On spatial memory specifically, the historical paradigm indicated place cells within the hippocampus process a large degree of spatial information based on the firing and long term potentiation (O'Keefe, 1979). Although the *OBiden* mouse shows global and CA1 specific AIS changes, it wasn't confirmed if place cell populations were altered or spared in our model. Also, memory processes are continually shown to be more complex and interconnected than previously understood (Aristovich et al., 2016; Eagle et al., 2015; Liska et al., 2015). This indicates that although the cortical-hippocampal connections are likely disrupted in the *OBiden* mouse, the connections carrying spatial information may be spared at this early disease point. More

investigation is needed to determine exactly what type of neurons are impacted at the current stage of the *OBiden* mouse model.

Importantly, these behavioral changes were the first indication that stochastic metabolic stress in oligodendrocytes could secondarily alter organismal behavior. The behavioral tests run in this work are by no means exhaustive, though, and more tests could be utilized in the future to determine what other pathways may be effected in the *OBiden* mouse.

General Secondary Neurodegenerative Changes

The final stage of this work was to identify where and what neuronal phenotypes occurred in the *OBiden* mouse. Neurodegeneration in MS patients has only recently been reinvestigated in part because imaging techniques have reached the sophistication necessary to detect changes *in vivo,* and because neurodegeneration is unaffected by current treatments.

In the *OBiden* mouse, a survey of various brain regions was conducted by using Western blotting to detect levels of the various neurofilament proteins in gray matter. Neurofilament proteins help to maintain axonal diameter and support the microtubule and actin cytoskeleton necessary for intracellular transport (Elder et al., 1998a; Elder et al., 1998b; Jacomy et al., 1999). Disruptions to neurofilament proteins have been noted in axonal pathologies such as spheroids and swellings, and within the soma of principal neurons. The *OBiden* mice showed a buildup of non-phosphorylated neurofilament heavy (nNF) and light chain (NF-L) in the rostral entorhinal and piriform cortices. Importantly, cortical punches from MS patient tissue obtained through the Human Brain and Spinal Fluid Resource Center (HBSFRC) also showed an increase in nNF. The changes in the *OBiden* mouse and MS patients were in normal appearing gray matter areas indicated by the normal levels of the neuronal marker, NeuN and synaptic marker synapsin-1. Whether this buildup was due to axonal or somatic accumulation of neurofilament proteins was not determined but could be analyzed in the future.

A final area that showed changes was the dorsal hippocampus. This area, along with the entorhinal cortex, are implicated in recognition memory so degenerative changes match the *in vivo* behavioral deficit. The dorsal hippocampus showed a decrease in nNF, rather than an increase, nevertheless, *OBiden* mice were different than Control animals in a behavioral relevant area. Although no hippocampal from MS patients was obtained for this study, previous work has shown that hippocampal degeneration occurs in MS patients, again showing similarities to the *OBiden* mouse (Pardini et al., 2014).

Specific Secondary Axon Initial Segment Changes

The neurofilament changes in the *OBiden* mouse are a good indication of pathology, but do not specifically show how secondary neuronal pathology could be manifesting as a behavioral deficit *in vivo*. Therefore, the final analysis was to determine what specific neuronal or axonal change was occurring in the *OBiden* mouse. Through a battery of immunocytochemical (ICC) stains looking at the axon, dendrites and synapses, the axon initial segment (AIS) was identified as a region that was altered in the *OBiden* mouse. Because the AIS integrates depolarization from the soma and axo-axonic inputs before it propagates and action potential, it is sensitive to upstream or downstream reciprocal feedback and can alter its length, proximity to the soma and ion channel composition accordingly (Kuba et al., 2014; Kuba et al., 2015).

The AIS is typically defined through staining for the structural protein ankyrin-G (AnkG). AnkG is expressed during development, sets up neuronal polarity and allows for the clustering of ion channels that contain an ankyrin-interacting domain. In the *OBiden* mouse, there was a shortening of the AIS in the rostral entorhinal cortex. Interestingly, this shortening did not extend into the caudal-medial entorhinal cortex showing a very specific localization. However, upon Western blotting for AIS related proteins, the entorhinal cortex showed a significant increase in expression of potassium channel variant 7.2 ($K_v7.2$) that was not seen in the rostral entorhinal cortex. These two phenotypes in theory would act to cause different effects on action potentials

in their local area. The shortening of the AIS would likely bring ion channels closer to the soma and allow spreading depolarization to reach the AIS with less current thereby increasing action potential generation. Increasing $K_v7.2$ abundance without altering the AIS location should suppress action potential generation. $K_v7.2$ can form a tetrameric structure and this channel then controls the M-current at the AIS, causing a prolonged efflux of potassium, hyperpolarizing the cell and decreasing the frequency of action potentials. However, these are hypothesis based on the known function of the AIS and ion channels, and *in vivo* or *in vitro* electrophysiological experiments in the *OBiden* mouse would be necessary to confirm the hypothesis.

The rostral and caudal portions of the entorhinal cortex have reciprocal connections with the dorsal hippocampus (Igarashi et al., 2014). The CA1 layer of the dorsal hippocampus was analyzed for AIS expression of AnkG and $K_v7.2$. The CA1 was used for the analysis because it is a downstream integration center receiving inputs form within the hippocampus as well as inputs form distributed cortical areas. If region upstream of the hippocampus was sufficiently effect, the CA1 should also show changes to the AIS if it has altered its firing properties. In fact, there was a decrease in the apparent immunoreactivity of the AnkG and $K_v7.2$ antibodies at the AIS of CA1 principal cells. In this case there was a decrease in $K_v7.2$ expression, indicating a potential increase in action potential frequency. Because the tracts between entorhinal cortices and dorsal hippocampus are extensively myelinated and because of the specific behavioral deficit in recognition memory, it is not surprising to see changes to the action potential generating AIS. However, the order of change is not known and that temporal degeneration is an area of work for a future project.

Finally, AIS proteins were analyzed in MS tissue. ICC staining of the AIS did not work under any conditions tested, however Western blotting from punches of cortex showed the potential for changes specifically to deep cortical neurons. Neurons in layer 5 and 6 express a negative regulator of transcription called Ctip2, and because of the specificity of that antibody for layers 5 and 6 it was used to normalize AIS protein signals from MS patients. Although no results

were significant due to variability between samples, there are indications that with increased number of samples a decrease in AIS proteins in MS cortex could be detected. This result would tie together with changes in the *OBiden* mouse AIS and give another point of correlation between the model and disease. In addition, showing changes to the AIS in MS cortex could tie in with ongoing electroencephalographic (EEG) studies in MS that could be replicated in the *OBiden* mouse and show that the molecular changes effect connectivity and alter behavior.

Conclusion

The *OBiden* mouse model is not the first model to show that activating the UPR in oligodendrocytes will cause metabolic stress, cell death and demyelination. However, it is unique in the method of causing stress by utilizing an endogenous oligodendrocyte protein. Also, the stochastic, episodic stress only effects subsets of cells rather than all oligodendrocytes allowing for the development of focal pathology. The focal pathology is similar to the seen in MS patients. In addition, behavioral and secondary neuronal changes in the *OBiden* mice show similarities to changes in MS patients and patient tissue. Taken together, the *OBiden* mouse model represents a novel look into the effect of oligodendrocytes on neuronal health and function and the cellular interactions within the CNS.

APPENDIX A – CHAPTER 2 SUPPLEMENT FIGURES AND TABLES

Supplemental Figure 2.1 – Forced Swim Learned Helplessness Comparison

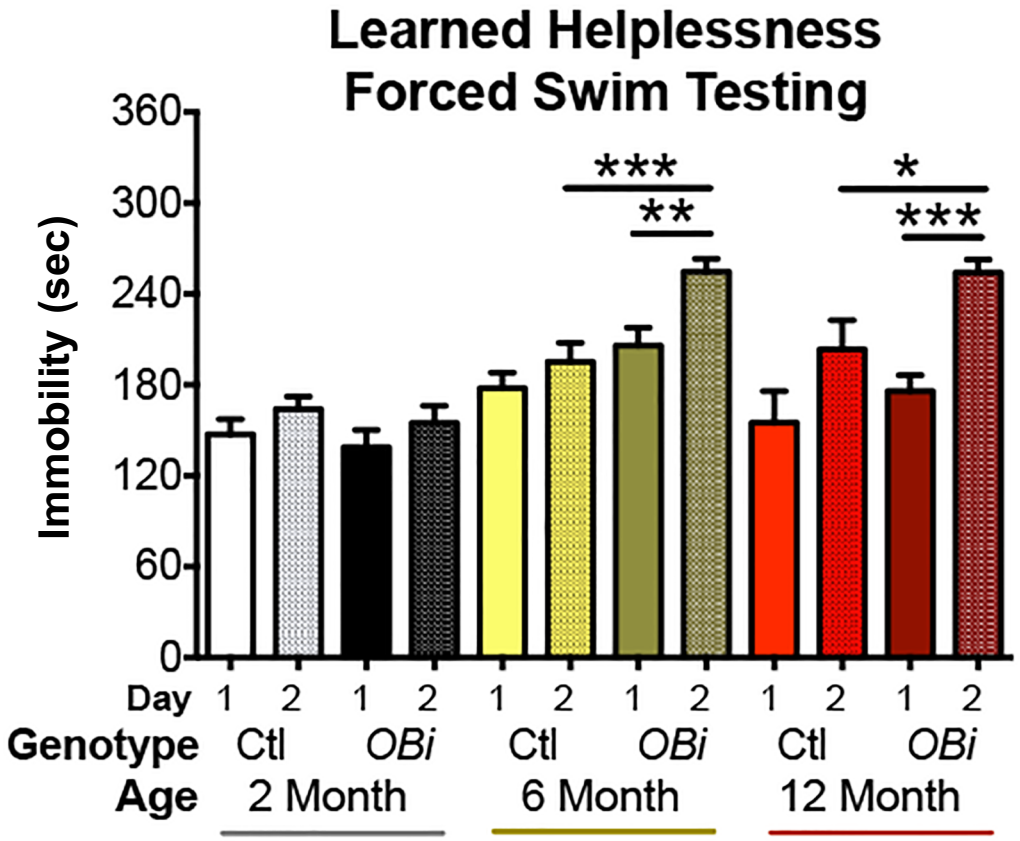

Supplemental Figure 2.1 – Graph of the Forced Swim test quantified for each day of tests (1 vs. 2) in each genotype (Control – Ctl vs. *OBiden* – *OBi*) and at each age a cohort was tested (2 months – gray, 6 months – yellow, 12 months – red). All 2 month old mice are resilient to learned helplessness in the forced swim paradigm. At 6 months, the *OBiden* mice are susceptible to learned helplessness (indicated by the significant difference between the 1 and 2 bars in the *OBi* at 6 months). This is also true at 12 months were the *OBiden* mice are still susceptible and increase their time immobile on Day 2. The Control mice show no susceptibility to learned helplessness at 6 or 12 months.

Supplemental Table 2.1 – Forced Swim Learned Helplessness Day 1 vs. 2

	Day 1 vs 2	Summary	P-value
Control-Control	2 Month	ns	0.215
	6 Month	ns	0.151
	12 Month	ns	0.113
OBiden-OBiden	2 Month	ns	0.336
	6 Month	**	0.004
	12 Month	****	<0.0001

Supplemental Figure 2.2 – Novel Object Trace in the *OBiden* Mouse

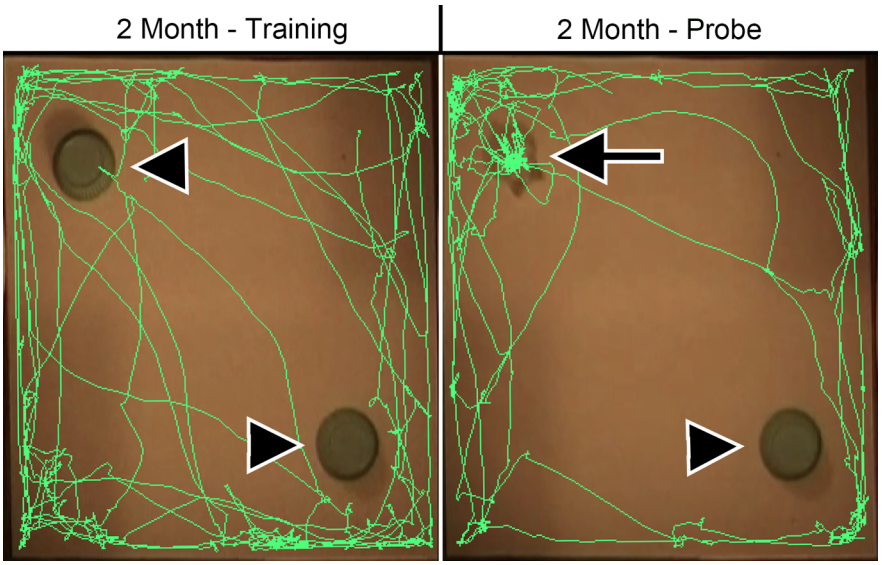

Supplemental Figure 2.2 – Tracing output from Ethovision of a control mouse at 2 months of age prior to gavage (green line). The training trial with the same objects (arrowheads) and the probe day with the novel object (arrow) are shown. On the training day, the mouse stays near the edge of the box as expected and investigates both objects. On the probe day, there is a shift and more of the trace falls around the novel object compared to the familiar object, as expected with this test.

APPENDIX B – CHAPTER 4 SUPPLEMENTAL FIGURES AND TABLES

Supplemental Figure 4.1 – Bielschowsky Silver Pathology in the *OBiden* Mouse

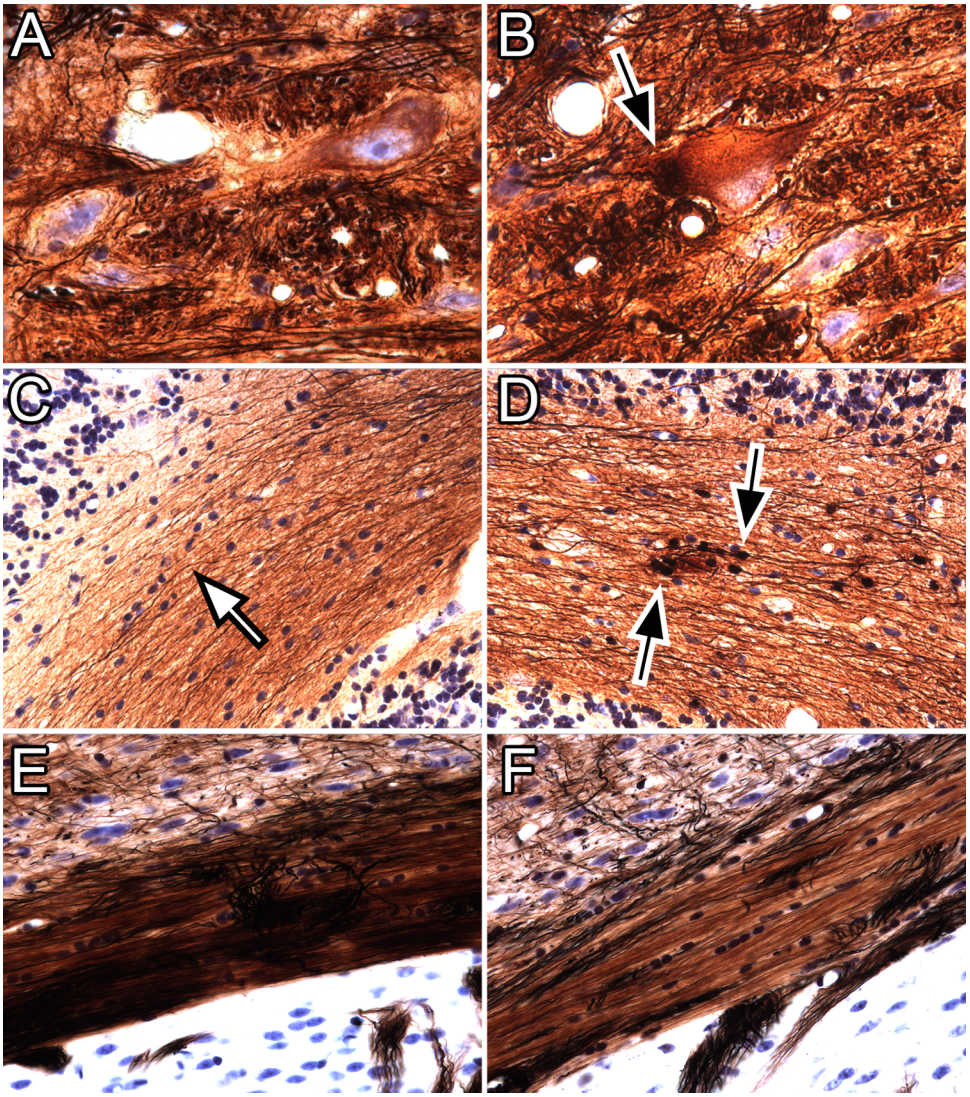

Supplemental Figure 4.1 – **A**) Control pons showing neurons and fibers. **B**) *OBiden* pons showing a swollen and enlarged cell (black arrow) and normal neurons and fibers. **C**) Control flocculus with normal nuclei and axons (white arrow). **D**) *OBiden* flocculus with nuclei, normal fibers but a grouping of black, axonal spheroids (black arrows) in a focal area. **E**) Left external capsule of a control mouse showing deep silver staining. **F**) Left external capsule from an *OBiden* mouse with lighter, less intense silver staining indicating possible axonal loss or

Supplemental Figure 4.2 – Coronal Brain Silver Stain in the *OBiden* Mouse

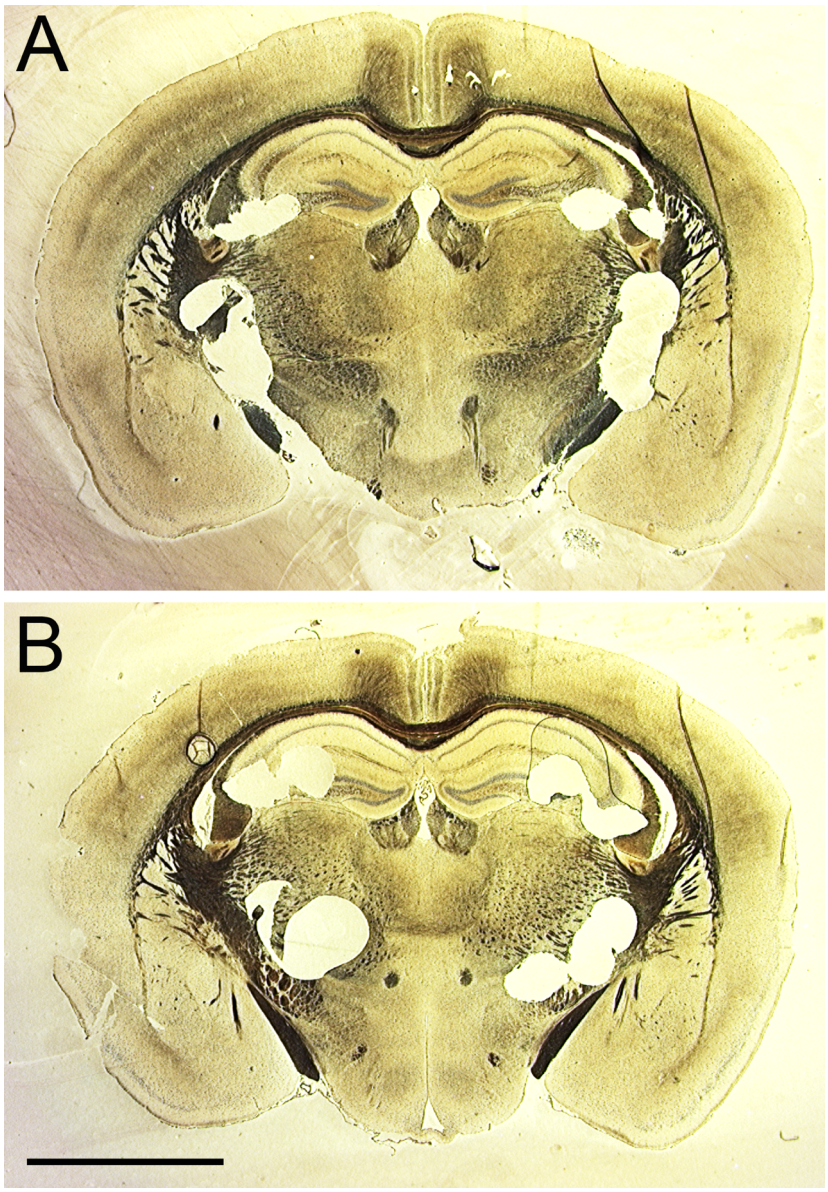

Supplemental Figure 4.2 – **A**) Coronal section through the neocortex of a control mouse at 12 month showing Bielschowsky silver stain roughly following the pattern of intact myelin tracts. **B**) Coronal section of *OBiden* mouse showing roughly similar staining pattern to that seen in control with possible subtle decreases in staining in the cortex and external capsule. Scale bar = 250μm.

Supplemental Figure 4.3 – CD68 Expression in Microglia of the *OBiden* Mouse

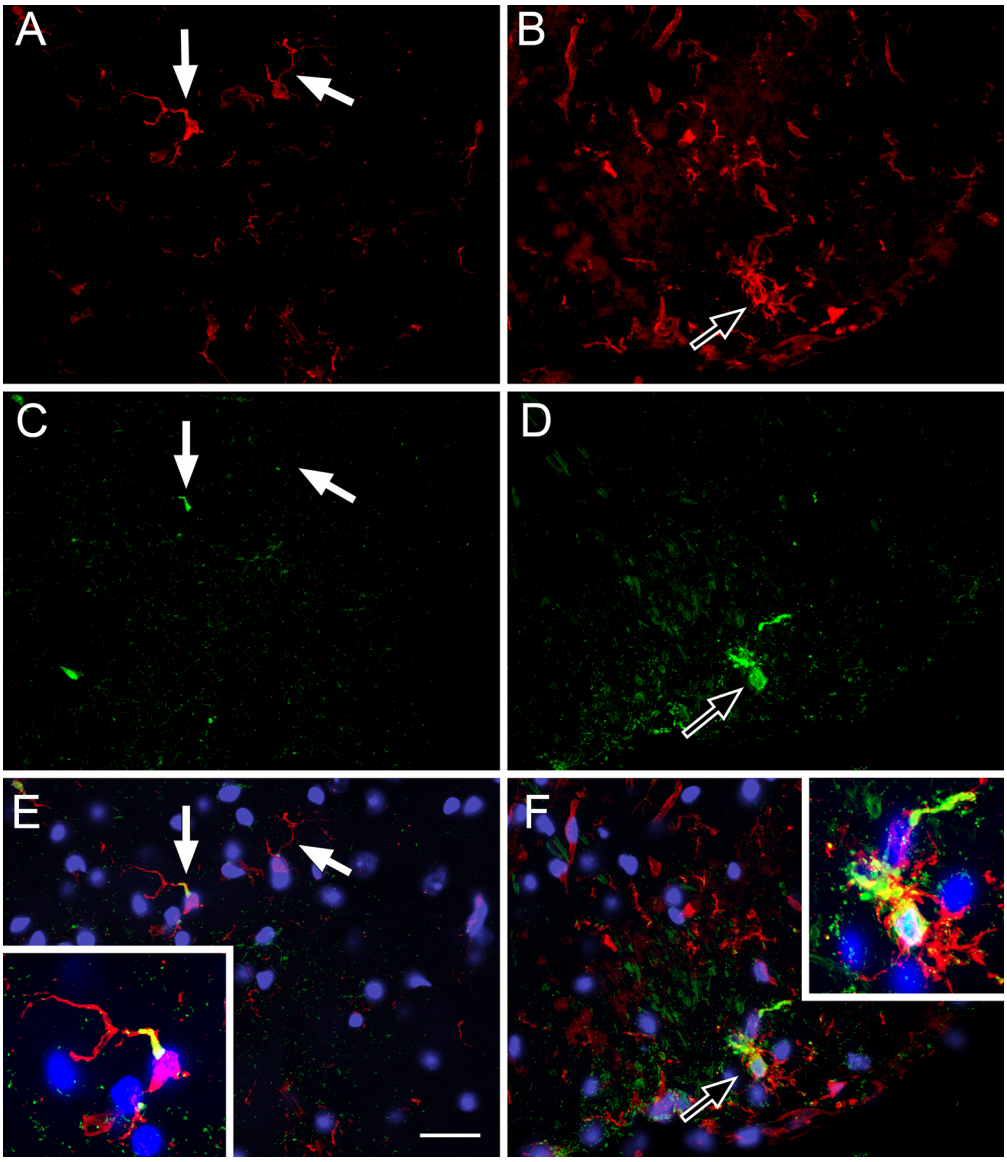

Supplemental Figure 4.2 – ICC staining of the ventral brainstem pons white matter for microglia (red) and CD68 activation marker (green). **A**) Control Iba-1 staining. **B**) *OBiden* Iba-1 staining. **C**) Control CD68 staining. **D**) *OBiden* CD68 staining. **E**) Control combine showing two cells (white arrows) in an inactive state given by no or low CD68 expression and thin Iba-1 processes. **F**) *OBiden* combine image highlighting an active microglia expressing high levels of CD68 with ramified processes. Scale bar = 25μm, inset = 12.5μm.

APPENDIX C – CHAPTER 5 SUPPLEMENTAL FIGURES AND TABLES

Supplemental Figure 5.1 – Piriform Cortex Neurofilament Western Blot

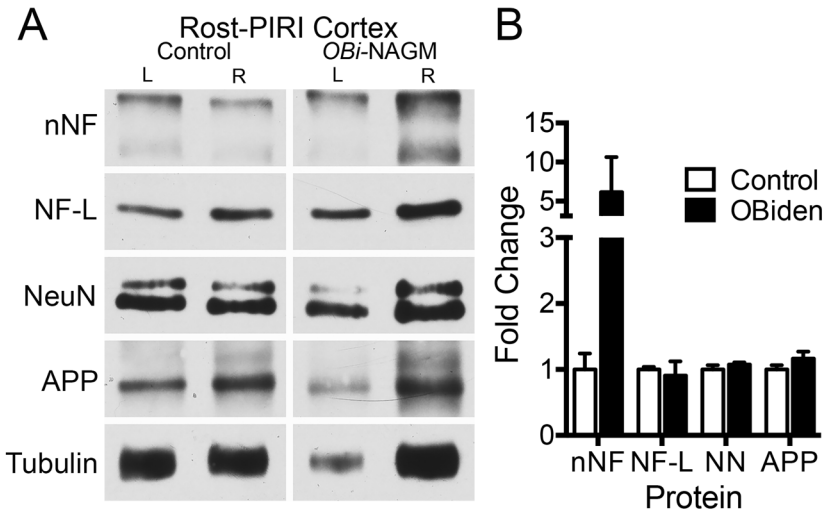

C

Rost-Piriform Cortex

ANOVA table	SS	DF	MS	F (DFn, DFd)	P value
Interaction	74.9	3	24.97	F (3, 56) = 0.5245	P = 0.6672
Protein	74.9	3	24.97	F (3, 56) = 0.5245	P = 0.6672
Genotype	24.15	1	24.15	F (1, 56) = 0.5074	P = 0.4792
Residual	2665	56	47.6		

Control - OBiden	Summary	Adjusted P Value
nNF	ns	0.4538
NF-L	ns	> 0.9999
NN	ns	> 0.9999
APP	ns	> 0.9999

Supplemental Figure 5.1 – **A**) Representative bilateral western blots from control and *OBiden* mouse rostral piriform cortex. **B**) Quantification of rostral piriform western blots showing no significant differences in amount of any protein between control and *OBiden* mice. **C**) 2-way ANOVA statistical table with no main effect differences between groups confirmed by no significant differences upon analysis with post-hoc t-tests.

Supplemental Figure 5.2 – Entorhinal Cortex Axon Initial Segment Lengths

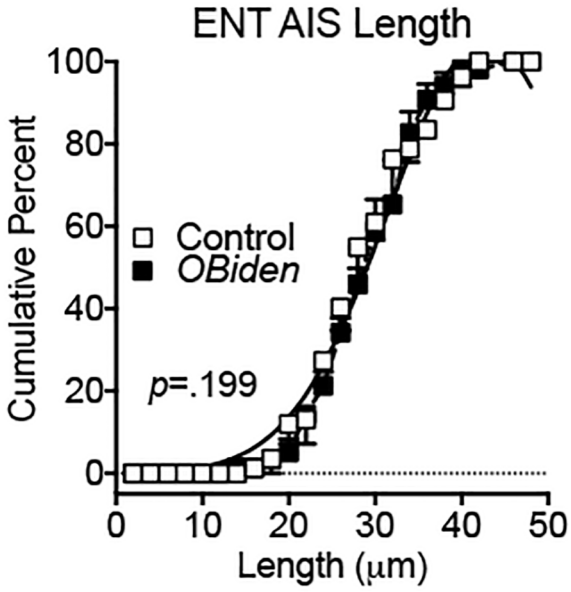

Comparison of Fits

Null hypothesis	One curve for all data sets
Alternative hypothesis	Different curve for each data set
P value	0.1985
Preferred model	One curve for all data sets
F (DFn, DFd)	1.575 (3,132)

Best-fit values	Control	*OBiden*
Mean	42.84	42.65
SD	11.68	10.88

Supplemental Figure 5.2 – Cumulative AIS length plot showing no differences between control and *OBiden* curves for the caudal portion of the entorhinal cortex, indicating no shortening of the AIS when measured using AnkG.

Supplemental Figure 5.3 – Dorsal Hippocampus Axon Initial Segment Western

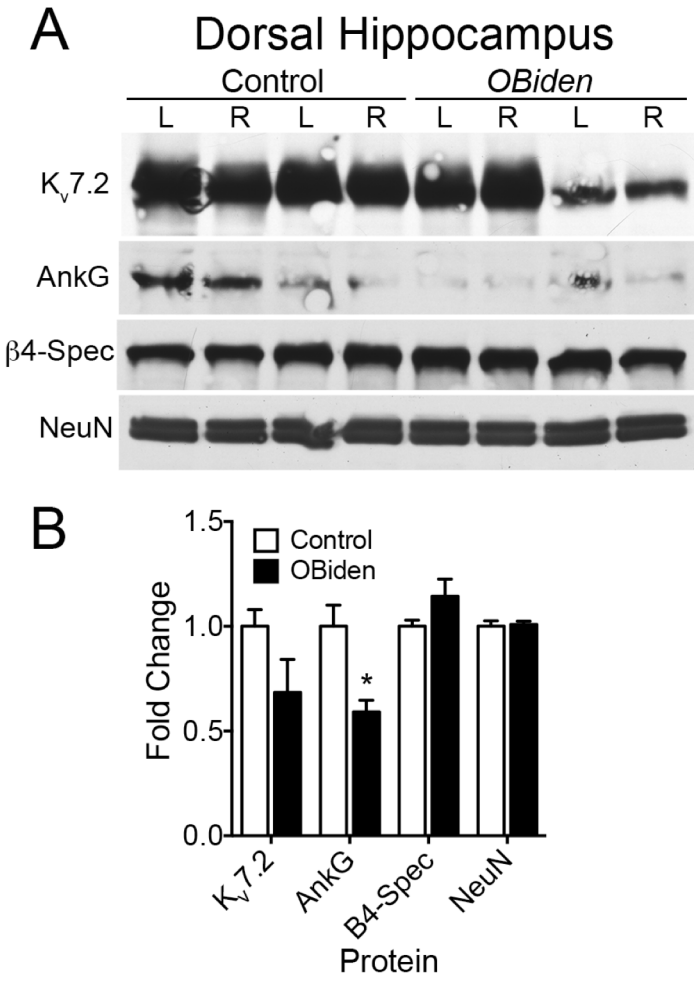

Supplemental Figure 5.3 – **A**) Western blots of AIS proteins obtained from tissue punches encompassing the entire dorsal hippocampus. NeuN blots between control and *OBiden* mice were compared and no difference was found and all AIS proteins were normalized to NeuN signal. **B**) Quantification of NeuN normalized AIS western blots showing a significant decrease in AnkG signal as well as a decreased in the mean $K_v7.2$ signal. Due to variability between animals the $K_v7.2$ was not significantly altered (n = 4 per group)

Supplemental Figure 5.4 – Ventral Hippocampus Axon Initial Segment Western

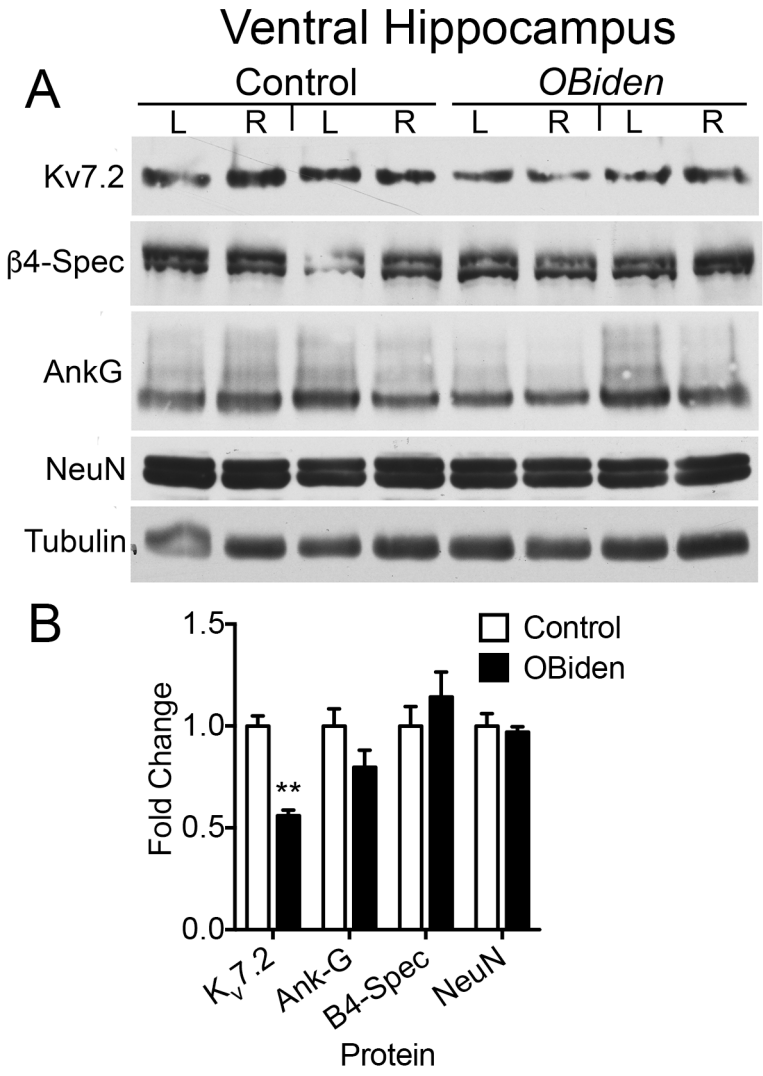

Supplemental Figure 5.4 – **A**) Representative bilateral western blots from the VHC of control and *OBiden* mice. **B**) Quantified, normalized signals show a significant decrease in the abundance of $K_v7.2$ in the *OBiden* mice compared to controls. Structural AIS proteins AnkG and β4-Spec were unaffected, as was neuronal marker NeuN (n= 4 per group).

Supplemental Table 5.1 – Dorsal and Ventral Hippocampus Axon Initial Segment Western Blot Statistics

Dorsal Hippocampus

ANOVA table	SS	DF	MS	F (DFn, DFd)	P value
Interaction	0.4103	3	0.1368	F (3, 24) = 5.235	P = 0.0064
Protein	0.4103	3	0.1368	F (3, 24) = 5.235	P = 0.0064
Genotype	0.164	1	0.164	F (1, 24) = 6.277	P = 0.0194
Residual	0.6271	24	0.02613		

Ventral Hippocampus

ANOVA table	SS	DF	MS	F (DFn, DFd)	P value
Interaction	0.3712	3	0.1237	F (3, 24) = 5.403	P = 0.0055
Protein	0.3712	3	0.1237	F (3, 24) = 5.403	P = 0.0055
Genotype	0.1405	1	0.1405	F (1, 24) = 6.134	P = 0.0207
Residual	0.5496	24	0.0229		

Dorsal Hippocampus

Control - OBiden	Summary	Adjusted P Value
Kv7.2	*	0.0425
AnkG	**	0.0061
B4-Spec	ns	0.633
NeuN	ns	> 0.9999

Ventral Hippocampus

Control - OBiden	Summary	Adjusted P Value
Kv7.2	**	0.0016
Ank-G	ns	0.2537
B4-Spec	ns	0.581
NeuN	ns	0.9977

Supplemental Figure 5.5 – Ctip2 Staining in the *OBiden* Mouse Cortex

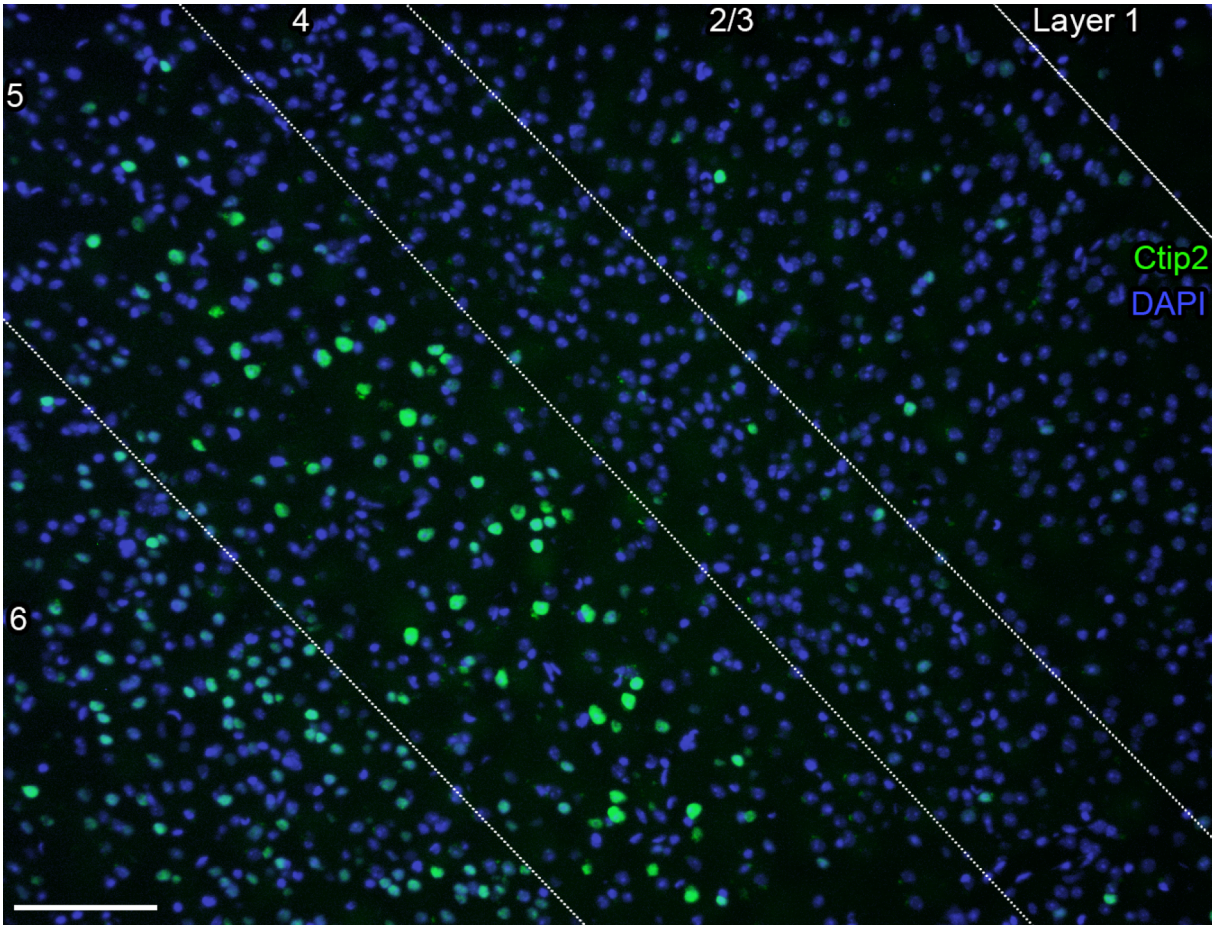

Supplemental Figure 5.5 – Staining from 12-month old control mouse in the rostral entorhinal cortex for Ctip2 (green) and DAPI (blue). The numbers and dashed lines indicate the layers of the cortex and Ctip2 staining predominates in layers 5 and 6. Scale bar = 100μm.

REFERENCES

1. Acharjee, S., Nayani, N., Tsutsui, M., Hill, M.N., Ousman, S.S., and Pittman, Q.J. (2013). Altered cognitive-emotional behavior in early experimental autoimmune encephalitis – Cytokine and hormonal correlates. Brain, Behavior, and Immunity *33*, 164-172.

2. Adams, R.D., and Kubik, C.S. (1952). The morbid anatomy of the demyelinative diseases. The American Journal of Medicine *12*, 510-546.

3. Aristovich, K.Y., Packham, B.C., Koo, H., Santos, G.S.d., McEvoy, A., and Holder, D.S. (2016). Imaging fast electrical activity in the brain with electrical impedance tomography. NeuroImage *124, Part A*, 204-213.

4. Aung, W.Y., Mar, S., and Benzinger, T.L.S. (2013). Diffusion tensor MRI as a biomarker in axonal and myelin damage. Imaging in medicine *5*, 427-440.

5. Bacioglu, M., Maia, Luis F., Preische, O., Schelle, J., Apel, A., Kaeser, Stephan A., Schweighauser, M., Eninger, T., Lambert, M., Pilotto, A.*, et al.* (2016). Neurofilament Light Chain in Blood and CSF as Marker of Disease Progression in Mouse Models and in Neurodegenerative Diseases. Neuron *91*, 56-66.

6. Battefeld, A., Tran, B.T., Gavrilis, J., Cooper, E.C., and Kole, M.H.P. (2014). Heteromeric Kv7.2/7.3 Channels Differentially Regulate Action Potential Initiation and Conduction in Neocortical Myelinated Axons. The Journal of Neuroscience *34*, 3719.

7. Bauer, J., Bradl, M., Klein, M., Leisser, M., Deckwerth, T.L., Wekerle, H., and Lassmann, H. (2002). Endoplasmic Reticulum Stress in PLP-Overexpressing Transgenic Rats: Gray Matter Oligodendrocytes Are More Vulnerable than White Matter Oligodendrocytes. Journal of Neuropathology & Experimental Neurology *61*, 12.

8. Bennett, M.L., Bennett, F.C., Liddelow, S.A., Ajami, B., Zamanian, J.L., Fernhoff, N.B., Mulinyawe, S.B., Bohlen, C.J., Adil, A., Tucker, A.*, et al.* (2016). New tools for studying microglia

in the mouse and human CNS. Proceedings of the National Academy of Sciences *113*, E1738-E1746.

9. Benveniste, H., Kim, K., Zhang, L., and Johnson, G.A. (2000). Magnetic Resonance Microscopy of the C57BL Mouse Brain. NeuroImage *11*, 601-611.

10. Bischoff, C.M.a.A. (1975). Oligodendroglial cell development in jimpy mice and controls. An electron-microscopic study in the optic nerve. Journal of the neurological sciences *26*, 517-528.

11. Bjartmar, C., and Trapp, B.D. (2001). Axonal and neuronal degeneration in multiple sclerosis: mechanisms and functional consequences. Curr Opin Neurol *14*.

12. Bjartmar, C., and Trapp, B.D. (2003). Axonal degeneration and progressive neurologic disability in multiple sclerosis. Neurotox Res *5*.

13. Boullerne, A.I. (2016). The history of myelin. Experimental Neurology *283, Part B*, 431-445.

14. Brockschnieder, D., Pechmann, Y., Sonnenberg-Riethmacher, E., and Riethmacher, D. (2006). An improved mouse line for Cre-induced cell ablation due to diphtheria toxin A, expressed from the Rosa26 locus. genesis *44*, 322-327.

15. Brown, R.E., Stanford, L., and Schellinck, H.M. (2000). Developing Standardized Behavioral Tests for Knockout and Mutant Mice. ILAR Journal *41*, 163-174.

16. Calabresi, P.A., Kieseier, B.C., Arnold, D.L., Balcer, L.J., Boyko, A., Pelletier, J., Liu, S., Zhu, Y., Seddighzadeh, A., Hung, S.*, et al.* (2014). Pegylated interferon beta-1a for relapsing-remitting multiple sclerosis (ADVANCE): a randomised, phase 3, double-blind study. The Lancet Neurology *13*, 657-665.

17. Can, A., Dao, D.T., Arad, M., Terrillion, C.E., Piantadosi, S.C., and Gould, T.D. (2012). The Mouse Forced Swim Test. Journal of Visualized Experiments : JoVE, 3638.

18. Chen, B., Wang, S.S., Hattox, A.M., Rayburn, H., Nelson, S.B., and McConnell, S.K. (2008). The Fezf2–Ctip2 genetic pathway regulates the fate choice of subcortical projection neurons in the developing cerebral cortex. Proceedings of the National Academy of Sciences *105*, 11382-11387.

19. Chen, L., Faas, G.C., Ferando, I., and Mody, I. (2015). Novel insights into the behavioral analysis of mice subjected to the forced-swim test. Transl Psychiatry *5*, e551.

20. Chen, S.-K., Tvrdik, P., Peden, E., Cho, S., Wu, S., Spangrude, G., and Capecchi, M.R. (2010). Hematopoietic Origin of Pathological Grooming in Hoxb8 Mutant Mice. Cell *141*, 775-785.

21. Chitnis, T., Ghezzi, A., Bajer-Kornek, B., Boyko, A., Giovannoni, G., and Pohl, D. (2016). Pediatric multiple sclerosis: Escalation and emerging treatments. Neurology *87*, S103-S109.

22. Chung, N.-C., Huang, Y.-H., Chang, C.-H., Liao, J.C., Yang, C.-H., Chen, C.-C., and Liu, I.Y. (2015). Behavior Training Reverses Asymmetry in Hippocampal Transcriptome of the Cav 3.2 Knockout Mice. PLoS ONE *10*, e0118832.

23. Coles, A., Deans, J., and Compston, A. (2004). Campath-1H treatment of multiple sclerosis: lessons from the bedside for the bench. Clin Neurol Neurosurg *106*.

24. Coles, A.J., Compston, D.A., Selmaj, K.W., Lake, S.L., Moran, S., and Margolin, D.H. (2008). Alemtuzumab vs. interferon beta-1a in early multiple sclerosis. N Engl J Med *359*.

25. Conel, J.L. (1953). Contribution of S. Ramon y Cajal to the Knowledge of the Anatomy of the Cerebral Cortex. New England Journal of Medicine *248*, 541-543.

26. Confavreux, C., and Vukusic, S. (2006). Age at disability milestones in multiple sclerosis. Brain *129*.

27. Corbin, J.G., Kelly, D., Rath, E.M., Baerwald, K.D., Suzuki, K., and Popko, B. (1996). Targeted CNS Expression of Interferon-γ in Transgenic Mice Leads to Hypomyelination, Reactive Gliosis, and Abnormal Cerebellar Development. Molecular and Cellular Neuroscience *7*, 354-370.

28. Dautigny, A., Mattei, M.G., Morello, D., Alliel, P.M., Pham-Dinh, D., Amar, L., Arnaud, D., Simon, D., Mattei, J.F., Guenet, J.L., *et al.* (1986). The structural gene coding for myelin-associated proteolipid protein is mutated in jimpy mice. Nature *321*, 867-869.

29. Deacon, R.M.J. (2013). Measuring the Strength of Mice. Journal of Visualized Experiments : JoVE, 2610.

30. Deacon, R.M.J., and Rawlins, J.N.P. (2006). T-maze alternation in the rodent. Nat Protocols *1*, 7-12.

31. Delmas, P., and Brown, D.A. (2005). Pathways modulating neural KCNQ/M (Kv7) potassium channels. Nat Rev Neurosci *6*, 850-862.

32. Denninger, A.R., Breglio, A., Maheras, K.J., LeDuc, G., Cristiglio, V., Deme, B., Gow, A., and Kirschner, D.A. (2015). Claudin-11 Tight Junctions in Myelin Are a Barrier to Diffusion and Lack Strong Adhesive Properties. Biophys J *109*, 1387-1397.

33. Dousset, V., Brochet, B., Vital, A., Gross, C., Benazzouz, A., Boullerne, A., Bidabe, A.M., Gin, A.M., and Caille, J.M. (1995). Lysolecithin-induced demyelination in primates: preliminary in vivo study with MR and magnetization transfer. American Journal of Neuroradiology *16*, 225-231.

34. Duddy, M., and Palace, J. (2015). The UK Risk-Sharing Scheme for interferon-beta and glatiramer acetate in multiple sclerosis. Outcome of the year-6 analysis. Pract Neurol.

35. Eagle, A.L., Gajewski, P.A., Yang, M., Kechner, M.E., Al Masraf, B.S., Kennedy, P.J., Wang, H., Mazei-Robison, M.S., and Robison, A.J. (2015). Experience-Dependent Induction of Hippocampal ΔFosB Controls Learning. The Journal of Neuroscience *35*, 13773-13783.

36. Edgar, J.M., McCulloch, M.C., Montague, P., Brown, A.M., Thilemann, S., Pratola, L., Gruenenfelder, F.I., Griffiths, I.R., and Nave, K.A. (2010). Demyelination and axonal preservation in a transgenic mouse model of Pelizaeus‐Merzbacher disease. EMBO Molecular Medicine *2*, 42.

37. Elder, G.A., Friedrich, V.L., Bosco, P., Kang, C., Gourov, A., Tu, P.-H., Lee, V.M.Y., and Lazzarini, R.A. (1998a). Absence of the Mid-sized Neurofilament Subunit Decreases Axonal Calibers, Levels of Light Neurofilament (NF-L), and Neurofilament Content. The Journal of Cell Biology *141*, 727.

38. Elder, G.A., Friedrich, V.L., Kang, C., Bosco, P., Gourov, A., Tu, P.-H., Zhang, B., Lee, V.M.Y., and Lazzarini, R.A. (1998b). Requirement of Heavy Neurofilament Subunit in the Development of Axons with Large Calibers. The Journal of Cell Biology *143*, 195.

39. Evans, Mark D., Dumitrescu, Adna S., Kruijssen, Dennis L.H., Taylor, Samuel E., and Grubb, Matthew S. (2015). Rapid Modulation of Axon Initial Segment Length Influences Repetitive Spike Firing. Cell Reports *13*, 1233-1245.

40. Feinstein, A., Freeman, J., and Lo, A.C. (2015). Treatment of progressive multiple sclerosis: what works, what does not, and what is needed. The Lancet Neurology *14*, 194-207.

41. Filippi, M.M. (2001). Diffusion tensor magnetic resonance imaging in multiple sclerosis. Neurology *56*, 304-311.

42. Fischer, M.T., Wimmer, I., Höftberger, R., Gerlach, S., Haider, L., Zrzavy, T., Hametner, S., Mahad, D., Binder, C.J., Krumbholz, M.*, et al.* (2013). Disease-specific molecular events in cortical multiple sclerosis lesions. Brain *136*, 1799-1815.

43. Fish, K.N., Hoftman, G.D., Sheikh, W., Kitchens, M., and Lewis, D.A. (2013). Parvalbumin-Containing Chandelier and Basket Cell Boutons Have Distinctive Modes of Maturation in Monkey Prefrontal Cortex. The Journal of Neuroscience *33*, 8352.

44. Franklin, R.J., Crang Aj Fau - Blakemore, W.F., and Blakemore, W.F. (1993). The reconstruction of an astrocytic environment in glia-deficient areas of white matter.

45. Funkhouser, E.B. (1915). THE VISUAL CORTEX, ITS LOCALIZATION, HISTOLOGICAL STRUCTURE, AND PHYSIOLOGICAL FUNCTION. The Journal of Experimental Medicine *21*, 617.

46. Gao, X., Gillig, T.A., Ye, P., D'Ercole, A.J., Matsushima, G.K., and Popko, B. (2000). Interferon-γ Protects against Cuprizone-Induced Demyelination. Molecular and Cellular Neuroscience *16*, 338-349.

47. Garbern, J.Y. (2007). Pelizaeus-Merzbacher disease: Genetic and cellular pathogenesis. Cellular and Molecular Life Sciences *64*, 50-65.

48. Gardinier, V., and Macklin, W.B. (1988). Myelin Proteolipid Protein Gene Expression in Jimpy and Jimpymsd Mice. Journal of Neurochemistry *51*, 360-369.

49. Garrosa, J.R.I.-R.a.M. (2012). Glia with very few processes (oligodendroglia) by Pio del Rio-Hortega. Clinical Neuropathology *31*, 440-459.

50. Garven, H.S.D., and Gairns, F.W. (1952). THE SILVER DIAMMINE ION STAINING OF PERIPHERAL NERVE ELEMENTS AND THE INTERPRETATION OF THE RESULTS: WITH A MODIFICATION OF THE BIELSCHOWSKY-GROS METHOD FOR FROZEN SECTIONS. Quarterly Journal of Experimental Physiology and Cognate Medical Sciences *37*, 131-142.

51. Gencic, S., and Hudson, L.D. (1990). Conservative amino acid substitution in the myelin proteolipid protein of jimpymsd mice. The Journal of Neuroscience *10*, 117.

52. Giovannoni, G., Gold, R., Selmaj, K., Havrdova, E., Montalban, X., Radue, E.-W., Stefoski, D., McNeill, M., Amaravadi, L., Sweetser, M.*, et al.* (2014). Daclizumab high-yield process in relapsing-remitting multiple sclerosis (SELECTION): a multicentre, randomised, double-blind extension trial. The Lancet Neurology *13*, 472-481.

53. Glasser, M.F., Coalson, T.S., Robinson, E.C., Hacker, C.D., Harwell, J., Yacoub, E., Ugurbil, K., Andersson, J., Beckmann, C.F., Jenkinson, M.*, et al.* (2016). A multi-modal parcellation of human cerebral cortex. Nature *advance online publication*.

54. Goldberg, J., Clarner, T., Beyer, C., and Kipp, M. (2015). Anatomical Distribution of Cuprizone-Induced Lesions in C57BL6 Mice. Journal of Molecular Neuroscience *57*, 166-175.

55. Gow, A. (2011). Chapter nine - Using Temporal Genetic Switches to Synchronize the Unfolded Protein Response in Cell Populations In Vivo. In Methods in Enzymology, P.M. Conn, ed. (Academic Press), pp. 143-161.

56. Gow, A., Friedrich, V.L., and Lazzarini, R.A. (1992). Myelin basic protein gene contains separate enhancers for oligodendrocyte and Schwann cell expression. The Journal of Cell Biology *119*, 605-616.

57. Gow, A., Friedrich, V.L., and Lazzarini, R.A. (1994a). Intracellular transport and sorting of the oligodendrocyte transmembrane proteolipid protein. Journal of Neuroscience Research *37*, 563-573.

58. Gow, A., Friedrich, V.L., and Lazzarini, R.A. (1994b). Many naturally occurring mutations of myelin proteolipid protein impair its intracellular transport. Journal of Neuroscience Research *37*, 574-583.

59. Gow, A., and Lazzarini, R.A. (1996). A cellular mechanism governing the severity of Pelizaeus-Merzbacher disease. Nat Genet *13*, 422-428.

60. Gow, A., Southwood, C.M., and Lazzarini, R.A. (1998). Disrupted proteolipid protein trafficking results in oligodendrocyte apoptosis in an animal model of Pelizaeus-Merzbacher disease. J Cell Biol *140*, 925-934.

61. Gow, A., and Wrabetz, L. (2009). CHOP and the endoplasmic reticulum stress response in myelinating glia. Current Opinion in Neurobiology *19*, 505-510.

62. Gschwind, M., Hardmeier, M., Van De Ville, D., Tomescu, M.I., Penner, I.-K., Naegelin, Y., Fuhr, P., Michel, C.M., and Seeck, M. (2016). Fluctuations of spontaneous EEG topographies predict disease state in relapsing-remitting multiple sclerosis. NeuroImage: Clinical *12*, 466-477.

63. Gusel'nikova, V.V., and Korzhevskiy, D.E. (2015). NeuN As a Neuronal Nuclear Antigen and Neuron Differentiation Marker. Acta Naturae *7*, 42-47.

64. Hamada, M.S., and Kole, M.H.P. (2015). Myelin Loss and Axonal Ion Channel Adaptations Associated with Gray Matter Neuronal Hyperexcitability. The Journal of Neuroscience *35*, 7272.

65. Hampton, D.W., Serio, A., Pryce, G., Al-Izki, S., Franklin, R.J.M., Giovannoni, G., Baker, D., and Chandran, S. (2013). Neurodegeneration progresses despite complete elimination of clinical relapses in a mouse model of multiple sclerosis. Acta Neuropathologica Communications *1*, 84.

66. Hares, K., Redondo, J., Kemp, K., Rice, C., Scolding, N., and Wilkins, A. (2016). Axonal motor protein KIF5A and associated cargo deficits in multiple sclerosis lesional and normal‐appearing white matter. Neuropathology and Applied Neurobiology.

67. Harrison, F.E., Reiserer, R.S., Tomarken, A.J., and McDonald, M.P. (2006). Spatial and nonspatial escape strategies in the Barnes maze. Learning & Memory *13*, 809-819.

68. Hasselmann, H., Bellmann-Strobl, J., Ricken, R., Oberwahrenbrock, T., Rose, M., Otte, C., Adli, M., Paul, F., Brandt, A.U., Finke, C.*, et al.* (2016). Characterizing the phenotype of multiple sclerosis–associated depression in comparison with idiopathic major depression. Multiple Sclerosis Journal.

69. Haussleiter, I.S., Brüne, M., and Juckel, G. (2009). Review: Psychopathology in multiple sclerosis: diagnosis, prevalence and treatment. Therapeutic Advances in Neurological Disorders *2*, 13-29.

70. Hemmer, B., Kerschensteiner, M., and Korn, T. (2015). Role of the innate and adaptive immune responses in the course of multiple sclerosis. The Lancet Neurology *14*, 406-419.

71. Henderson, N.D. (1968). Genetic analysis of acquisition and retention of a conditioned fear in mice. Journal of comparative & physiological psychology *65*, 325-330.

72. Hernandez, C.C., Zaika, O., Tolstykh, G.P., and Shapiro, M.S. (2008). Regulation of neural KCNQ channels: signalling pathways, structural motifs and functional implications. The Journal of Physiology *586*, 1811-1821.

73. Ho, T.S., Zollinger, D.R., Chang, K.J., Xu, M., Cooper, E.C., Stankewich, M.C., Bennett, V., and Rasband, M.N. (2014). A hierarchy of ankyrin-spectrin complexes clusters sodium channels at nodes of Ranvier. Nat Neurosci *17*, 1664-1672.

74. Huizinga, R., Gerritsen, W., Heijmans, N., and Amor, S. (2008). Axonal loss and gray matter pathology as a direct result of autoimmunity to neurofilaments. Neurobiology of Disease *32*, 461-470.

75. Igarashi, K.M., Lu, L., Colgin, L.L., Moser, M.-B., and Moser, E.I. (2014). Coordination of entorhinal-hippocampal ensemble activity during associative learning. Nature *510*, 143-147.

76. Ikeda, S.R., and Kammermeier, P.J. (2002). M Current Mystery Messenger Revealed? Neuron *35*, 411-412.

77. Ikenaka, K., Furuichi, T., Iwasaki, Y., Moriguchi, A., Okano, H., and Mikoshiba, K. (1988). Myelin proteolipid protein gene structure and its regulation of expression in normal and jimpy mutant mice. Journal of Molecular Biology *199*, 587-596.

78. Inda, M.C., DeFelipe, J., and Muñoz, A. (2006). Voltage-gated ion channels in the axon initial segment of human cortical pyramidal cells and their relationship with chandelier cells. Proceedings of the National Academy of Sciences of the United States of America *103*, 2920-2925.

79. Inoue, K., Osaka, H., Imaizumi, K., Nezu, A., Takanashi, J.-I., Arii, J., Murayama, K., Ono, J., Kikawa, Y., Mito, T.*, et al.* (1999). Proteolipid protein gene duplications causing Pelizaeus-Merzbacher disease: molecular mechanism and phenotypic manifestations. Annals of neurology *45*, 624-632.

80. Inoue, Y., Kagawa, T., Matsumura, Y., Ikenaka, K., and Mikoshiba, K. (1996). Cell death of oligodendrocytes or demyelination induced by overexpression of proteolipid protein depending on expressed gene dosage. Neuroscience Research *25*, 161-172.

81. Jacobs, L., O'Malley, J., Freeman, A., Murawski, J., and Ekes, R. (1982). Intrathecal interferon in multiple sclerosis. Archives of Neurology *39*, 609-615.

82. Jacomy, H., Zhu, Q., Couillard-Despres, S., Beaulieu, J., and Julien, J. (1999). Disruption of Type IV Intermediate Filament Network in Mice Lacking the Neurofilament Medium and Heavy Subunits. Journal of neurochemistry *73*, 972-984.

83. Kappos, L., Hartung, H.-P., Freedman, M.S., Boyko, A., Radü, E.W., Mikol, D.D., Lamarine, M., Hyvert, Y., Freudensprung, U., Plitz, T.*, et al.* (2014). Atacicept in multiple sclerosis (ATAMS): a randomised, placebo-controlled, double-blind, phase 2 trial. The Lancet Neurology *13*, 353-363.

84. Karim, S.A., Barrie, J.A., McCulloch, M.C., Montague, P., Edgar, J.M., Kirkham, D., Anderson, T.J., Nave, K.A., Griffiths, I.R., and McLaughlin, M. (2007). PLP overexpression perturbs myelin protein composition and myelination in a mouse model of Pelizaeus-Merzbacher disease. Glia *55*, 341-351.

85. Kaufman, R.J. (2002). Orchestrating the unfolded protein response in health and disease. The Journal of Clinical Investigation *110*, 1389-1398.

86. Kearney, H., Miszkiel, K.A., Yiannakas, M.C., Altmann, D.R., Ciccarelli, O., and Miller, D.H. (2015). Grey matter involvement by focal cervical spinal cord lesions is associated with progressive multiple sclerosis. Mult Scler.

87. Kilsdonk, I.D., Jonkman, L.E., Klaver, R., van Veluw, S.J., Zwanenburg, J.J.M., Kuijer, J.P.A., Pouwels, P.J.W., Twisk, J.W.R., Wattjes, M.P., Luijten, P.R., *et al.* (2016). Increased cortical grey matter lesion detection in multiple sclerosis with 7 T MRI: a post-mortem verification study. Brain *139*, 1472-1481.

88. Kitamura, T., Macdonald, C.J., and Tonegawa, S. (2015). Entorhinal–hippocampal neuronal circuits bridge temporally discontiguous events. Learning & Memory *22*, 438-443.

89. Knapp, P.F., Skoff, R.P., and Redstone, D.W. (1986). Oligodendroglial cell death in jimpy mice: an explanation for the myelin deficit.

90. Koenig, K.A., Sakaie, K.E., Lowe, M.J., Lin, J., Stone, L., Bermel, R.A., Beall, E.B., Rao, S.M., Trapp, B.D., and Phillips, M.D. (2014). Hippocampal volume is related to cognitive decline and fornicial diffusion measures in multiple sclerosis. Magnetic Resonance Imaging *32*, 354-358.

91. Kohno, K., Normington, K., Sambrook, J., Gething, M.J., and Mori, K. (1993). The promoter region of the yeast KAR2 (BiP) gene contains a regulatory domain that responds to the presence of unfolded proteins in the endoplasmic reticulum. Molecular and Cellular Biology *13*, 877-890.

92. Kole, M.H.P., Ilschner, S.U., Kampa, B.M., Williams, S.R., Ruben, P.C., and Stuart, G.J. (2008). Action potential generation requires a high sodium channel density in the axon initial segment. Nat Neurosci *11*, 178-186.

93. Kole, Maarten H.P., and Stuart, Greg J. (2012). Signal Processing in the Axon Initial Segment. Neuron *73*, 235-247.

94. Kornek, B., and Lassmann, H. (1999). Axonal Pathology in Multiple Sclerosis. A Historical Note. Brain Pathology *9*, 651-656.

95. Kuba, H., Adachi, R., and Ohmori, H. (2014). Activity-Dependent and Activity-Independent Development of the Axon Initial Segment. The Journal of Neuroscience *34*, 3443-3453.

96. Kuba, H., Yamada, R., Ishiguro, G., and Adachi, R. (2015). Redistribution of Kv1 and Kv7 enhances neuronal excitability during structural axon initial segment plasticity. Nat Commun *6*.

97. Kuhlmann, T., Ludwin, S., Prat, A., Antel, J., Brück, W., and Lassmann, H. (2017). An updated histological classification system for multiple sclerosis lesions. Acta Neuropathologica *133*, 13-24.

98. Lee, M.K., Marszalek, J.R., and Cleveland, D.W. (1994). A mutant neurofilament subunit causes massive, selective motor neuron death: Implications for the pathogenesis of human motor neuron disease. Neuron *13*, 975-988.

99. Lidster, K., Jackson, S.J., Ahmed, Z., Munro, P., Coffey, P., Giovannoni, G., Baker, M.D., and Baker, D. (2013). Neuroprotection in a Novel Mouse Model of Multiple Sclerosis. PLOS ONE *8*, e79188.

100. Liska, A., Galbusera, A., Schwarz, A.J., and Gozzi, A. (2015). Functional connectivity hubs of the mouse brain. NeuroImage *115*, 281-291.

101. Liu, Y., Staal, J.A., Canty, A.J., Kirkcaldie, M.T.K., King, A.E., Bibari, O., Mitew, S.T., Dickson, T.C., and Vickers, J.C. (2013). Cytoskeletal changes during development and aging in the cortex of neurofilament light protein knockout mice. Journal of Comparative Neurology *521*, 1817-1827.

102. Llufriu, S., Martinez-Heras, E., Fortea, J., Blanco, Y., Berenguer, J., Gabilondo, I., Ibarretxe-Bilbao, N., Falcon, C., Sepulveda, M., Sola-Valls, N.*, et al.* (2014). Cognitive functions in multiple sclerosis: impact of gray matter integrity. Multiple Sclerosis Journal *20*, 424-432.

103. Lorscheider, J., Buzzard, K., Jokubaitis, V., Spelman, T., Havrdova, E., Horakova, D., Trojano, M., Izquierdo, G., Girard, M., Duquette, P.*, et al.* (2016). Defining secondary progressive multiple sclerosis. Brain *139*, 2395.

104. Lublin, F., Miller, D.H., Freedman, M.S., Cree, B.A.C., Wolinsky, J.S., Weiner, H., Lubetzki, C., Hartung, H.-P., Montalban, X., Uitdehaag, B.M.J.*, et al.* (2016). Oral fingolimod in primary progressive multiple sclerosis (INFORMS): a phase 3, randomised, double-blind, placebo-controlled trial. The Lancet *387*, 1075-1084.

105. Maheras, K.J., and Gow, A. (2013). Increased anesthesia time using 2,2,2-tribromoethanol-chloral hydrate with low impact on mouse psychoacoustics. J Neurosci Methods *219*, 61-69.

106. Maytin, E.V., Ubeda, M., Lin, J.C., and Habener, J.F. (2001). Stress-Inducible Transcription Factor CHOP/gadd153 Induces Apoptosis in Mammalian Cells via p38 Kinase-Dependent and -Independent Mechanisms. Experimental Cell Research *267*, 193-204.

107. Montalban, X., Hauser, S.L., Kappos, L., Arnold, D.L., Bar-Or, A., Comi, G., de Seze, J., Giovannoni, G., Hartung, H.-P., Hemmer, B.*, et al.* (2016). Ocrelizumab versus Placebo in Primary Progressive Multiple Sclerosis. New England Journal of Medicine *376*, 209-220.

108. Morellini, F., Sivukhina, E., Stoenica, L., Oulianova, E., Bukalo, O., Jakovcevski, I., Dityatev, A., Irintchev, A., and Schachner, M. (2010). Improved Reversal Learning and Working Memory and Enhanced Reactivity to Novelty in Mice with Enhanced GABAergic Innervation in the Dentate Gyrus. Cerebral Cortex *20*, 2712-2727.

109. Nijeholt, G.J., van Walderveen, M.A., Castelijns, J.A., van Waesberghe, J.H., Polman, C., Scheltens, P., Rosier, P.F., Jongen, P.J., and Barkhof, F. (1988). Brain and spinal cord abnormalities in multiple sclerosis. Correlation between MRI parameters, clinical subtypes and symptoms. Brain (London, England : 1878) *121 (Pt 4)*, 687-697.

110. O'Keefe, J. (1979). A review of the hippocampal place cells. Progress in Neurobiology *13*, 419-439.

111. O'Leary, T.P., Savoie, V., and Brown, R.E. (2011). Learning, memory and search strategies of inbred mouse strains with different visual abilities in the Barnes maze. Behavioural Brain Research *216*, 531-542.

112. Oluich, L.-J., Stratton, J.A.S., Lulu Xing, Y., Ng, S.W., Cate, H.S., Sah, P., Windels, F., Kilpatrick, T.J., and Merson, T.D. (2012). Targeted Ablation of Oligodendrocytes Induces Axonal Pathology Independent of Overt Demyelination. The Journal of Neuroscience *32*, 8317-8330.

113. Oosten, B.W.v., Hodgkins, S., Barkhof, F., Miller, D.H., Moseley, I.F., Thompson, A.J., Rudge, P., McDougall, A., Mcleod, J.G., Ader, H.J.*, et al.* (1997). Treatment of multiple sclerosis with the monoclonal anti-CD4 antibody cM-T412: results of a randomized, double-blind, placebo-controlled, MR-monitored phase II trial. Neurology *49*, 351-357.

114. Ozawa, K., Suchanek, G., Breitschopf, H., Br€ck, W., Budka, H., Jellinger, K., and Lassmann, H. (1994). Patterns of oligodendroglia pathology in multiple sclerosis. Brain *117*, 1311-1322.

115. Padilla-Coreano, N., Bolkan, Scott S., Pierce, Georgia M., Blackman, Dakota R., Hardin, William D., Garcia-Garcia, Alvaro L., Spellman, Timothy J., and Gordon, Joshua A. (2016). Direct Ventral Hippocampal-Prefrontal Input Is Required for Anxiety-Related Neural Activity and Behavior. Neuron *89*, 857-866.

116. Palay, S.L., Sotelo, C., Peters, A., and Orkand, P.M. (1968). THE AXON HILLOCK AND THE INITIAL SEGMENT. The Journal of Cell Biology *38*, 193.

117. Panitch, H.S.H. (1987). Exacerbations of multiple sclerosis in patients treated with gamma interferon. Lancet *1*, 893-895.

118. Pardini, M., Bergamino, M., Bommarito, G., Bonzano, L., Luigi Mancardi, G., and Roccatagliata, L. (2014). Structural correlates of subjective and objective memory performance in multiple sclerosis. Hippocampus *24*, 436-445.

119. Peters, A. (1960). THE FORMATION AND STRUCTURE OF MYELIN SHEATHS IN THE CENTRAL NERVOUS SYSTEM. The Journal of Biophysical and Biochemical Cytology *8*, 431.

120. Polak, P.E., Kalinin, S., and Feinstein, D.L. (2011). Locus coeruleus damage and noradrenaline reductions in multiple sclerosis and experimental autoimmune encephalomyelitis. Brain *134*, 665-677.

121. Polman, C.H., Reingold, S.C., Banwell, B., Clanet, M., Cohen, J.A., Filippi, M., Fujihara, K., Havrdova, E., Hutchinson, M., Kappos, L.*, et al.* (2011). Diagnostic criteria for multiple sclerosis: 2010 Revisions to the McDonald criteria. Annals of Neurology *69*, 292-302.

122. Porsolt, R.D., Bertin, A., and Jalfre, M. (1977). Behavioral despair in mice: a primary screening test for antidepressants. Archives internationales de pharmacodynamie et de thérapie *229*, 327-336.

123. Prineas, J.W., Kwon, E.E., Cho, E.-S., and Sharer, L.R. (1984). Continual Breakdown and Regeneration of Myelin in Progressive Multiple Sclerosis Plaquesa. Annals of the New York Academy of Sciences *436*, 11-32.

124. Pryce, G., O'Neill, J.K., Croxford, J.L., Amor, S., Hankey, D.J., and East, E. (2005). Autoimmune tolerance eliminates relapses but fails to halt progression in a model of multiple sclerosis. J Neuroimmunol *165*.

125. Rasband, M.N. (2010). The axon initial segment and the maintenance of neuronal polarity. Nat Rev Neurosci *11*, 552-562.

126. Raskind, W.H., Williams, C.A., Hudson, L.D., and Bird, T.D. (1991). Complete deletion of the proteolipid protein gene (PLP) in a family with X-linked Pelizaeus-Merzbacher disease. American Journal of Human Genetics *49*, 1355-1360.

127. Rasminsky, Z.J.K.a.M. (1972). A computer simulation of conduction in demyelinated nerve fibres. The Journal of physiology *227*, 351-364.

128. Readhead, C., Schneider, A., Griffiths, I., and Nave, K.A. (1994). Premature arrest of myelin formation in transgenic mice with increased proteolipid protein gene dosage. Neuron *12*, 583-595.

129. Reuter, E., Gollan, R., Grohmann, N., Paterka, M., Salmon, H., Birkenstock, J., Richers, S., Leuenberger, T., Brandt, A.U., Kuhlmann, T.*, et al.* (2015). Cross-Recognition of a Myelin Peptide by CD8+ T Cells in the CNS Is Not Sufficient to Promote Neuronal Damage. The Journal of Neuroscience *35*, 4837-4850.

130. Rio-Hortega, P.d. (1921). Estudios sobre al neurologia. La glia de escasas radiaciones (oligodendroglia). Boletin de la Real Sociedad Espanola de Histroia Natural *21*, 63-92.

131. Rivers, T.M., Sprunt, D.H., and Berry, G.P. (1933). OBSERVATIONS ON ATTEMPTS TO PRODUCE ACUTE DISSEMINATED ENCEPHALOMYELITIS IN MONKEYS. The Journal of Experimental Medicine *58*, 39.

132. Rosenbluth, J., Stoffel, W., and Schiff, R. (1996). Myelin structure in proteolipid protein (PLP)-null mouse spinal cord. The Journal of Comparative Neurology *371*, 336-344.

133. Rovaris, M., Confavreux, C., Furlan, R., Kappos, L., Comi, G., and Filippi, M. (2006). Secondary progressive multiple sclerosis: current knowledge and future challenges. Lancet Neurol *5*.

134. Schafer, D.P., Jha, S., Liu, F., Akella, T., McCullough, L.D., and Rasband, M.N. (2009). Disruption of the Axon Initial Segment Cytoskeleton Is a New Mechanism for Neuronal Injury. The Journal of Neuroscience *29*, 13242-13254.

135. Scherzinger, A.L., and Hendee, W.R. (1985). Basic Principles of Magnetic Resonance Imaging—An Update. Western Journal of Medicine *143*, 782-792.

136. Schumacher, G.A., Beebe, G., Kibler, R.F., Kurland, L.T., Kurtzke, J.F., McDowell, F., Nagler, B., Sibley, W.A., Tourtellotte, W.W., and Willmon, T.L. (1965). PROBLEMS OF EXPERIMENTAL TRIALS OF THERAPY IN MULTIPLE SCLEROSIS: REPORT BY THE PANEL ON THE EVALUATION OF EXPERIMENTAL TRIALS OF THERAPY IN MULTIPLE SCLEROSIS. Annals of the New York Academy of Sciences *122*, 552-568.

137. Seewann, A., Vrenken, H., van der Valk, P., and et al. (2009). Diffusely abnormal white matter in chronic multiple sclerosis: Imaging and histopathologic analysis. Archives of Neurology *66*, 601-609.

138. Seo, D.-o., Funderburk, S.C., Bhatti, D.L., Motard, L.E., Newbold, D., Girven, K.S., McCall, J.G., Krashes, M., Sparta, D.R., and Bruchas, M.R. (2016). A GABAergic Projection from the Centromedial Nuclei of the Amygdala to Ventromedial Prefrontal Cortex Modulates Reward Behavior. The Journal of Neuroscience *36*, 10831.

139. Shah, S.N., and Salamy, A. (1980). Auditory-Evoked Far-Field Potentials in Myelin Deficient Mutant Quaking Mice. Neuroscience *5*, 2321-2323.

140. Sharma, R., and Gow, A. (2007). Minimal role for caspase 12 in the unfolded protein response in oligodendrocytes in vivo. Journal of neurochemistry *101*, 889-897.

141. Shaw, C.-M., Alvord, E.C., Fahlberg, W.J., and Kies, M.W. (1962). ADJUVANT-ANTIGEN RELATIONSHIPS IN THE PRODUCTION OF EXPERIMENTAL "ALLERGIC" ENCEPHALOMYELITIS IN THE GUINEA PIG. The Journal of Experimental Medicine *115*, 169.

142. Shimai, S.S. (1982). Effects of bilateral amygdala lesions on neophobia and conditioned taste aversion in mice. Perceptual and motor skills *54*, 127-130.

143. Shipton, O.A., El-Gaby, M., Apergis-Schoute, J., Deisseroth, K., Bannerman, D.M., Paulsen, O., and Kohl, M.M. (2014). Left–right dissociation of hippocampal memory processes in mice. Proceedings of the National Academy of Sciences *111*, 15238-15243.

144. Şık, A., van Nieuwehuyzen, P., Prickaerts, J., and Blokland, A. (2003). Performance of different mouse strains in an object recognition task. Behavioural Brain Research *147*, 49-54.

145. Snodgress, A.B., Dorsey, C.H., and Lacey, L.B. (1961). Luxol fast blue staining of degenerating myelinated fibers. The Anatomical Record *140*, 83-90.

146. Song, A.-h., Wang, D., Chen, G., Li, Y., Luo, J., Duan, S., and Poo, M.-m. (2009). A Selective Filter for Cytoplasmic Transport at the Axon Initial Segment. Cell *136*, 1148-1160.

147. Southwood, C.M., Fykkolodziej, B., Dachet, F., and Gow, A. (2013). Potential For Cell-mediated Immune Responses In Mouse Models Of Pelizaeus-Merzbacher Disease. Brain Sci *3*, 1417-1444.

148. Southwood, C.M., Fykkolodziej, B., Maheras, K.J., Garshott, D.M., Estill, M., Fribley, A.M., and Gow, A. (2016). Overexpression of CHOP in Myelinating Cells Does Not Confer a Significant Phenotype under Normal or Metabolic Stress Conditions. The Journal of Neuroscience *36*, 6803-6819.

149. Southwood, C.M., Garbern, J., Jiang, W., and Gow, A. (2002). The Unfolded Protein Response Modulates Disease Severity in Pelizaeus-Merzbacher Disease. Neuron *36*, 585-596.

150. Staugaitis, S.M., Chang, A., and Trapp, B.D. (2012). Cortical pathology in multiple sclerosis: experimental approaches to studies on the mechanisms of demyelination and remyelination. Acta Neurologica Scandinavica *126*, 97-102.

151. Susuki, K., and Rasband, M.N. (2008). Spectrin and ankyrin-based cytoskeletons at polarized domains in myelinated axons. Exp Biol Med (Maywood) *233*, 394-400.

152. Szabadics, J., Varga, C., Molnár, G., Oláh, S., Barzó, P., and Tamás, G. (2006). Excitatory Effect of GABAergic Axo-Axonic Cells in Cortical Microcircuits. Science *311*, 233.

153. Tang, Y., and Le, W. (2016). Differential Roles of M1 and M2 Microglia in Neurodegenerative Diseases. Molecular Neurobiology *53*, 1181-1194.

154. Traka, M., Podojil, J.R., McCarthy, D.P., Miller, S.D., and Popko, B. (2016). Oligodendrocyte death results in immune-mediated CNS demyelination. Nat Neurosci *19*, 65-74.

155. Trapp, B.D., Bö, L., Mörk, S., and Chang, A. (1999). Pathogenesis of tissue injury in MS lesions. Journal of Neuroimmunology *98*, 49-56.

156. Trapp , B.D., Peterson , J., Ransohoff , R.M., Rudick , R., Mörk , S., and Bö , L. (1998). Axonal Transection in the Lesions of Multiple Sclerosis. New England Journal of Medicine *338*, 278-285.

157. Trimmer, James S. (2015). Subcellular Localization of K+ Channels in Mammalian Brain Neurons: Remarkable Precision in the Midst of Extraordinary Complexity. Neuron *85*, 238-256.

158. Turnley, A.M., Morahan, G., Okano, H., Bernard, O., Mikoshiba, K., Allison, J., Bartlett, P.F., and Miller, J.F.A.P. (1991). Dysmyelination in transgenic mice resulting from expression of class I histocompatibility molecules in oligodendrocytes. Nature *353*, 566-569.

159. van Noort, J.M., van Sechel, A.C., Bajramovic, J.J., Ouagmiri, M.E.I., Polman, C.H., Lassmann, H., and Ravid, R. (1995). The small heat-shock protein [alpha]B-crystallin as candidate autoantigen in multiple sclerosis. Nature *375*, 798-801.

160. Vogel, F.S. (1951). DEMYELINIZATION INDUCED IN LIVING RABBITS BY MEANS OF A LIPOLYTIC ENZYME PREPARATION. The Journal of Experimental Medicine *93*, 297.

161. Walker, L.A.S., Osman, L., Berard, J.A., Rees, L.M., Freedman, M.S., MacLean, H., and Cousineau, D. (2016). Brief International Cognitive Assessment for Multiple Sclerosis (BICAMS): Canadian contribution to the international validation project. Journal of the Neurological Sciences *362*, 147-152.

162. Wang, X., and Sun, Q.-Q. (2012). Characterization of axo-axonic synapses in the piriform cortex of Mus musculus. The Journal of Comparative Neurology *520*, 832-847.

163. Warshawsky, I., Rudick, R.A., Staugaitis, S.M., and Natowicz, M.R. (2005). Primary progressive multiple sclerosis as a phenotype of a PLP1 gene mutation. Annals of Neurology *58*, 470-473.

164. Waxman, S.G. (1975). Electron-microscopic observations on preterminal fibers in the oculomotor nucleus of the cat. With special reference to the relation between axon diameter and myelin thickness in mammalian gray matter. Journal of the neurological sciences *26*, 395-400.

165. Wefelmeyer, W., Cattaert, D., and Burrone, J. (2015). Activity-dependent mismatch between axo-axonic synapses and the axon initial segment controls neuronal output. Proceedings of the National Academy of Sciences *112*, 9757-9762.

166. Wenngren, B.-I., and Anniko, M. (1988). A Frequency-specific Auditory Brainstem Response Technique Exemplified in the Determination of Age-related Auditory Thresholds. Acta Otolaryngology *106*, 238-243.

167. Witter, M.P. (2006). Connections of the subiculum of the rat: Topography in relation to columnar and laminar organization. Behavioural Brain Research *174*, 251-264.

168. Yamada, R., and Kuba, H. (2016). Structural and Functional Plasticity at the Axon Initial Segment. Frontiers in Cellular Neuroscience *10*, 250.

169. Yamamoto, T., and Hirano, A. (1986). A COMPARATIVE STUDY OF MODIFIED BIELSCHOWSKY, BODIAN AND THIOFLAVIN S STAINS ON ALZHEIMER'S NEUROFIBRILLARY TANGLES. Neuropathology and Applied Neurobiology *12*, 3-9.

170. Yeager, C.L. (1950). THE ADAPTATION OF ELECTROENCEPHALOGRAPHY TO MEDICINE. California Medicine *73*, 350-354.

171. Young, I.R., Hall, A.S., Pallis, C.A., Bydder, G.M., Legg, N.J., and Steiner, R.E. (1981). NUCLEAR MAGNETIC RESONANCE IMAGING OF THE BRAIN IN MULTIPLE SCLEROSIS. The Lancet *318*, 1063-1066.

172. Zingg, B., Hintiryan, H., Gou, L., Song, Monica Y., Bay, M., Bienkowski, Michael S., Foster, Nicholas N., Yamashita, S., Bowman, I., Toga, Arthur W.*, et al.* (2014). Neural Networks of the Mouse Neocortex. Cell *156*, 1096-1111

ABSTRACT

ANALYSIS OF THE SECONDARY NEURODEGENERATIVE CONSEQUENCES OF PRIMARY OLIGODENDROCYTE STRESS THROUGH THE USE OF THE NOVEL *OBIDEN* MOUSE MODEL

by

DANIEL ZDZISLAW RADECKI

May 2017

Advisor: Alexander Gow, Ph.D.

Major: Molecular Biology and Genetics

Degree: Doctor of Philosophy

The work of this project was to develop, test and characterize a potential novel mouse model of the neurodegenerative disease Multiple Sclerosis (MS). Historically, MS has been identified as a primary autoimmune disease of the central nervous system (CNS). However, treatments based on this view have met with limited success, and in most cases, fail to prevent progression of MS from mild to moderate and severe forms. Original observations regarding axonal and neuronal pathology in the white and gray matter of the CNS were rediscovered in the 1990s. These observations indicated that even in the absence of the immune system, degeneration can be widespread throughout the CNS. In addition, observations on the demyelinating leukodystrophy Pelizaeus-Merzbacher Disease (PMD), that could present with MS-like symptoms led to a new hypothesis on the etiology of MS.

This hypothesis was that primary metabolic stress in oligodendrocytes could be contributing to the etiology and pathology of MS. To test this, our lab developed the *OBiden* model, where we can induce metabolic stress in mature, myelinating oligodendrocytes. The method of metabolic stress induction is well characterized and therefore allows for the study of the secondary behavioral and neurodegenerative changes that occur in the *OBiden* mouse.

The *OBiden* mouse was found to develop a depression-like endophenotype at 6 months of age that persisted through until 12 months of age. Deficits in working and novel memory also developed at 12 months of age, and both behavioral changes are analogous to those noted in MS patients. Next, secondary lesions in white matter as well as extensive gliosis were identified in the *OBiden* animals, both of these results match closely with observations on MS tissue. Finally, secondary gray matter changes were noted throughout the CNS, specifically in cortical and hippocampal areas closely associated with the noted behavioral decline. These changes included structural neurofilament alterations and the novel identification of changes to the proximal axon called the axon initial segment (AIS). The AIS is intimately associated with action potential generation and changes to AIS structure or function are noted to coincide with neuronal firing changes. These neuronal changes are likely the cause of the behavioral deficits noted in the *OBiden* mice and develop solely as a secondary result to the primary oligodendrocyte stress.

Together, these results indicate that the *OBiden* mouse shares a number of similarities to MS patients including cognitive behavioral changes and molecular degeneration phenotypes. These degenerative consequences occur without the invasion of the peripheral immune system and instead are a result of primary metabolic stress in oligodendrocytes. Therefore, the *OBiden* mouse may represent a novel insight into MS pathology and allow more general research into the communication and interaction between oligodendrocytes and neurons.

AUTOBIOGRAPHICAL STATEMENT

EDUCATION

Doctor of Philosophy — Wayne State University, Detroit, MI 48201
2010-2017 — Molecular Biology and Genetics

Bachelor of Arts — State University of New York at Buffalo, Buffalo, NY 14261
2006-2010 — Major: Biological Sciences

Professional Memberships

Society for Neuroscience	2010-present
American Assocaite for the Advancement of Science	2011-present
International Society for Neurochemistry	2014-present

Publications

"Corticohippocampal Damage from Primary Oligodendrocyte Stress in the *OBiden* Model of Multiple Sclerosis Pathology." **DZ Radecki**, A Brown, N Meshkin, SA Perrine, A Gow. *In preparation*.

"Oligodendrocyte Metabolic Stress in Neurodegeneration." **DZ Radecki**, A Gow. In: Neurodegenerative diseases – Processes, Prevention, Protection and Monitoring Change, RC-C, Ho, JY-S, eds, *InTech*, pp. 535-557.

Grants

National Multiple Sclerosis Society	2011-2016

Fellowships and Awards

Thomas C. Rumble Fellowship	2014-2015
International Society of Neurochemistry Travel Award	2015
Wayne State Graduate Exhibition 3rd Place Poster Award	2015
ASN Neuro Journal Graduate Student Poster Award-9th Great Lakes Glia	2013
IBS Program Fellowship	2010-2013